# 國立交通大學

# 材料科學與工程學系

# 博 士 論 文

## 奈 米 碳 管 應 用 於 場 發 射 元 件 之 研 究

**Study of Carbon Nanotubes on Field Emission Device**

研 究 生：陳光中

指導教授：陳家富、黃華宗　教授

中 華 民 國 九 十 七 年 六月

# 奈米碳管應用於場發射元件之研究

# Study of Carbon Nanotubes on Field Emission Device


研 究 生：陳光中　　Student：Kuang-Chung Chen

指導教授：陳家富、黃華宗　Advisor：Dr. Chia-Fu Chen

Dr. Wha-Tzong Whang


國 立 交 通 大 學

國立交通大學材料科學與工程學系

博 士 論 文

A Thesis

Submitted to Department of Materials Science and Engineering

College of Engineering, National Chiao Tung University

in partial Fulfillment of the Requirements

for the Degree of Ph. D.

in Materials Science and Engineering

June 2008

Hsinchu, Taiwan, Republic of China

中華民國九十七年六月

# 國　立　交　通　大　學

## 研 究 所 博 士 班

## 論文口試委員會審定書

本校 **材料科學與工程** 學系 陳光中 君

所提論文 奈米碳管應用於場發射元件之研究

Study of Carbon Nanotubes on Field Emission Device

合於博士資格水準、業經本委員會評審認可。

口試委員：

| | |
|---|---|
| | |
| | 許鈺泉 |
| | 孫 宏 |
| | |
| 指導教授： | 黃華宗 |

系主任： 韋光華 教授

中　華　民　國　九十七　年六月　十　日

# 奈米碳管應用於場發射元件之研究

研究生：陳光中　　指導教授：陳家富博士、

黃華宗博士

國立交通大學材料科學與工程研究所　博士班

## 摘 要

奈米碳管(CNTs)具有高深寬比、高傳導性、與高機械強度等特性，被視為應用於場發射元件最適合的材料之一。而以奈米碳管作為發射源的應用之中，奈米碳管場發射顯示器(CNT-FED)最受青睞，為了達到低製造成本，可大尺寸化等要求，搭配網印技術厚膜成型於玻璃基板，成為量產的最可能方式之一。受限於一般玻璃基板耐溫低於 550℃，故以往技術是先合成奈米碳管後，調配成漿料方式，再網印於電極之上，但此法需再額外作活化處理，才能提升奈米碳管的場發射特性。

故在此篇論文中，主要目的就是要在低溫下合成或沈積奈米碳管於網印厚膜結構之中，並得到合適的場發射特性運用於場發射元件。著重討論奈米碳管合成與沈積技術以及沈積之後的特性。首先提出兩種觸媒成型方式-溶液沈積法與溶膠-凝膠法，可搭配漿料與網印技術，製作於厚膜結構之中，加上微波電漿化學沈積法(MPCVD)，以 $CH_4$ /$H_2$ 氣體系，低溫選擇性成長於玻璃基材上，實驗結果顯示兩種方式所成型的觸媒，經合成後之奈米碳管，其型態為不規則捲曲，中間帶有魚骨狀結構，且為多層壁。觸媒成型為溶液沈積法，合成之碳管其發射源啟動電場(turn-on electric field)約 3.2 V/$\mu$m(電流為 10 $\mu$A/cm$^2$)。另一藉由溶膠-凝膠法成型之觸媒，其合成之碳管其發射源啟動電場約 5.4 V/$\mu$m。

為了在低溫下大面積合成奈米碳管，本論文也嘗試使用易於大尺寸化的熱化

學沈積法(thermal CVD)，同樣採用溶膠-凝膠法成型觸媒，搭配漿料與網印技術，以 $C_2H_2$ /$H_2$ 氣體系成長於厚膜銀電極之上，研究結果顯示此法可於 480℃之下合成奈米碳管，其型態為不規則捲曲的多層壁結構，在二極與三極結構中量測，呈現均勻場發射影像與高亮度，發射源啟動電場約 3.85 V/μm(電流為 10 μA/$cm^2$)，當電流達到 1 mA/$cm^2$時，電場強度為 5 V/μm。後續也探討陰極結構的形狀效應，對奈米碳管合成的影響，為了搭配三極結構製作的便利性，觸媒改採濺鍍方式，藉由控制反應氣體氣流的變化，成功於三極結構中合成奈米碳管。

最後基於化學氣相沈積法低溫合成時，會有碳管品質不佳的問題，著手採用電泳法(EPD)直接於三極結構中擇區沈積奈米碳管，藉由兩台電壓源分別於閘極與陰極提供不同的電壓，隨著電場分佈，奈米碳管會被閘極排斥，而被陰極吸引而沈積。此電壓控制的設計，具有不需要使用光阻或犧牲層覆蓋電極的優點，並可在常溫下進行。

# Study of Carbon Nanotubes on Field Emission Device

Student：Kuang-Chung Chen　　Advisor：Dr. Chia-Fu Chen,

Dr. Wha-Tzong Whang

Institute of Material Science and Engineering

National Chiao Tung University

## Abstract

Carbon nanotubes(CNTs) exhibit excellent field emission characteristics due to their high aspect ratios, small tip radius of curvature and low work function. A low cost process combines arc-discharge producing CNTs as a paste and screen-printing technologies which was developed to prepare field emitters on the glass substrate. Unfortunately, using CNTs paste by screen-printing technology has a relatively low resolution and needs a surface rubbing technology or other activated steps to enhance field emission characteristics. By using chemical vapor deposition (CVD) process, CNTs can directly grow on the predefined catalyst layer, and also achieve high yield and uniformity. Therefore, the development of direct growth CNTs on the glass substrates at low temperature by a low cost technology will play an important role in practical field emission display (FED) applications.

In this thesis, we successfully combined the advantages of screen printing process, microwave plasma chemical vapor deposition (MPCVD) and thermal CVD process to pattern catalyst/Ag cathode by screen printing technology and grow CNTs on patterned Ni-catalyst of cathode electrode on glass substrates below 550℃. Two novel

ways can be applied to coat catalyst-Ni with Ag powders in a solution phase by the solution deposition method and sol-gel method.

However, the mass flow transport behaviors of precursor gas play important roles for CVD technology especially in the stepped electronic structures. The depth dimension of dielectric holes in thick-film normal triode structures may range from 10μm to 50μm. In order to solve the gas transport problem in such narrow and deep dielectric holes, we controlled the pumping system and precursor concentration during the CVD process. The relationship between CNTs synthesis and aspect ratio of dielectric holes was investigated in this work. The cathode with high aspect ratio dielectric holes for field emission devices was properly produced.

Another novel way applied to deposit CNTs in triode structure was the electrophoretic deposition (EPD) method. Two power supplies were used to provide the gate electrode and cathode electrode with different voltages, respectively. Following the electric field distribution, CNTs were forced to be dragged toward the cathode electrode but repelled out of the gate electrode. By conducting this designed voltage-controlling method, CNTs were able to be deposited in the selected-area without any photo-resist or sacrificial layer at the room temperature.

# 致謝

衷心感謝指導教授-陳家富老師的教導，陳老師雖身負研究、教學與行政等重任，仍抽出時間不時給予親切關懷與悉心指導，也承蒙共同指導教授-黃華宗老師的教導與鼓勵，在兩位老師的指點之下，本文才得以順利完成，在此謹向陳老師與黃老師致以誠摯的謝意。

感謝實驗室的多位學長姐與學弟妹-佳倫、陳密、建良、建仲、建銘、士塵、華琦、鴻鈞、泰霖、振航、依璇、騰凱、厥陽、淙琦、方慈、昱顯等，在實驗與生活上的協助與支持，我才能克服一個個的困難，走到最後。

還有感謝在工研院的同事，正中、名君、悠揚、明宏多年來給予支持，讓我能投入論文研究之中，尤其立雄不厭其煩，在實驗的規劃與論文的撰寫上持續給予指導與寶貴意見，貞慧、良祐、淑幸、國峰、建良、日舜、宏吉、小芬、又萱、耀誠、寬鑫、炳南、姿蘭、曉玟、曉萍、怡凱、德皓、偉義、麟恩、傳旭、寶鳴、振豪、家充、偉浩、雲嬌、明良、志嘉、鑫茂、鈞道、詩文、玉涵、仲文、士杰、世杰、志榮、慶勳、仁豪、福光、裕淵、盈憲、智平、宏元、志成等伸出溫暖的雙手，鼎立襄助，這段時間能和各位相遇、相交、相知是人生中最快樂的時光。

最後謹向我的父母和兩位弟弟表示誠摯的謝意，感謝他們對我的支持與體諒，尤其父母對我的身教與言教，更讓我終生受益無窮，我的點滴成就都來自他們。在論文即將完成之際，原本該要如釋重負，但心情卻還是無法平靜，因為我的父親未能及時看到此論文付梓，身為人子總覺有一絲遺憾，願父親在另一個世界能過得更好，母親與家人永遠健康快樂！

## Contents

## List of Figures

# List of Tables



# Chapter 1 Introduction

Carbon nanotubes (CNTs), since their discovery in 1991 [1], have been considered for use in many different applications. The small dimensions, strength and remarkable physical properties of these materials make them the very promising emitters for field emission devices. Electron field emitters are now becoming increasingly attractive for flat panel displays. This resurgence is largely due to the recent development of cheap and robust field emitting materials. Although field emission devices based on microfabricated Mo tips are commercially available, researchers are actively looking for alternative materials. The ideal field emitter should be very long and very thin, made of conductive material with high mechanical strength, be robust, and cheap and easy to process [2]. CNTs show remarkable electronic [3-6] and mechanical [7-12] properties that have triggered an ever stronger effort towards applications. The power of CNTs as electron field emitters was already apparent from the first articles reporting extremely low turn-on fields and high current densities in 1995 [13-15]. Field emission devices based on CNTs have exhibited remarkable emission characteristics and good current stability [15,16], because of the high-aspect-ratio and electrical conductivity, as well as a mechanical stiffness of the CNTs [9,17]. This chapter introduces the motivation and outline of this study.

## 1.1 Background

Carbon nanotubes (CNTs) were first discovered by Iijima in 1991 using transmission electron microscopy (TEM) [1]. Due to their high aspect ratios, small tip radius of curvature and low work function, CNTs exhibit excellent field emission characteristics. Geometry, high mechanical strength and high chemical stability are the advantage of CNTs used as field emitters [18-21].

Numerous methods to grow CNTs have been developed, including arc-discharge, chemical vapor deposition and pulsed laser ablation [22-24]. Among various growth methods, both arc-discharge produced CNTs [25] and CVD [26] were usually reported to be the electronic device application such as field emission display. A low cost process combines arc-discharge producing CNTs as a paste and screen-printing technologies which was developed to prepare field emitters on glass substrate [27]. Unfortunately, using CNTs paste by screen-printing technology has a relatively low resolution and needs a surface rubbing technology or other activated steps to enhance field emission characteristics [27].

### 1.2 Motivation

For CVD synthesizing CNTs, it can directly grow on the predefined catalyst layer and has high yield and uniformity. Many researchers have succeeded in synthesizing CNTs on Si substrate at a relatively high temperature by various CVD methods [28]. In order to suit for FED applications, the growth temperature limits below 550℃ to avoid glass substrate deformation. Recently, the study of direct growth CNTs at low temperature on glass substrates by CVD method has been reported [29-31].

However, in previous works, it is required to deposit patterned catalyst metal on cathode electrode on glass substrate by semiconductor processes, such as sputtering or thermal evaporating etc. As we know, the cost increase of the semiconductor processes is many times larger than screen-printing processes. Therefore, development of the direct growth or direct deposit CNTs in triode structure on glass substrates at low temperature by a low cost technology will play an important role in practical FED applications. In this work, we combined the advantages of screen printing process and CVD/EPD process to manufacture cathode structure by screen printing technology and grew/deposited CNTs on cathode electrode on glass substrate at low temperature.

### 1.3 Outline of this Thesis

There are other four chapters in the thesis; a concisely summary of these chapters is as follows:

**Chapter 2 Literature Review:** The aim of this chapter is to provide a basic understanding about CNTs and the field emission. First, carbon materials, fullerence and carbon nanofiber, are introduced. Second, structures and properties of CNTs are focused. Third, synthesis methods of CNTs are interpreted. Finally, field emission theory and applications are presented.

**Chapter 3 Experimental Details:** Related deposition systems are illustrated. The major analysis instruments used includes SEM, micro-Raman spectroscopy and HRTEM. Field emission properties were measured by an I-V measurement.

**Chapter 4 Results and Discussion:** There are five subjects in this chapter. Research objectives listed above are interpreted, and the more concerned literature review is also discussed in this chapter.

**Chapter 5 Conclusions:** The results of the present investigation are summarized.

# Chapter 2 Literature Review

Through the achievements of the pioneers and other procedures, many research records about the CNTs applied in field emission can be found in a readable literature. In fact, there are many review paragraphs appeared in papers, reports, theses and CNTs handbooks. However, the aim of this chapter is to provide a basic understanding about the field emission related subject, and the material aspect of CNTs.

## 2.1 Introduction to Carbon Materials

Carbon is the sixth element of the periodic table and is listed at the top of column IV. Carbon materials can be found in various forms as diamond, graphite, carbon fibers, fullerences, and CNTs. Crystal structures of these carbon materials are shown schematically in Fig. 2.1. The reason why carbon assumes many structural forms is that a carbon atom can form several distinct types of valence bonds (or hybridization of orbitals).

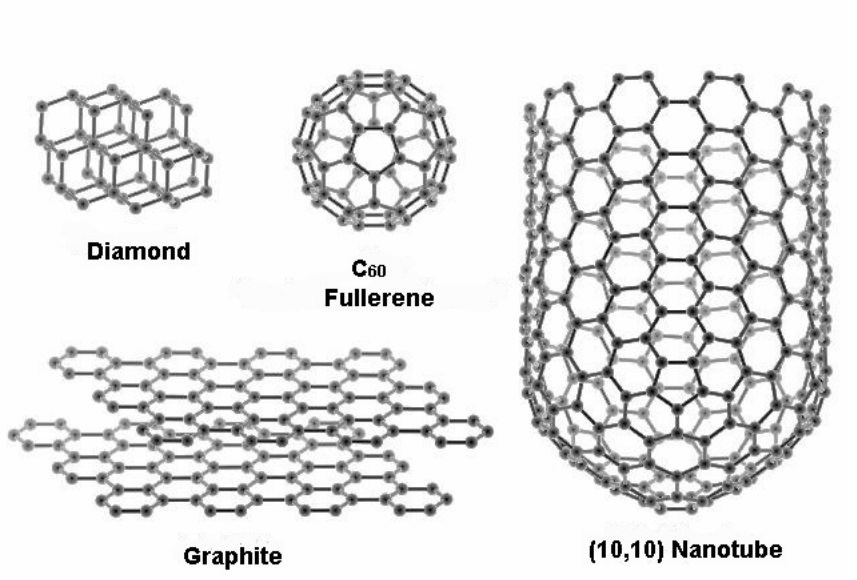


Fig. 2.1. Various forms of carbon: diamond, fullerene, graphite, and CNT [34].

Each carbon atom has six electrons $1s^2$, $2s^2$, and $2p^2$ theoretically. In carbon, there are three possible hybridized orbitals sp, $sp^2$, and $sp^3$. The $sp^n$ hybridization is important for

determining the dimensionality of carbon-based molecules and carbon-based solids. Carbon shows a variety of stable forms ranging from 0D fullerenes [32] to 1D conducting or semiconducting CNTs to 2D semi-metallic graphite to 3D semiconducting diamond, as shown in Table 2.1 [33]. In $sp^n$ hybridization, (n+1) σ bonds per carbon atom are formed. These σ bonds make a frame for the local structure of the n-dimensional structure.

Table 2.1 Isomers of carbon [33]

| Dimension | 0-D | 1-D | 2-D | 3-D |
|---|---|---|---|---|
| Isomer | $C_{60}$<br>Fullerene | CNT<br>Carbyne | Graphite<br>Fiber | Diamond<br>Amorphous |
| Hybridization | $sp^2$ | $sp^2$ ( sp) | $sp^2$ | $sp^3$ |
| Density<br>[g / $cm^3$] | 1.72 | 1.2-2.0<br>2.68-3.13 | 2.26<br>~2 | 3.515<br>2-3 |
| Bond Length<br>[Å] | 1.4 (C=C )<br>1.46 (C-C) | 1.44 (C=C ) | 1.42 (C=C )<br>1.44 (C=C) | 1.54 (C-C) |
| Electronic Properties | Semiconductor<br>Eg = 1.9 eV | Metal or Semiconductor | Semimetal | Insulating<br>Eg = 5.47 eV |

In $sp^3$ hybridization, 4 σ bonds defining a regular tetrahedron are sufficient to form a 3D diamond structure. In $sp^2$ hybridization, it forms a planar structure in 2D graphite, and also forms a planar local structure in the closed polyhedron (0D) of fullerence and in the cylinders (1D) of CNT. Carbon fiber is macroscopic 1D material, because of the high length to diameter ratio. However, it consists of many graphitic planes and microscopically exhibits electronic properties that are mainly 2D. In sp hybridization, two σ bonds make only a 1D chain structure, which is known as a carbyne. Besides, amorphous carbon is a disorder, 3D material in which both of $sp^2$ and $sp^3$ hybridization are present randomly. Amorphous graphite is the

graphite with random stacking of graphitic layer segments, which consists mainly of $sp^2$ hybridization. Amorphous graphite can behave like a 2D material.

Next, fullerences and carbon fibers, which are closely related to CNTs, are introduced. The main research object of this thesis, CNTs, is introduced apart in Section 2.2.

### 2.1.1 Fullerenes

Fullerence is an abbreviation of buckminsterfullerenes that honored the famous architect Buckminster Fuller, who designed and invented geodesic dome that was similar to the structure of $C_{60}$. In 1985, Kroto, Smalley, Curl and coworkers [35] began a famous series of experiments on the vaporization of graphite. In the distribution of gas-phase carbon clusters, $C_{60}$ was the dominant species. This dominance became even more marked under conditions which maximized the amount of time the clusters were 'annealed' in the helium. Figure 2.2 shows $C_{60}$, which is a closed cluster containing precisely 60 carbon atoms would have a structure of unique stability and symmetry. The discovery of $C_{60}$ marked the beginning of a new area in carbon science [36-39].

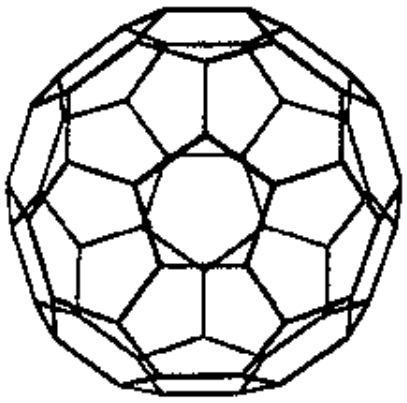

Fig. 2.2. C60 buckminsterfullerence [37].

### 2.1.2 Carbon Nanofibers

Carbon fibers represent an important class of graphite-related materials which are closely connected to CNTs, because of the high length to diameter ratio. Carbon fibers synthesized by traditional methods of extrusion from polymer slurries and from catalytic CVD vary in morphology and structure from fiber to fiber and area to area on each fiber. Despite the many precursors that can be used to synthesize carbon fibers, each having a different cross-sectional morphology, as shown in Fig. 2.3. Figure 2.3(a) shows carbon fibers as-deposited at 1100℃, and Fig. 2.3(b) shows carbon fibers which after treatment to 3000℃. The morphologies for commercial mesophase pitch fibers are shown in Fig. 2.3(c) for a "PAN-man" cross section with a radical arrangement of straight graphene ribbons and a missing wedge and Fig. 2.3(d) for a PAN-AM cross-sectional arrangement of graphene plane. A PAN fiber is shown in Fig. 2.3(e) with a circumferential arrangement of ribbons in the sheath region and a random structure in the core. The preferred orientation of the graphene planes is parallel to the fiber axis for all carbon fibers, thereby accounting for the high mechanical strength [40].

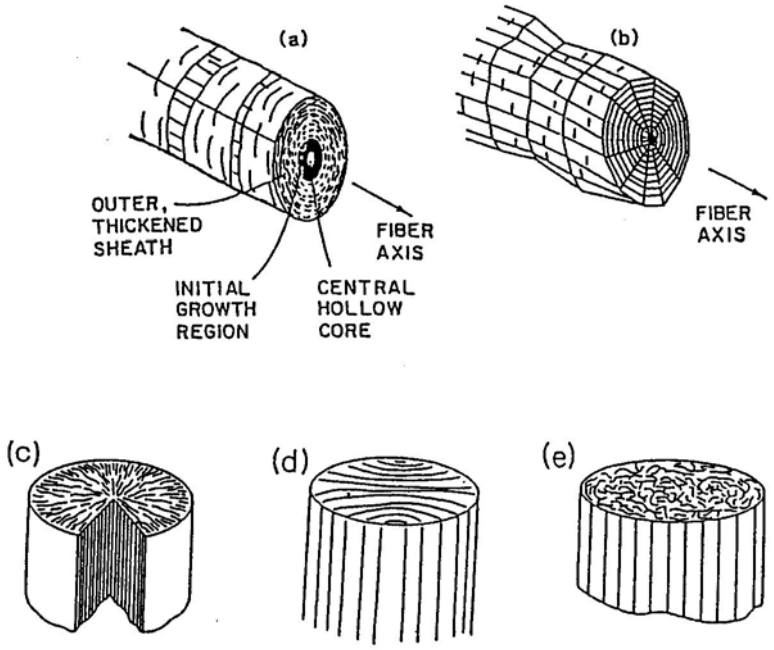


Fig. 2.3. Sketch illustrating the morphology of vapor grown carbon fibers [32].

### 2.1.3 Structure and Properties of Carbon Nanotubes

The main research object of this thesis, CNTs, is introduced here. Following paragraphs provide an overview of the structural and properties of CNTs, and there are many review articles [41-44] and books [32,45,46] surround this subject.

#### 2.1.3.1 Structure

The detail structure of CNTs is discussed here. In the ideal case, a CNT consists of either one cylindrical graphene sheet (Single-walled nanotube, SWCNT) or of several nested cylinders with an inter-layer spacing of 0.34 - 0.36 nm that is close to the typical spacing of turbostratic graphite, i.e. MWCNT. There are many possibilities to form a cylinder with a graphene sheet [4] and a few configurations are shown in Fig. 2.4. Figure 2.4(a)-(c) are SWCNTs of (a) zig-zag, (b) armchair and (c) chiral type. Figure 2.4(d) represents a MWCNT formed by four tubes of increasing diameter with a layer spacing of 0.34 nm. One can roll up the sheet along one of the symmetry axis: this gives either a zig-zag tube, or an armchair tube. It is also possible to roll up the sheet in a direction that differs from a symmetry axis: one obtains a chiral CNT. Besides the chiral angle, the circumference of the cylinder can also be varied.

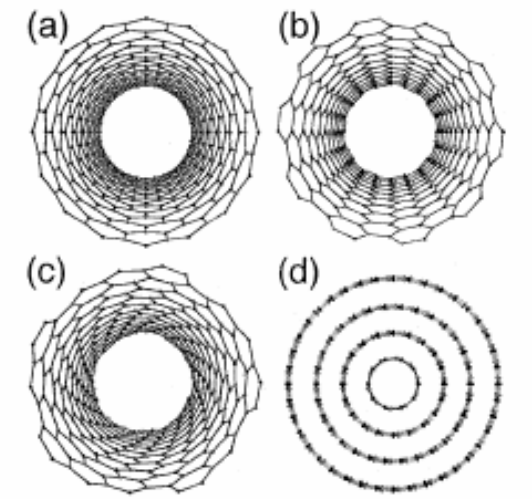


Fig. 2.4. Models of different CNT structures [2].

Figure 2.5 shows the cutting graphite sheet along the dotted lines which connects two crystalline graphite equivalent sites on a 2-D [47]. Each carbon atom has three nearest neighbors, rolling sheet of graphite into cylinder form CNTs. The circumference of CNTs can be expressed in term of the chiral vector, $C_h$, and chiral angle, $\theta$. The chiral vector is given by Eq. (1):

$$C_h = na_1 + ma_2 \equiv (n,m) \tag{1}$$

(n, m are integers, $0 \leqq |m| \leqq n$ ),

where $a_1$ and $a_2$ are the primitive vectors length of which are both equal to $\sqrt{3}\ l_{C\text{-}C,}$ with $l_{C\text{-}C}$ is the length of C-C bond. The chiral angel determines the amount of twist in the tube. The chiral angles exist two limiting cases that are at $0^\circ$ and $30^\circ$. The chiral angle is defined in Eq. (2) as

$$\cos\theta = \frac{C_h \cdot a_1}{|C_h| \cdot |a_1|} = \frac{2n+m}{2\sqrt{nm+m^2+n^2}} \tag{2}$$

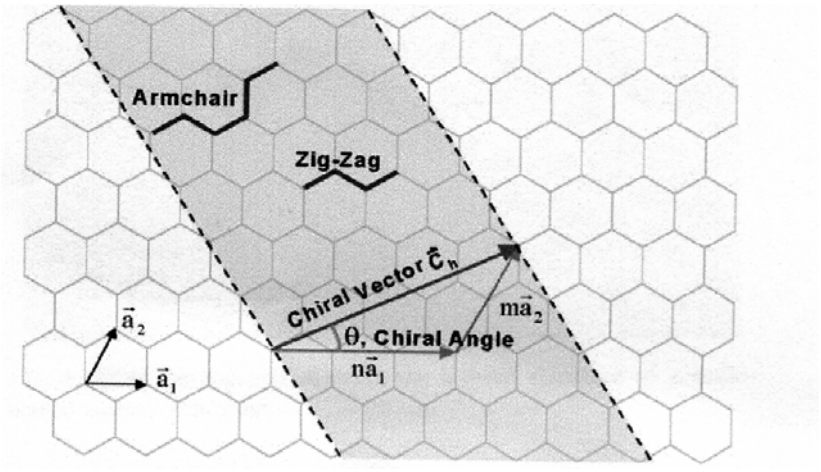


Fig. 2.5. Schematic diagram showing how a hexagonal sheet of graphite is rolled to form a CNT [47].

The zig-zag CNT corresponds to the case of m = 0, and the armchair CNT corresponds to the case of n = m. The chiral CNT corresponds to the other (n, m) chiral vectors. The zig-zag CNT (n, 0) is generated from hexagon with θ= 0°, and armchair CNT (n, n) is formed from hexagon with θ= 30°. The chiral CNT is formed from hexagon with $0° < \theta < 30°$.

The inter-atomic spacing of carbon atom is known so that the rolled up vector of CNT can define the CNT diameter. The properties of carbon CNTs depend on the atomic arrangement, diameter, length, and the morphology [48].

This diversity of possible configurations is indeed found in practice, and no particular type is preferentially formed. In most cases, the layers of MWCNTs are chiral [1,49] and of different helicities [50]. The lengths of SWCNTs and MWCNTs are usually well over 1 μm and diameters range from ~1 nm (for SWCNTs) to ~50 nm (for MWCNTs). Pristine SWCNTs are usually closed at both ends by fullerene-like halfspheres that contain both pentagons and hexagons [4]. A SWCNT with a well-defined spherical tip is shown in Fig. 2.6. A MWCNT where the shape of the cap is more polyhedral than spherical is represented in Fig. 2.6(b). An open MWCNT where the ends of the graphene layers and the internal cavity of the tube are exposed is shown in Fig. 2.6(c). Defects in the hexagonal lattice are usually present in the form of pentagons and heptagons. Pentagons produce a positive curvature of the graphene layer and are mostly found at the cap as shown in Fig. 2.6(b) where each knick in the graphene layers points to the presence of pentagons in the carbon network. Heptagons give rise to a negative curvature of the tube wall [51]. Defects consisting of several pentagons and/or heptagons have also been observed. A simple model indicates that the diameter and/or chirality of the tube is changed from one side of the defect to the other [52]. Such an arrangement forms therefore a link between two different tubes and is accordingly called a junction.

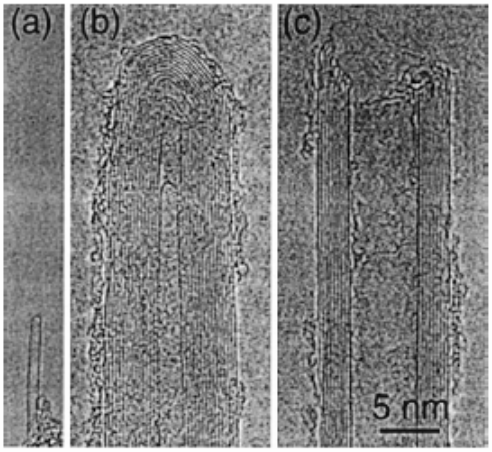


Fig. 2.6. TEM pictures of the ends of (a) a SWCNT, (b) a closed MWCNT, and (c) an open MWCNT. Each black line corresponds to one graphene sheet viewed edge-on [2].

### 2.1.3.2 Properties

This section is an overview of the mechanic and electronic properties of CNTs. The electronic properties of SWCNTs have been studied in a large number of theoretical works [3,4,53-55]. These models show that the electronic properties vary in a calculable way from metallic to semiconducting, depending on the tube chirality (n, m) given by [32]

Metallic properties: n-m = 0 or (n-m)/3 = integer

Semiconducting properties: (n-m)/3 ≠ integer

The study shows that about 1/3 of SWCNTs are metallic, while the other 2/3 of SWCNT are semiconducting with a band gap inversely proportional to the tube diameter. This is due to the very unusual band structure of graphene and is absent in systems that can be described with usual free electron theory. Graphene is a zero-gap semiconductor with the energy bands of the p-electrons crossing the Fermi level at the edges of the Brillouin zone, leading to a Fermi surface made of six points [56]. Graphene should show a metallic behavior at room temperature since electrons can easily cross from the valence to the conduction band. However, it behaves as a semi-metal because the electronic density at the Fermi level is quite low [32,56]. Rolling up the graphene sheet into a cylinder imposes periodic boundary conditions along the circumference and only a limited number of wave vectors are allowed in

the direction perpendicular to the tube axis. When such wave vectors cross the edge of the Brillouin zone, and thus the Fermi surface, the CNT is metallic. This is the case for all armchair tubes and for one out of three zig-zag and chiral tubes. Otherwise, the band structure of the CNT shows a gap leading to semiconducting behavior, with a band gap that scales approximately with the inverse of the tube radius. Band gaps of 0.4-1 eV can be expected for SWCNTs (corresponding to diameters of 1.6-0.6 nm) [3,4,54]. This simple model does not take into account the curvature of the tube which induces hybridization effects for very small tubes [53] and generates a small band gap for most metallic tubes [55]. The exceptions are armchair tubes that remain metallic due to their high symmetry.

These theoretical predictions made in 1992 were confirmed in 1998 by scanning tunneling spectroscopy [5,6]. The scanning tunneling microscope has since then been used to image the atomic structure of SWCNTs [57,58], the electron wave function [59] and to characterize the band structure [58,60]. Numerous conductivity experiments on SWCNTs and MWCNTs yielded additional information [61-72]. At low temperatures, SWCNTs behave as coherent quantum wires where the conduction occurs through discrete electron states over large distances. Transport measurements revealed that metallic SWCNTs show extremely long coherence lengths [65,72,73]. MWCNTs show also these effects despite their larger diameter and multiple shells [74,75].

The fact that both MWCNT and SWCNT have indeed extraordinary mechanical properties has been indicated by a growing body of experimental evidence. Yakobson et al [76,77] inspected the instability of CNTs beyond linear response. Their simulation results show that CNTs are remarkably resilient, sustaining extreme strain with no signs of brittleness or plasticity. Besides, some experimental measures of the Young's modulus of CNTs have been reported. Treacy et al. [78] obtained a relation between amplitude of the tip oscillations and the Young's modulus. Through TEM observations of some CNTs, they defined the amplitude of those oscillations and obtained an average value of 1.8 TPa for the Young's modulus.

Another way to probe the mechanical properties of CNTs is to use the tip of AFM to bend anchored CNT. Young's modulus can be extracted while simultaneously recording the force exerted by the tube as a function of the displacement from its equilibrium position. By this way, Wong et al. [9] reported a mean value of 1.28±0.59 TPa with no dependence on tube diameter for MWCNT. Walters et al. [79] investigated the elastic strain of CNTs bundles with the AFM. An experimental strain measurement and an elastic modulus of 1.25 TPa was assumed. Then yield strength of 45±7 GPa was calculated.

Yu et al. [12,80] reported the tensile of SWCNTs and MWCNTs ropes. For MWCNTs ropes, the tensile strengths of the outermost layer ranged from 11 to 63 GPa and the elastic modulus ranged from 27 to 950 GPa. For SWCNT ropes, the tensile strengths in the range from 13 to 52 GPa and the average elastic modulus of 320 to 1470 GPa were obtained.

In term of mechanical properties, CNTs are among the strongest and most elastic materials known to exist in nature [81]. Table 2.2 shows the mechanical properties of CNTs with other materials. It indicates that MWCNTs are of the most superior mechanical characteristic. The hollow structure and close topology of CNTs form a distinct mechanical response in CNT compared to other graphitic structure.

Table 2.2 Mechanical properties of CNTs compared with other Materials [81]

| Materials | Young's modulus (GPa) | Tensile strength (GPa) | Density (g/cm$^3$) |
|---|---|---|---|
| SWCNT | 1054 | ~150 | |
| MWCNT | 1200 | ~150 | 2.6 |
| (10,10) Nanorope | 563 | ~75 | 1.3 |
| Type I carbon fiber | 350 | 2.5 | 2.6 |
| Steel | 208 | 0.4 | 7.8 |
| Epoxy | 3.5 | 0.05 | 1.25 |
| Wood | 16 | 0.08 | 0.6 |

## 2.2 Carbon Nanotube Synthesis

There are three major methods to synthesize CNTs: arc discharge, laser ablation and catalytically chemical vapor deposition.

### 2.2.1 Arc Discharge

The arc discharge was the first available method for the production of both MWCNTs [1,82] and SWCNTs [83,84]. This is the classic method of preparing MWCNTs, and produces the best quality samples. The method has been in use for a long time for the production of carbon fibers. Therefore, it is very possible that CNTs were observed but not recognized before Iijima observed CNTs synthesized from this method in 1991 [85,86].

Figure 2.7 shows the schematic of arc discharge system and TEM micrograph of the grown CNT [2]. The arc discharge apparatus involves the use of two graphite rods as the anode and cathode. The rods are brought together under a gas atmosphere (usually He, but $H_2$ [87] and Ar have also been used) and a voltage is applied until a stable arc is achieved. As the anode is consumed, a gap (~ 1mm) between cathode and anode is maintained by adjusting the position of anode. Carbon materials are deposited on the cathode to form CNTs and other carbon particles. MWCNTs produced by arc discharge are long and straight tubes closed at both ends with graphitic walls running parallel to the tube axis, as shown in Fig. 2.7.

Several factors have been shown to be important in producing a good yield of high quality of CNTs. Harris [88] repotted that perhaps the most important is the pressure of the helium in the chamber, as demonstrated by Ebbesen and Ajayan [82]. The Current in the arc discharge method is another important factor [89,90]. Efficient cooling of the electrodes and the chambers has also been shown to be essential in producing good quality CNT samples [89-91].

To synthesize SWCNTs, Iijima et al. [83] and Bethune et al. [84] reported in 1993 that an arc discharge with a cathode containing metal catalysts (such as cobalt, iron or nickel) mixed

to graphite powder results in a deposit containing SWCNTs. The yield has been significantly increased by optimizing the catalyst mixture [92] and the deposition conditions [93].

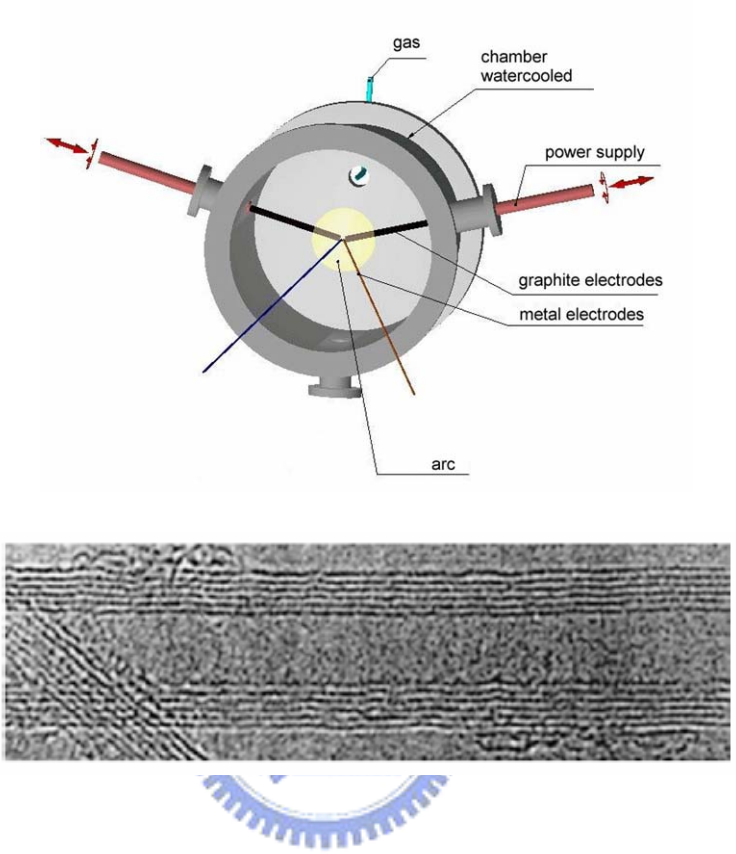


Fig. 2.7. Schematic illustration of the arc discharge system and TEM micrograph of the grown CNT [2].

### 2.2.2 Laser Ablation

Laser ablation was first used for synthesis of $C_{60}$ in 1985 by Kroto et al. [35], and was demonstrated to grow SWCNTs and MWCNTs in 1995 by Samlley's group at Rice University [94]. Subsequent refinements to this method led to the production of SWCNTs with unusually uniform diameter [95]. However, the length of MWCNTs grown by this method is much shorter than that by arc discharge method [94].

Thess et al. [95] showed that the synthesis could be carried out in a horizontal flow tube under a flow of inert gas at controlled pressure. In this setup the flow tube is heated to

~1200°C by a tube furnace as displayed in Fig. 2.8. Laser pulses enter the tube and strike a target consisting of a mixture of graphite and a metal catalyst such as Co or Ni. SWCNTs condense from the laser vaporization plume and are deposited on a collector outside the furnace zone [96]. The size of carbon sources limited the volume of sample. Besides, purification steps are necessary to separate the tube from undesirable by-product. Nevertheless, this method has still become an important technique for synthesizing SWCNTs due to the high yield of CNTs.

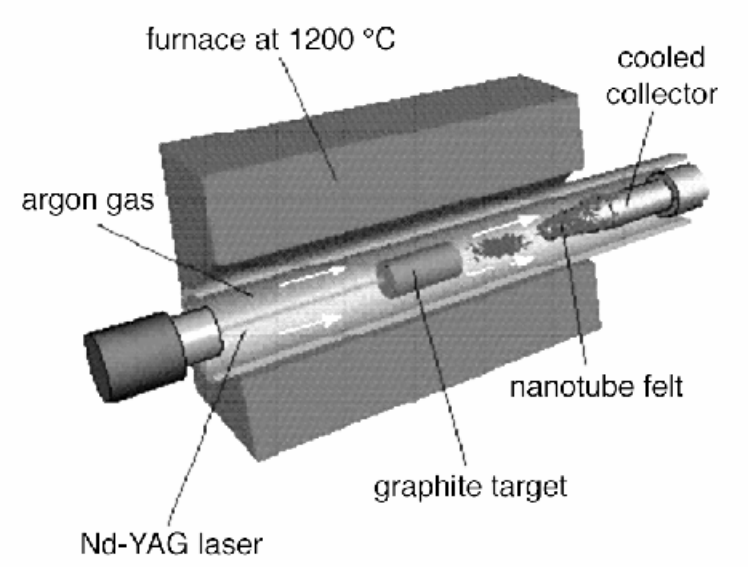


Fig. 2.8. Schematic illustration of the laser ablation apparatus [43].

### 2.2.3 Catalytically Chemical Vapor Deposition (CVD)

The catalytic growth of CNTs is an alternative to the arc discharge and laser ablation methods. It is based on the decomposition of the hydrocarbon gas over transition metals to grow CNTs by using chemical vapor deposition (CVD). Since the 1960s [97], carbon filaments and fibers have been produced by thermal decomposition of hydrocarbons. Usually, a catalyst is necessary to promote the growth [98]. A similar approach was used to grow MWCNTs from the decomposition of acetylene over iron particles in 1993 [99]. A tube

produced by catalytic growth is shown in Fig. 2.9. In general, the diameter of CNTs grown by catalytic growth is larger than that of arc discharge, but along with an imperfectly graphitized crystalline structure. To grow MWCNTs, acetylene is usually used as carbon source at temperatures typically between 600-800°C. To grow SWCNTs, the temperature has to be significantly higher (900-1200°C) due to the fact that they have a higher energy of formation. In this case carbon monoxide or methane must be used because of their increased stability at higher temperatures as compared to acetylene.

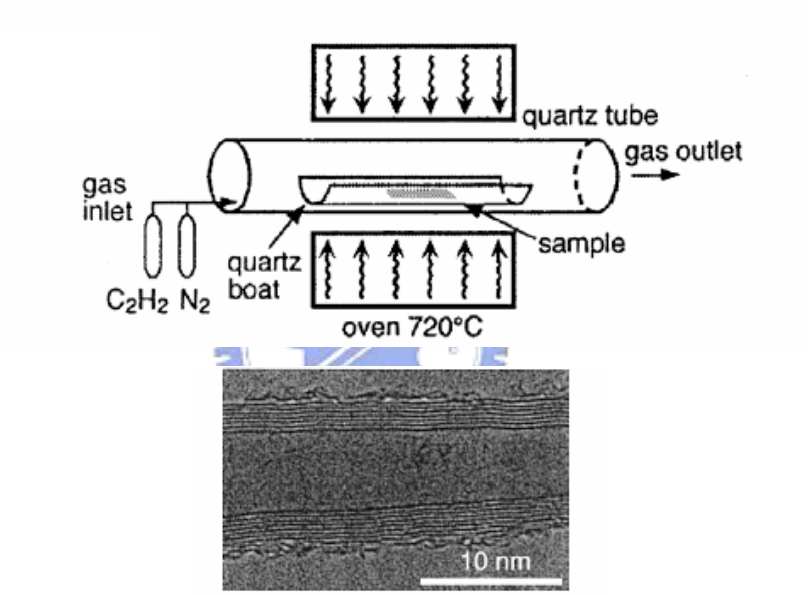


Fig. 2.9. Schematic illustration of the catalytic deposition and TEM micrograph of the grown CNT [2].

Up to now, the catalytic CVD has undergone many improvements. Co catalysts supported on silica particles produced straight as well as coiled MWCNTs [100], and the yield of CNTs was significantly increased by using zeolites as catalyst supports [101,102]. It was also reported that the continuous production of SWCNTs, where both the carbon and the catalyst are supplied in the gas phase. Besides, the yield and average diameter of SWCNTs could be varied by controlling the process parameters [103]. In addition, the type of catalyst support was found to control the formation of individual or bundled SWCNTs [104]. Transition metal

(e.g. Fe, Co, Ni) particles are known to be catalysts for vapor grown CNTs synthesis, in which hydrocarbons are used as carbon source. Metal catalysts are generally necessary to activate CNTs growth. A variety of other catalysts, hydrocarbons and catalyst supports have been used successfully by various groups the world wide to synthesize CNTs [105, 106]. Various metal compounds used as catalysts are listed in Table 2.3 [107]

The catalytic CVD is also an ideal method to grow CNTs on planar substrate (e.g. silicon or glass). Dense MWCNT arrays were thus deposited on mesoporous silica that was prepared by a sol-gel process [108] and long aligned CNTs were obtained over several square millimeters by using large-area mesoporous silica substrates [109]. Aligned MWCNTs were generated by pyrolysis of a triazine compound at 950°C with nearly no by-products [110]. There are some reasons behind the development of catalytic techniques to grow CNTs on planar substrates. First, in many cases, purification steps are unnecessary because there is no or very few by-product. Second, substrates can be directly patterned with catalysts using lithographic techniques followed by catalytic growth.

CNTs were also deposited by plasma-assisted CVD (PACVD) of methane and hydrogen at 950°C [111], and the synthesis temperature could be decreased below 660°C by using plasma-enhanced hot filament CVD [112]. Since then, several papers describing the synthesis of films of CNTs on silicon substrates have been published [113-116]. Moreover, microwave plasma-enhanced CVD of methane and hydrogen allowed to lower further the deposition temperature below 600°C on Ni-coated silicon [117], nickel [118], steel and Ni-coated glass [119] substrates. The synthesis of well-aligned CNTs on a variety of substrates was accomplished by the use of PACVD where the plasma is excited by a DC source [120] or a microwave source [121-123]. It was reported [108] that the ability to grow straight CNTs over a large area with uniformity in length, diameter, density, and straightness.

Table 2.3 Metals and metal compounds catalysts for SWCNT synthesis [107]

| Metal/compound | Experimental conditions[1] | Locations of SWCNT[2] | Density of SWCNT[3] |
|---|---|---|---|
| Fe | Fullerence | Soot | High |
| | | Extended deposition | High |
| | Tube | Soot | Low |
| Ni | Fullerence | Soot | High |
| | | Extended deposition | High |
| | Tube | Soot | Low |
| Co | Fullerence | Soot | Low |
| | Tube | Soot | High |
| | | Weblike | High |
| Fe/Ni | Fullerence | Soot | Very high |
| | Tube | Soot | Very high |
| | | Weblike | Very high |
| Fe/Co | Fullerence | Soot | Low |
| | Tube | Soot | High |
| | | Weblike | Very high |
| Ni/Co | Fullerence | Soot | Very high |
| | Tube | Soot | Very high |
| | | Weblike | Very high |
| Ni/Cu | Tube | Soot | Low |
| Ni/Ti | Tube | Soot | Very low |
| Cu/Co | Tube | Soot | Low |
| Mg/Ni | Tube | Soot | Low |
| $Y_2O_3$/Co | Tube | Soot | Low, radial |
| $YC_2$ | Tube | Soot | High, radial |

[1] "Fullerence" for arc discharge at 100-Torr He and "Tube" at 550 Torr.

[2] "Soot" and "Extended deposit" protruding from the usual cathodic deposit, and "Weblike deposit".

[3] Categorised as very high, high, low and very low.

CVD technique deals with gas phase system in CNTs are formed by the deposition of carbon-containing gas [108]. The gas phase techniques are amenable to continuous process since the carbon source is continually replaced by flowing gas. In addition, the final purity of CNTs can be quite high enough to minimize purification steps. The advantage of CVD technique is that CNTs can be synthesized continually and thus the growing pure CNTs could be obtained in the optimum condition. That is a very good way to synthesize large quantities of CNTs under relatively controlled conditions. So the CVD has advantages for scale-up and commercial productions.

## 2.3 Catalytic Growth Mechanisms of Carbon Nanotubes

Due to huge amount compound and various atomic bonding of carbon, plenty of kinds of methods are used for the growth of carbon related nanomaterials. Each method has its advantages, disadvantages, distinguishing feature, and a range for suitable use. Most of them have been successfully synthesize carbon nanotubes.

The model used for describing the growth of nanomaterials still is an issue because of the difficulty for observation under such extremely small scale. Even though, several mechanisms are brought up to characterize the behavior for the growth. Here we discuss some growth models which are considered to be the major mechanism for nanosize material.

Growth mechanism of various kind of bottom-up nanosize materials are generally considered to be three models: Vapor-Solid (VS) model, Vapor-Liquid-Solid (VLS) model, and recently, Solution-Liquid-Solid (SLS) model. Some modifications [124] have also been published which will not be discussed here.

### Vapor-Solid (VS) Model

Figure 2.10 shows an approximately growth model of vapor-solid growth mechanism. The diagram takes the growth of GaN for example. Epitaxial growth can be achieved without

catalyst or liquid phase. The sum of thermodynamic surface energy and heat of fusion become the driving force for VS growth. The growth rate of VS is dominated by the rate of atoms or molecules diffusion and rearrangement. Compare with the growth mechanism with catalyst, the VS mechanism has a lower growth rate.

**Vapor-Liquid-Solid (VLS) Model**

The mechanism [125] was first introduced in the 1960s to explain the growth of silicon whiskers or tubular structures [126]. In this model, growth occurs by precipitation from a supersaturated liquid-metal-alloy droplet located at the top of whisker, into which silicon atoms are preferentially absorbed from the vapor phase. The similarity between the growth of carbon nanotubes and the VLS model has also been pointed out by Saito et al [127,128] on the basis of their experimental findings for multi-walled nanotube growth in a purely carbon environment (Fig. 2.11). Solid carbon sublimates before it melts at ambient pressure, and therefore these investigators suggested that some other disordered carbon form with high fluidity, possibly induced by ion irradiation, should replace the liquid droplet.

**Solid-Liquid-Solid (SLS) Model**

Figure 2.12 [129] shows diagram of solution-liquid-solid growth mechanism which takes Ⅲ-Ⅴ materials for example. No catalyst is used for solution-phase synthesis. The materials are produced as polycrystalline fibers or near-single-crystal whiskers having width of 10 to 150 nanometers and length of up to several micrometers [130]. This mechanism shows that process analogous to vapor-liquid-solid growth operated at low temperatures, while requirement of a catalyst that melts below the solvent boiling point to be its potential limitation.

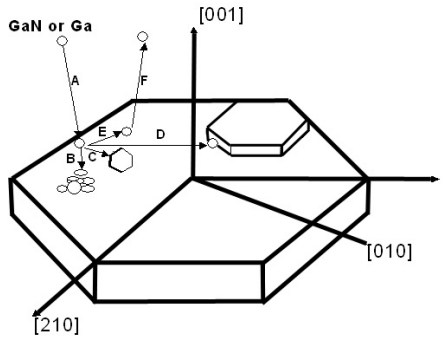


Fig. 2.10 Schematic diagram of vapor-solid (VS) growth model.

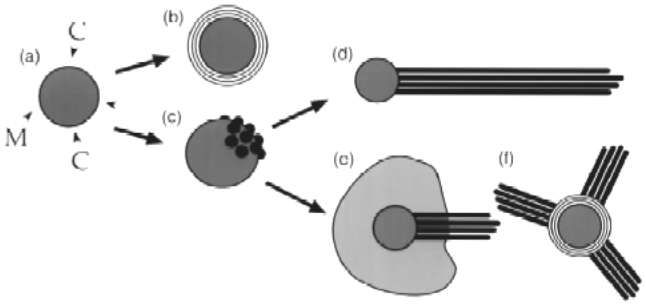


Fig. 2.11 Schematic diagram of VLS growth mechanism for nanotubes.

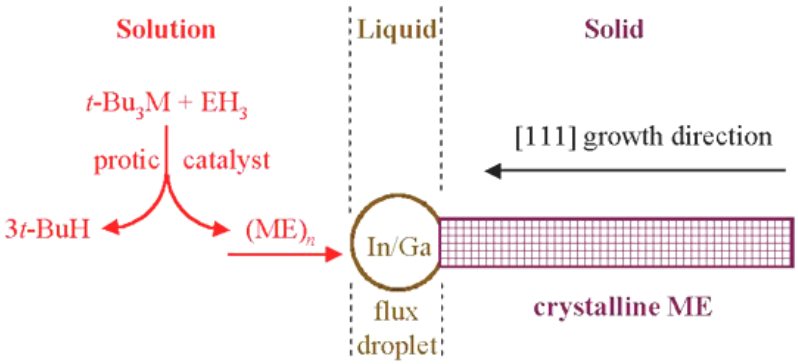


Fig. 2.12 Schematic depiction of SLS growth mechanism.

## 2.4 Field Emission Theory

### 2.4.1 Introduction to Field Emission Theory

The science of field emission began in 1928 [131], when Fowler and Nordheim presented the first quantum mechanical model for describing field induced electron emission from a metallic surface; a model still in use today. In deriving their model, Fowler and Nordheim first assumed that the conduction electrons in the emitting metal are describable as a free-flowing 'electron cloud' - following Fermi-Dirac statistics -and are bound to the metal by an energy barrier at the surface. Under the influence of a field, these conduction electrons can be induced to tunnel through the barrier into vacuum, producing a field-induced electron emission from the metal surface. The presence of the electric field makes the width of the potential barrier finite and therefore permeable to the electrons. This can be seen in Fig. 2.13 which presents a diagram of the electron potential energy at the surface of a metal. Fowler and Nordheim further assumed that the surface barrier can be approximated with a one dimensional energy function without losing significant accuracy.

**Field Emission from Metals**

The dashed line in Figure 2.13 shows the shape of the barrier in the absence of an external electric field. The height of the barrier is equal to the work function of the metal, φ, which is defined as the energy required removing an electron from the Fermi level $E_F$ of the metal to a rest position just outside the material (the vacuum level). The solid line in Figure 2.13 corresponds to the shape of the barrier in the presence of the external electric field. As can be seen, in addition to the barrier becoming triangular in shape, the height of the barrier in the presence of the electric field E is smaller, with the lowering given by [132]

$$\Delta\phi = \left( \frac{eE}{4\pi\varepsilon_0} \right)^{1/2} \tag{1}$$

where e is the elementary charge and $\varepsilon_0$ is the permittivity of vacuum.

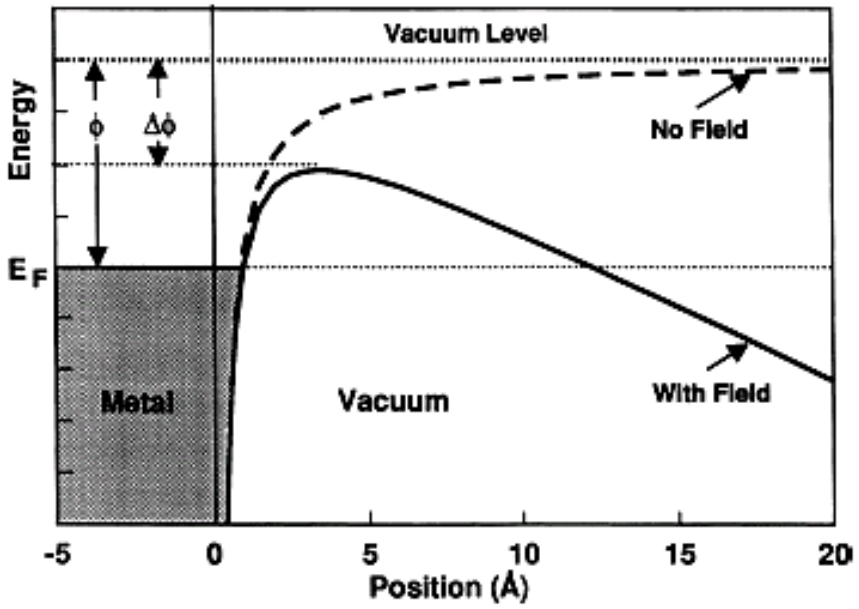


Fig. 2.13 Diagram of potential energy of electrons at the surface of a metal.

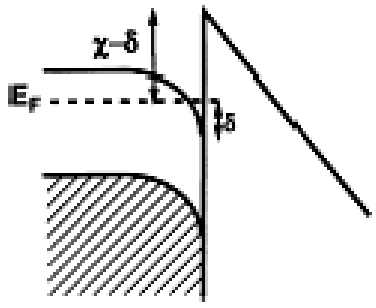


Fig. 2.14 Diagram of the potential energy of electrons at the surface of an n-type semiconductor with field penetrates into the semiconductor interior.

Knowing the shape of the energy barrier, one can calculate the probability of an electron with a given energy tunneling through the barrier. Integrating the probability function multiplied by an electron supply function in the available range of electron energies leads to an expression for the tunneling current density J as a function of the external electric field E. The tunneling current density can be expressed by Eq. (2) which is often referred to as the Fowler-Nordheim equation [131,133]

$$J = \frac{e^3 E^2}{8\pi h \phi t^2(y)} \exp\left[\frac{-8\pi(2m)^{1/2}\phi^{3/2}}{3heE} v(y)\right] \qquad (2)$$

where $y=\Delta\varphi/\varphi$ with $\Delta\varphi$ given by Eq. (1), h is the Planck's constant, m is the electron mass, and t(y) and v(y) are the Nordheim elliptic functions; to the first approximation $t^2(y)= 1.1$ and $v(y) =0.95 - y^2$. Substituting these approximations in Eq. (2), together with Eq. (1) for y and values for the fundamental constants, one obtains

$$J = 1.42\times10^{-6} \frac{E^2}{\phi} \exp\left(\frac{10.4}{\phi^{1/2}}\right) \exp\left(\frac{-6.44\times10^7 \phi^{3/2}}{E}\right) \qquad (3)$$

where J is in units of A $cm^{-2}$, E is in units of V $cm^{-1}$ and φ in units of eV. Plotting log ($J/E^2$) vs. 1/E results in a straight line with the slope proportional to the work function value, φ, to the 3/2 power. Eq. (3) applies strictly to temperature equal to $0^oK$. However, it can be shown that the error involved in the use of the equation for moderate temperatures ($300^oK$) is negligible [134].

**Field Emission From Semiconductors**

To a large degree, the theory for electron emission from semiconductors can be derived parallel to the theory for metals. However, special effects are associated with semiconductors due to the state of their surface and the fact that an external field applied to a semiconductor may penetrate to a significant distance into the interior. For the case when the external electric field penetrates into the interior of an n-type semiconductor and the surface states are neglected, log($J/E^2$) is shown to be a linear function of 1/E [135]. However, in place of the

work function φ in the Fowler-Nordheim equation one needs to substitute a quantity χ-δ, where χ is the electron affinity defined as the energy required for removing an electron from the bottom of the conduction band of the semiconductor to a rest position in the vacuum, and δ denotes the band bending below the Fermi level. These parameters are illustrated in Fig. 2.14. The linear dependence of $\log(J/E^2)$ on 1/E is expected only if the density of the current flowing through the sample is much smaller than the current limiting density $J_{lim} = en\mu_n E/\varepsilon$, where $\mu_n$ is the electron mobility and n is the electron concentration in the bulk of the semiconductor [136,137]. At $J \approx J_{lim}$, the Fowler-Nordheim character of the relationship J(E) passes into the Ohm's law (if the dependence of electron mobility on the electric field is neglected) which results in the appearance of the saturation region in the emission current vs. voltage curve [138]. Such saturation regions were observed experimentally for lightly doped n-type semiconductors and for p-type semiconductors [139,140]. Electron emission from semiconductors has been a subject of more recent theoretical considerations which takes into account complications due to electron scattering, surface state density, temperature, and tip curvature [141-143].

**Local Field Enhancement Factor**

The Fowler-Nordheim equation predicts that a field of $l0^7$ V/cm would be necessary to generate an emission current density of $10^8 A/cm^2$ from a tungsten tip. However, experimental emission data tends to be on the order of ten to one hundred times greater than the predicted emission current density. Schottky postulated that such an enhancement factor would be due to nanostructures on the tip surface. The geometry of these nanostructures concentrates the applied field locally and so they are locations of high electron concentrations. An example of this effect is shown in Figure 2.15(a). If a voltage is applied across two parallel plates separated by vacuum the field lines will concentrate at small structures, commonly nanometer scale structures.


Fig. 2.15 (a) Local Field Enhancement due to nanostructure (b) Model for local field enhancement

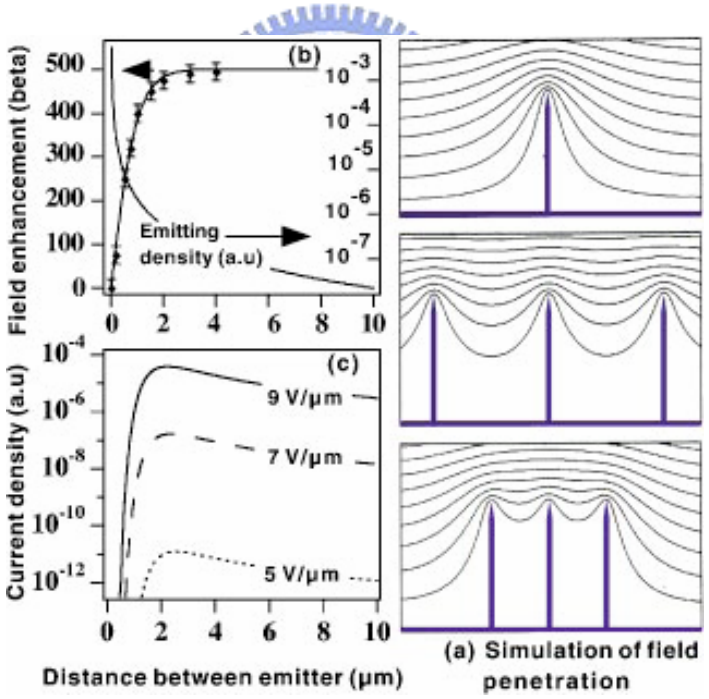


Fig. 2.16 (a)Simulation of the equipotential lines of the electrostatic field for tubes of 1 mm height and 2 nm radius, for distances between tubes of 4, 1, and 0.5 mm; along with the corresponding changes of the field enhancement factor ß and emitter density (b), and current density (c) as a function of the distance.

Consider a model of conductive sphere of charge Q suspended above a flat metal surface. The sphere and the metal surface are connected by a thin conductive path [Fig. 2.15(b)]. The sphere has radius r and the conductive path has length h. An applied field between two opposing parallel plates creates a potential at a distance h from the flat surface of:

$$\varphi = E_Q h = \frac{1}{4\pi\varepsilon_0}\frac{Q}{r} \tag{4}$$

Equating the potentials represents connecting the sphere to the plate, the substitution can be made:

$$E = \frac{\varphi}{r} = \frac{1}{4\pi\varepsilon_0}\frac{Q}{r^2} = \frac{h}{r}E_Q = \beta E_Q = \beta V \tag{5}$$

The apparent enhancement of the applied field is represented by the ß coefficient, which has been dubbed the "local field enhancement factor". The local field enhancement can be considered a product of the nanoscale protrusion from the metal surface. The local field enhancement can be similarly produced by other nanostructures.

To incorporate the local field enhancement factor and the constants into the previous equations, the substitution suggested by equation (5) is made. The simplified Fowler-Nordheim equation becomes:

$$I = J \times \alpha = A \times V^2 \exp\left(-B/V\right) \tag{6}$$

where

$$A = 1.42 \times 10^{-6} \times \alpha \times \beta^2 / \phi \times \exp\left(10.4/\phi^{1/2}\right) \tag{7}$$

$$B = 6.44 \times 10^7 \times \phi^{3/2} / \beta \tag{8}$$

Along with the I-V curve, a "Fowler-Nordheim plot" is generally shown for a material. Its linearity clearly illustrates whether or not the non-linear I-V curve can be represented by field emission. If the field emission data is properly described by the Fowler-Nordheim equation, the plot shows a straight line with a projected y-axis intercept of B and slope of A.

**Screening Effect**

The Fowler-Nordheim equation has predicted the field emission behavior for a film or a single emitter (which also include a single emitter in the gated device). However in normal cases, the field emission current does not achieve the predicted value since nanostructures are usually synthesized with massive units. In fact, for high density films, screening effects reduce the field enhancement and thus the emitted current. For films of medium density, there is an ideal compromise between the emitter density and the inter-emitter distance, which is sufficiently large to avoid screening effects. A better control of density and morphology (and hence of the $\beta$ factors) of the films is thus clearly required for future applications.

In the previous report [144,145], a predicted inter-emitter distance of about 2 times the height of the CNTs optimizes the emitted current per unit area. Simulation of an ideal density of $2.5 \times 10^7$ emitters/$cm^2$, or equivalently to 625 emitters per 50x50 mm2 pixel is obtained.

### 2.4.2 Field Emission Applications of Carbon Nanotube Films

Applications based on an assembly of CNTs films are discussed here. CNTs have been demonstrated to possess remarkable mechanical and electric properties for field emission application [15,48]. A powerful application of electronic emission sources can be expanded to flat panel display such as field emission display (FED). The application of CNTs to FEDs requires their vertical alignment on cathode electrodes for better emission. In FED, electrons coming from millions of tiny emitters pass through gates and excite phosphor to light up pixels on the screen. This principle is similar to that of cathode ray tube (CRT) in television sets [146], as shown in Fig. 2.17. In a CRT electrons from a triad of thermionic emitters are scanned across the phosphor screen with electromagnetic deflection coils. In a FED electrons from an addressable array of cold cathode impinge onto a precisely aligned phosphor anode. Instead of just one gun spraying electrons, there are millions of emitters in FED. Because of the simpler assembly, custom performance and special sizes are less costly to produce. FED technology also offers many advantages including brightness, lightness and speed [146].

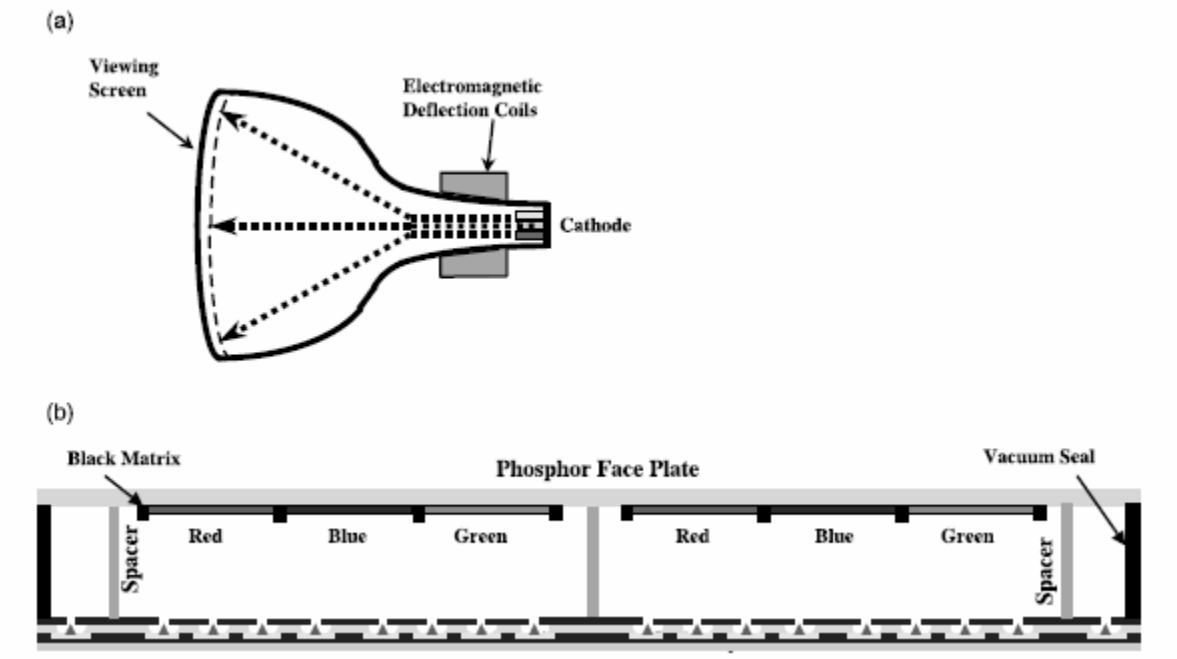


Fig. 2.17. CRTs and FEDs share many common features, including a glass vacuum envelope, and phosphor coated anode, and a cathode electron source [146].

CNT flat panel displays were proposed early on as an desirable alternative to other film emitters [13,15]. The first display with 32 × 32 matrix-addressable pixels in diode configuration has been fabricated using CNTs as the electron emission source by Wang et al. [147]. One demonstration structure constructed at Northwestern University consists of CNT-epoxy stripes on the cathode glass plate and phosphor-coated Indium-Tin-Oxide (ITO) stripes on the anode plate [147]. Pixels are formed at the intersection of cathode and anode stripes, as shown in Fig. 2.18. At a cathode-anode gap distance of 30 μm, 230 V is required to obtain the emission current density necessary to drive the diode display (~ 76 μ mA/mm$^2$). The device is operated using the half-voltage off-pixel scheme. Pulses of ±150 V are switched among anode and cathode stripes, respectively to produce an image.

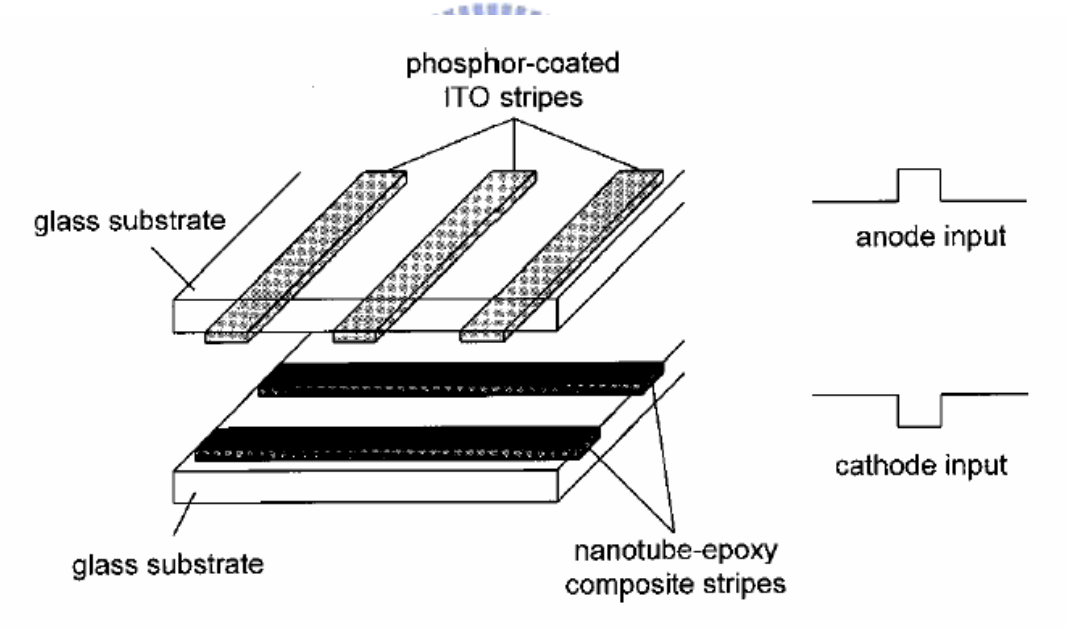


Fig. 2.18. Schematic structure of the matrix-addressed CNT display [147].

Recently, a fully sealed 4.5 inch three color field-emission display was demonstrated by Choi et al. [148,149], with SWCNT stripes on the cathode and phosphor-coated ITO stripes on the anode running orthogonally to the cathode stripes [148]. SWCNTs synthesized by the arc-discharge method were dispersed in isopropyl alcohol and then mixed with an organic

mixture of nitro cellulose. The paste was squeezed into sodalime glasses through a metal mesh, and then heat-treated to remove the organic binder. $Y_2O_2S$:Eu, ZnS:Cu,Al, and ZnS:Ag,Cl, phosphor-coated glass is used as the anode. This display has 128 addressable lines and works in diode configuration, as shown in Fig. 2.19. The emitting image of fully sealed SWCNT-FED at color mode with red, green, and blue phosphor columns. Since then, the Samsung research group has shown a 4.5 inch device displaying full-color images [150] and later a 9 inch full-color display with 576 × 242 pixels [151].

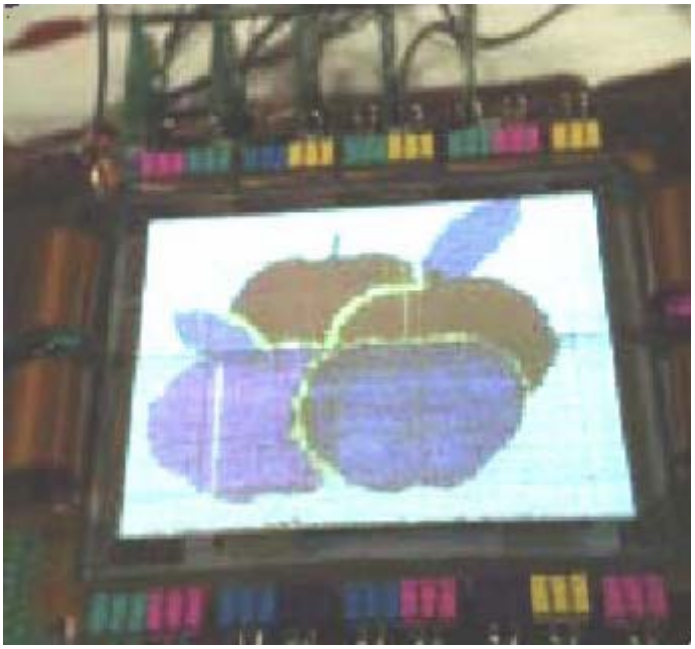

Fig. 2.19. Samsung's 9 inch full-color display [150].

Cathode ray tube (CRT) with CNTs as the field emitters has been developed by Saito et al. and is reportedly commercially available [152]. These CNT-based lighting elements have a triode-type design, and light is produced by bombarding a phosphor-coated surface with electrons. Figure 2.20(a) shows the longitudinal cross-section of a CRT fluorescent display with a FE cathode made of CNTs. The outer diameter and the length of the glass bulb are 20 mm and 74 mm, respectively. Figure 2.20(b) shows photographs of CRT lighting elements

emitting the three primary colors, green, red, and blue. Fluorescent materials are ZnS:Cu, Al for green, $Y_2O_3$:Eu for red, and ZnS:Ag for blue. The anode currents and voltages are 200 mA and 10 kV, respectively [152]. In the early models, cylindrical rods containing MWCNTs, formed as a deposit by the arc-discharge method, were cut into thin disks and were glued to stainless steel plates by silver paste. In later models, CNTs are now screen-printed onto the metal plates. A phosphor screen is printed on the inner surfaces of a glass plate. Different colors are obtained by using different fluorescent materials. The brightness is typically higher by a factor of 2 as compared to conventional thermoionic CRT lighting elements operated under similar conditions and can be used for giant outdoor displays [153]. Lifetimes of 8000 h have been demonstrated with such devices [154]. Moreover, H. Murakami et al. suggests a lifetime of exceeding 10 000 h [119].

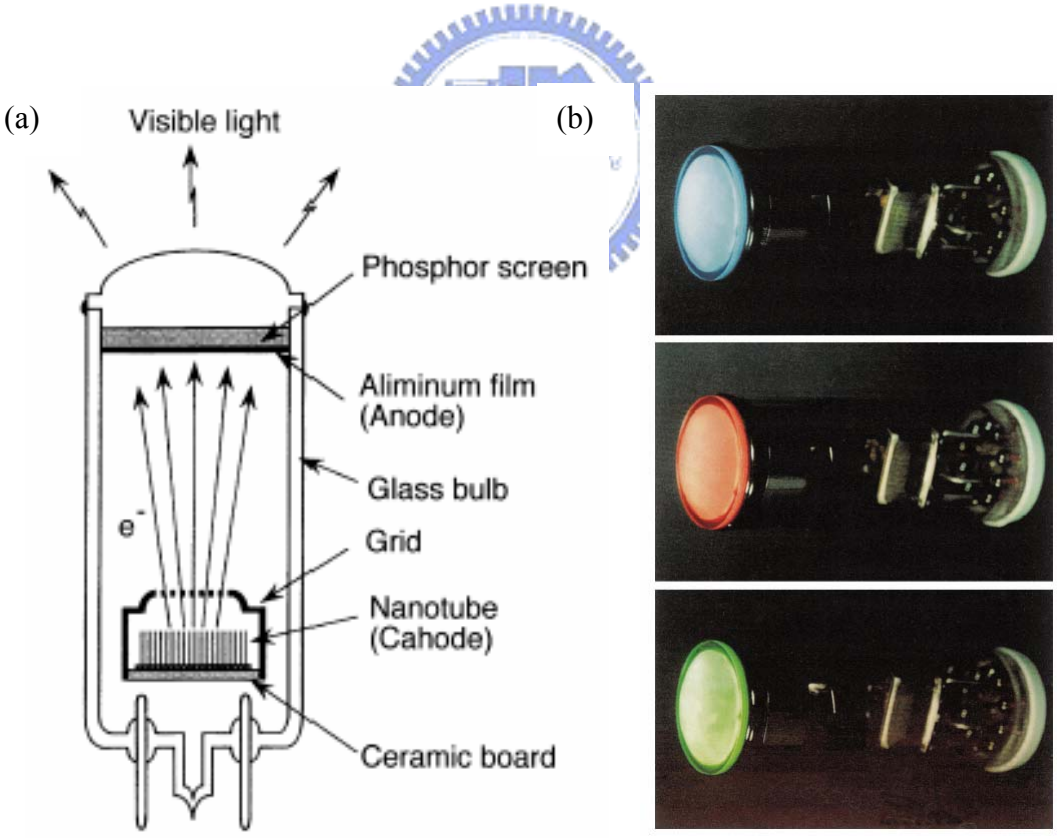


Fig. 2.20. (a) Cross-section of a CRT lighting element with a field emission cathode made of CNTs, and (b) photographs of CRT lighting elements emitting the three primary colors [152].

Field emitters are also of great interest for microwave amplification [155]. This type of application is very demanding because the current density must be at least 0.1 A/cm$^2$. Zhou et al. constructed a prototype based on a SWCNT cathode that is able to reach that lower limit to operate in microwave tubes [156,157].

The same group realized a gas discharge tube (GDT) that serves as an overvoltage protection [158]. GDT protectors, usually consisting of two electrodes parallel to each other in a sealed ceramic case filled with a mixture of noble gases, is one of the oldest methods used to protect against transient over-voltages in a circuit [159]. They are widely used in telecom network interface devices boxes and central office switching gear to provide protection from lightening and ac power cross faults on the telecom network. They are designed to be insulating under normal voltage and current flow. Under large transient voltages, such as from lightning, a discharge is formed between the metal electrodes, creating a plasma breakdown of the noble gases inside the tube. In the plasma state, the gas tube becomes a conductor, essentially short-circuiting the system and thus protecting the electrical components from over-voltage damage. These devices are robust, moderately inexpensive, and have a relatively small shunt capacitance, so they do not limit the bandwidth of high- frequency circuits as much as other nonlinear shunt components. Compared to solid state protectors, GDTs can carry much higher currents. However, the current GDT protector units are unreliable from the standpoint of mean turn-on voltage and run-to-run variability.

Prototype GDT devices using CNT coated electrodes have recently been fabricated and tested by a group from UNC and Raychem Co. [158]. Molybdenum electrodes with various interlayer materials were coated with SWCNTs and analyzed for both electron field emission and discharge properties. Figure 2.21 shows dc breakdown voltage of a GDT with SWCNT/Fe/Mo electrodes, filled with 15 Torr argon with neon added and 1 mm distance between the electrodes. The commercial GDTs are off-the-shell products with unknown filling gases but the same electrode–electrode gap distances. The breakdown voltage of the

GDT with SWCNT/Fe/Mo electrodes is 448.5 V with a standard deviation of 4.8 V over 100 surges. The commercial GDT from manufacturer 1 has a mean breakdown voltage of 594 V and a standard deviation of 20 V. The GDT from manufacturer 2 has a breakdown voltage of 563 V and a standard deviation of 93 V. The breakdown reliability of CNT-based GDTs is a factor of 4-20 better and the breakdown voltage is ~30 % lower than the two commercial products measured. It could be demonstrated that this device shows better performance than commercially available elements.

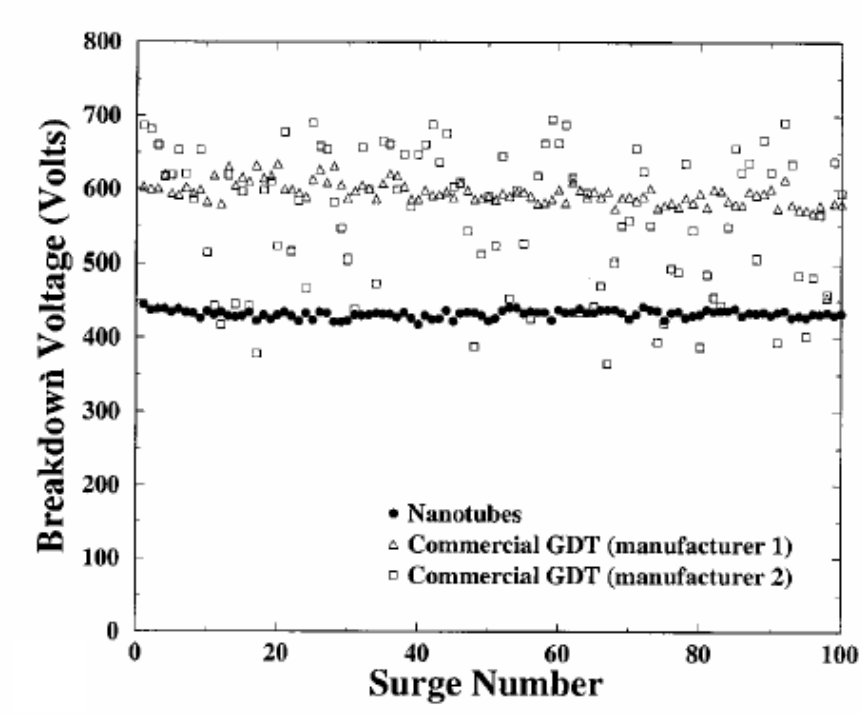


Fig. 2.21. Comparing of dc breakdown voltage of a CNT-based GDT and commercial GDTs [158].

In many field emission applications of CNTs, it is desirable to grow CNTs on cathode with well alignment for the reason of simplifying the process. Many researchers investigated the direct growth alignment CNTs methods which are compatible with current silicon fabrication techniques for electronic application. Kind et al [116] synthesized well-aligned CNTs on Si wafer using microcontact printing of catalysts. However, it is still a challenge to directly

fabricate the CNTs field emission for commercial application. Zhang et al. [160] investigated the fabrication of vertically aligned CNTs patterns by CVD for field emitters.

# Chapter 3 Experimental Instruments

## 3.1 Experimental Instruments

### 3.1.1 Deposition System- MPCVD

Schematic diagram of the MPCVD system is shown in Fig. 3.1. A quartz tube attached vertically to the rectangular wave-guide was used as the deposition chamber. The microwave from a magnetron source (model IMG 2502-S, IDX Tokyo, Japan) was supplied to the quartz tube through an isolator, three-stub tuner, and a power meter. Next, the microwave power was coupled to the quartz tube through an aluminum wave-guide with a hole drilled through a top and bottom face. Aluminum tubes extend out from both holes; the tube extensions are water-cooled as well. A sliding short circuit was then attached at the end of the wave-guide. The lower position of the quartz tube was connected a stainless steel chamber that was equipped with a rotary pump. The substrates were positioned in the middle of the quartz tube waveguide intersection and held vertically by a substrate holder. The substrate holder of 20 mm diameter is made of molybdenum. Under the holder, it was attached to Ta wire which was connected to the bias system; it was used as the lower electrode in the bias treatment stage [161]. A quartz protector under the holder to protect the plasma was not attracted to the Ta wire attached to the Mo. The upper electrode, a Mo disk of 20 mm diameter, was placed 40 mm above the substrate; it was also attached to a Ta wire. The flow rate of the source gases was introduced into the chamber by mass flow controllers (model 647B, MKS instrument, Inc., USA) from the upper end of the quartz tube. An optical pyrometer was used to monitor the temperature of the plasma through a small window on the waveguide.

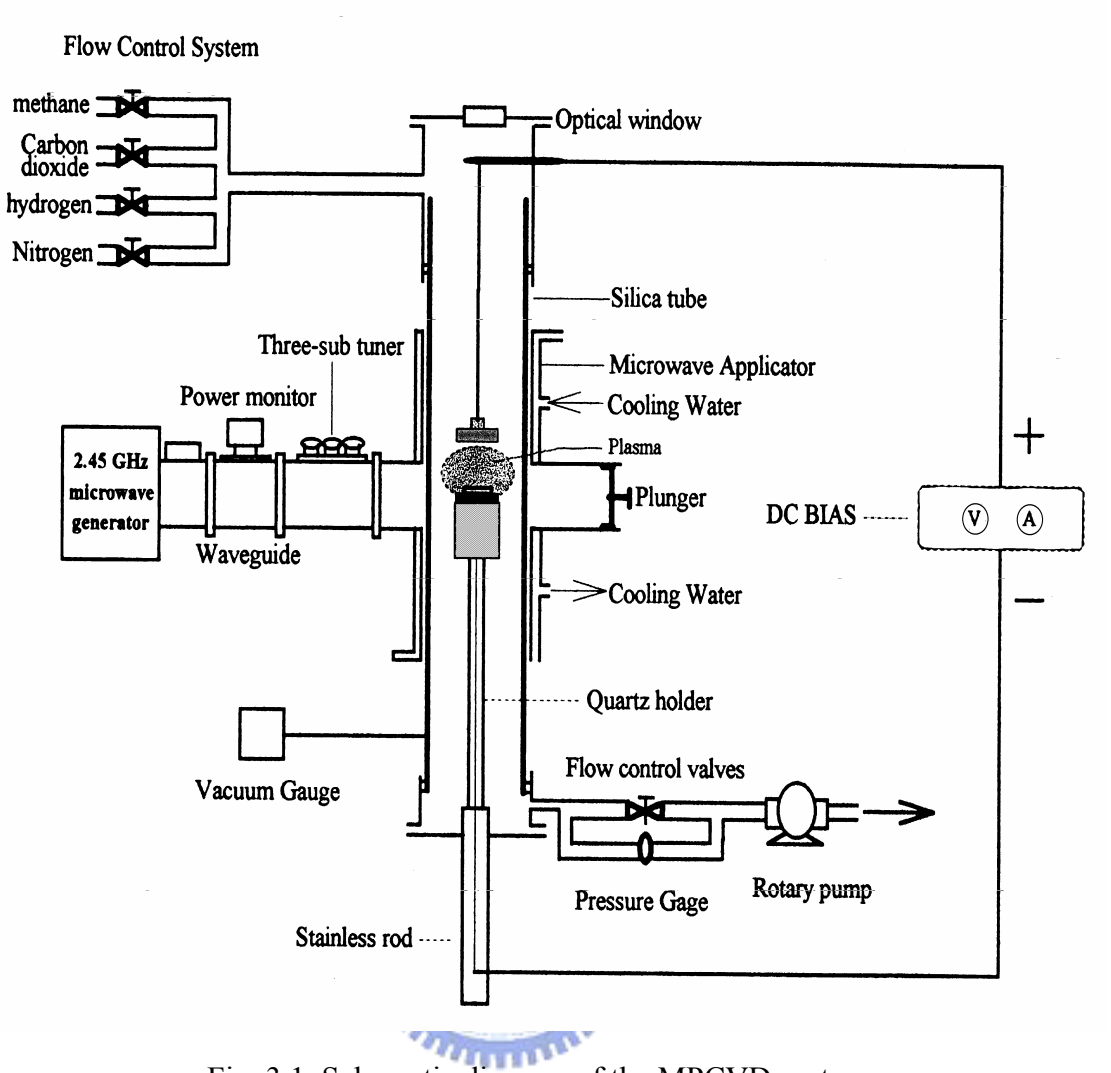


Fig. 3.1. Schematic diagram of the MPCVD system.

### 3.1.2 Deposition System- thermal CVD

A simplified thermal CVD method for synthesizing nanotubes is described here. Figure 3.2 presents the schematic diagram of the thermal CVD method. The proposed method eliminates nearly all of the complex and expensive machinery associated with conventional nanotube growth. This system consists of a heater, three gas flow meters, and a quartz tube used as a reaction vessel. The synthesis apparatus is similar to that used to deposit CVD diamond. However, in order to suit for FED applications, the growth temperature has a limit below 550 ℃ to avoid glass substrate deformation. The reduction step proceeded under $H_2$ and Ar atmospheres, followed by the CNTs growth step under $H_2$, Ar, and acetylene ($C_2H_2$) atmospheres.

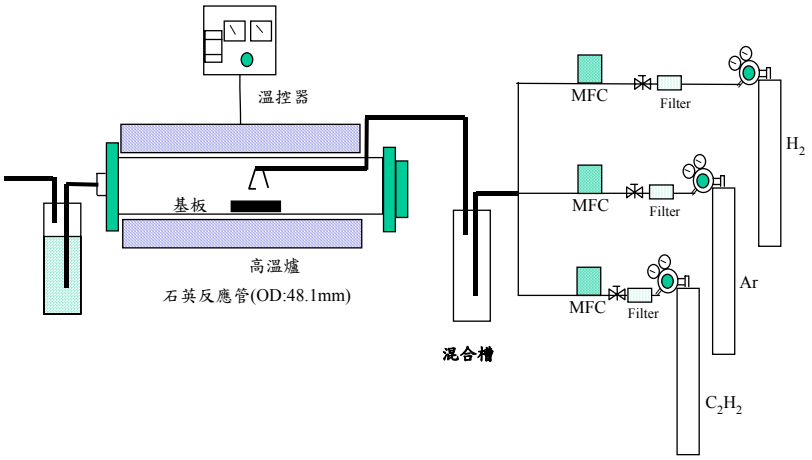


Fig. 3.2. Schematic diagram of the thermal CVD method.

### 3.1.3 Sputtering

Sputtering is a physical process whereby atoms in a solid target material are ejected into the gas phase due to bombardment of the material by energetic ions. It is commonly used for thin-film deposition, as well as analytical techniques. Standard physical sputtering is driven by momentum exchange between the ions and atoms in the material, due to collisions. The process can be thought of as atomic billiards, with the ion striking a large cluster of close-packed atoms (billiard balls). Although the first collision pushes atoms deeper into the cluster, subsequent collisions between the atoms can result in some of the atoms near the surface being ejected away from the cluster. The number of atoms ejected from the surface per incident particle is called the sputter yield and is an important measure of the efficiency of the sputtering process. Other things the sputter yield depends on are the energy of the incident ions, the masses of the ions and target atoms, and the binding energy of atoms in the solid. The ions for the sputtering process are supplied either by a plasma that is induced in the sputtering equipment, or an ion or electron accelerator. In the plasma sputtering devices, a variety of techniques are used to modify the plasma properties, especially ion density, to achieve the optimum sputtering conditions, including usage of RF (radio frequency)

alternating current, utilization of magnetic fields, and application of a bias voltage to the target.

### 3.2 Characterization of Carbon Nanotubes

A scanning electron microscope (SEM) was used to observe the original morphology and distribution of the CNTs. A Renishaw micro-Raman spectroscope was used to characterize the CNTs' quality. Transmission electron microscope (TEM) was used to further characterize CNTs. The I-V measurement was used to analyze the field emission properties of the CNTs.

#### 3.2.1 Optical Microscopy (OM)

The optical microscope is a type of microscope which uses visible light and a system of lenses to magnify images of small samples. Optical microscopes are the oldest and simplest of the microscopes. The optical components of a modern microscope are very complex and for a microscope to work well, the whole optical path has to be very accurately set up and controlled. Despite this, the basic optical principles of a microscope are quite simple. The objective lens is, at its simplest, a very high powered magnifying glass i.e. a lens with a very short focal length. This is brought very close to the specimen being examined so that the light from the specimen comes to a focus about 160 mm inside the microscope tube. This creates an enlarged image of the subject. This image is inverted and can be seen by removing the eyepiece and placing a piece of tracing paper over the end of the tube. By careful focusing a rather dim image of the specimen, much enlarged can be seen. It is this real image that is viewed by the eyepiece lens that provides further enlargement. In most microscopes, the eyepiece is a compound lens, which is made of two lenses one near the front and one near the back of the eyepiece tube forming an air separated couplet. In many designs, the virtual image comes to a focus between the two lenses of the eyepiece, the first lens bringing the real image to a focus and the second lens enabling the eye to focus on the now virtual image. In all

microscopes the image is viewed with the eyes focused at infinity. Headaches and tired eyes after using a microscope are usually signs that the eye is being forced to focus at a close distance rather than at infinity.

### 3.2.2 Scanning Electron Microscopy (SEM)

Scanning electron microscopy is used to observe the surface morphology of wide range kinds of objects. It has the advantage of rather easy sample preparation, high image resolution, large depth of field and high magnification. A common SEM contains an electron gun to generate electron beams, which will be accelerated under 0.4-40kV voltage. By deflecting the incident beams with the focusing coils, a two dimensional image can be obtained by detect the reflected secondary electrons and the backscatter electrons. The model we use here is JEOL 6500, with field emission electron source and 15kV accelerate voltage.

### 3.2.3 Micro-Raman Spectroscopy

Raman spectroscopy is an excellent technique for characterization of the CNTs. When photons illuminate a molecule or a crystal, they react with the atoms accompany with momentum change or energy exchange. Collecting the scatter photons, one can obtain a sequence of spectrum, including Raman scattering (Inelastic scattering) and Reyleigh scattering (Elastic scattering). The photon of Raman scattering can be classified into Stoke side and anti-Stoke side. Generally, Stoke side, which photons loss energy or the molecules gains energy, is used to characterize the material.

In this study, the CNTs' quality was analyzed by a Renishaw micro-Raman spectroscope (Model 2000). The laser light with the power of 200 mW was reflected by a half-mirror, and focused on to the sample with an objective lens. The spectral slit width is $0.4cm^{-1}$.

### 3.2.4 High Resolution Transmission Electron Microscopy (HRTEM)

In this study, HRTEM (Tecnai 20, Philips) was used to further characterize CNTs. One of the typical characters of CNTs is their small size. Although some structural features can be revealed by x-ray and neutron diffraction, direct imaging of the CNTs is only possible using TEM. TEM is unique because it can provide a real space image on the atom distribution in the nano-crystal and on its surface. With a finely focused electron probe, the structural characteristic of a single CNT can be fully characterized. Besides, the energy dispersive X-ray spectroscopy (EDX) attached on TEM system was used to characterize the chemical components of catalyst particles in the CNTs.

### 3.2.5 I-V Measurement

Field emission properties are obtained using a diode structure. As shown in Fig. 3.3, an anode, made of indium tin oxide glass (ITO glass), was separated by 150 μm from the tip of a cathode made of CNTs. The I-V properties were measured using an electrometer (Keithley SMU 237) in a vacuum of $1\times10^{-6}$ Torr and analyzed using the Fowler-Nordheim (F-N) model. The anode-to-cathode voltage was varied from 0 to 1100 V. The turn-on and threshold field, defined respectively for 10 $\mu A/cm^2$ and 10 $mA/cm^2$, have been used as the merit parameters to distinguish various emitter materials [2].

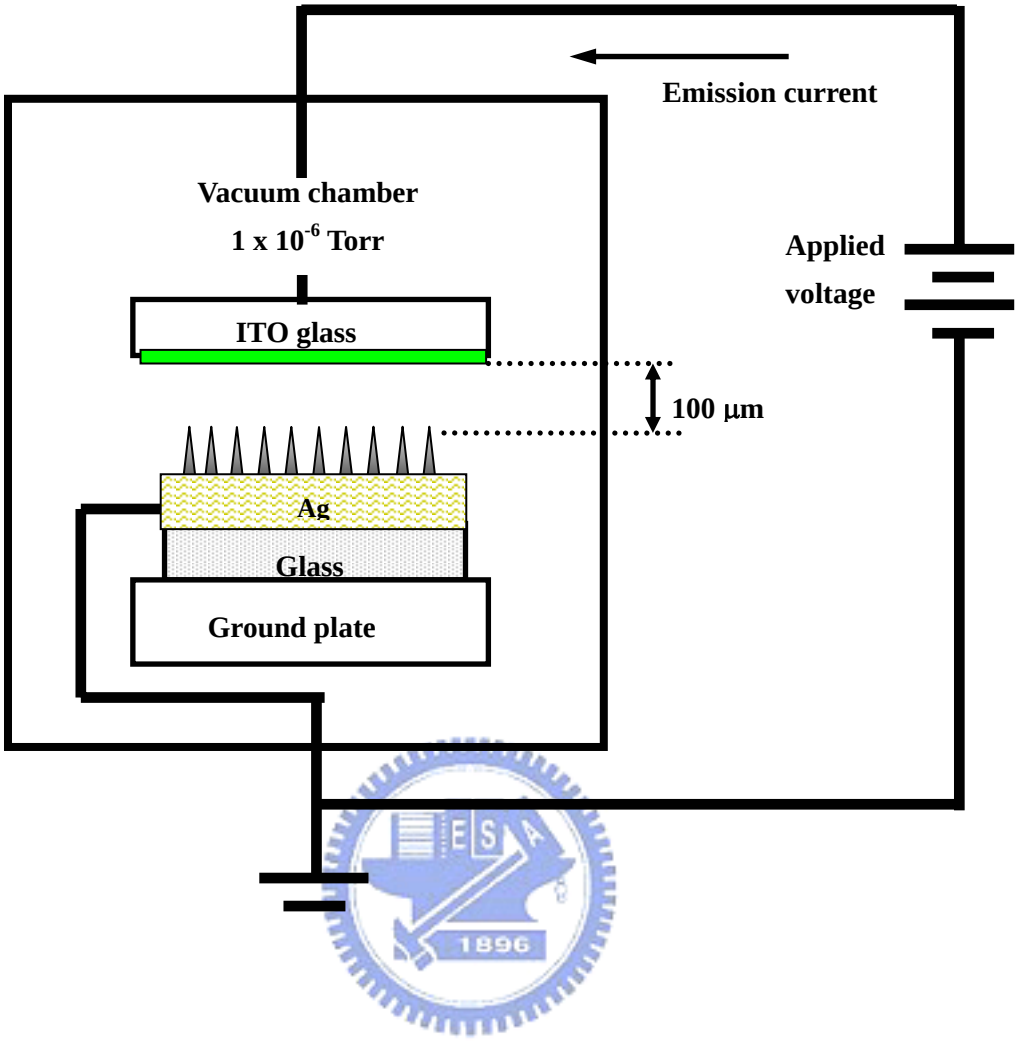


Fig. 3.3. Schematic diagram of the I-V measurement.

# Chapter 4 Results and Discussion

## 4.1 The growth of carbon nanotubes on patterned catalyst-Ni of cathode by MPCVD: catalyst preparation by solution deposition method

### 4.1.1 Introduction

Carbon nanotubes (CNTs) were first discovered by Iijima in 1991 under observation of transmission electron microscopy (TEM) [1]. Owing to the unique aspect ratios, CNTs exhibit excellent field emission characteristics. High mechanical strength and high chemical stability are also the advantages of CNTs for field emitters [18-21]. Numerous methods to grow CNTs have been developed, including arc-discharge, chemical vapor deposition and pulsed laser ablation [22-24]. Among various methods, both arc-discharge [25] and CVD [26] were usually reported to be used for field emission display. A low cost process combining arc-discharge produced CNTs and screen-printing technologies was developed to prepare field emitters on glass substrate [27]. Unfortunately, using CNTs paste by screen-printing technology has a relatively low resolution and needs a surface rubbing technology or other activated steps to enhance field emission characteristics [27].

For CVD process, it can directly grow on the predefined catalyst layer and has high yield and uniformity. Many researchers have succeeded in synthesizing CNTs on Si substrate at a relatively high temperature by various CVD methods [28]. In order to suit for FED applications, the growth temperature has a limit below 550℃ to avoid glass substrate deformation. Recently, the study of direct growth CNTs at low temperature on glass substrates by CVD method has been reported [29-31]. However, in previous works, it is required to deposit patterned catalyst metal on cathode electrode on glass substrate by semiconductor processes, such as sputtering or thermal evaporating etc. As we know, the cost increase of the semiconductor processes is many times larger than screen-printing processes. Therefore, development of the direct growth CNTs on glass substrates at low temperature by a low cost

technology will play an important role in practical FED applications.

In this work, we combined the advantages of screen printing process and MPCVD process to pattern catalyst/Ag cathode by screen printing technology and grew CNTs on patterned Ni-catalyst of cathode electrode on glass substrate at low temperature. A novel way can be applied to coat catalyst-Ni with Ag powders in solution phase by solution deposition method.

### 4.1.2 Experimental procedures

#### 4.1.2.1 Catalyst preparation by solution deposition method

For preparing the catalysts, the silver (Ag) powders were dispersed in the water and then the ammonia ($NH_3$) solution was added at 100℃ for 30 min. Next, $Ni(NO_3)_2 \cdot 6H_2O$ was added in the solution, and $NH_3$ solution also added in for maintaining pH value at 10.5 at 100℃ for 3 hr. The formaldehyde (HCHO) was added to make the nickel (Ni) ions deposit on Ag powders by heating at 100℃ for 30 min. Then the Ni /Ag powders were washed by DI water and dried at 110℃. The catalyst fabrication process is illustrated in Fig. 4.1.

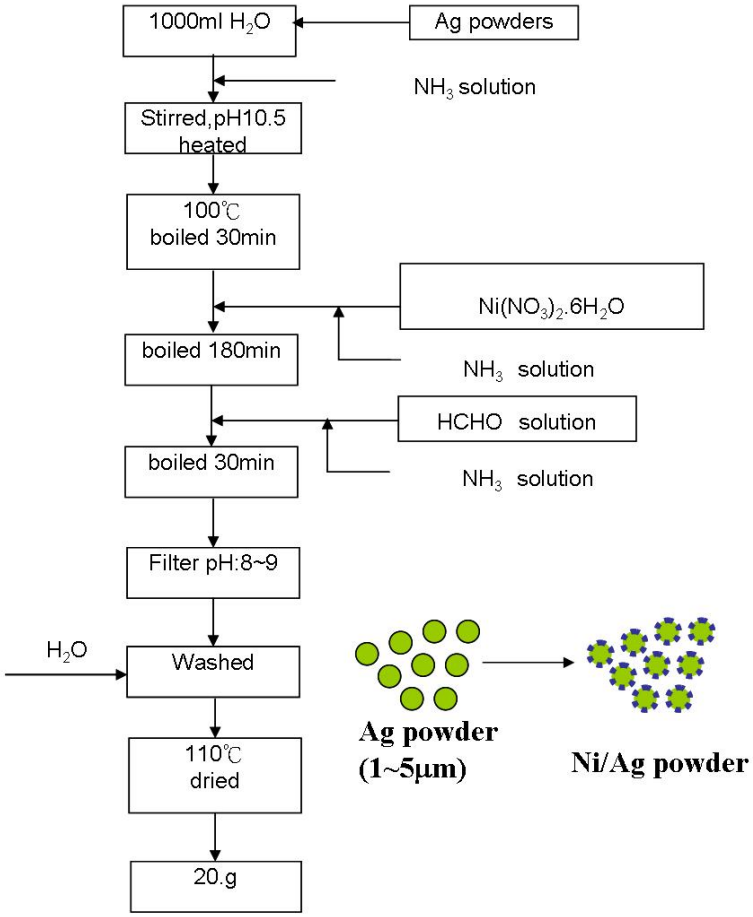


Fig. 4.1. A schematic illustration of the catalyst fabrication processes.

### 4.1.2.2 Samples preparation by screen printing

Dried Ni/Ag powders were then well-mixed with frit and organic vehicles by using ball mill and three-roller mill to make a printable paste (Fig. 4.2). The Ni/Ag paste was coated on the soda-lime glass substrate by screen-printing technology. After printing the Ag film was dried at 200℃ for 1 hr and heated at 400℃ for 2 hr to remove the organic materials in the paste, then the film was sintered at 560℃ for 10 min.

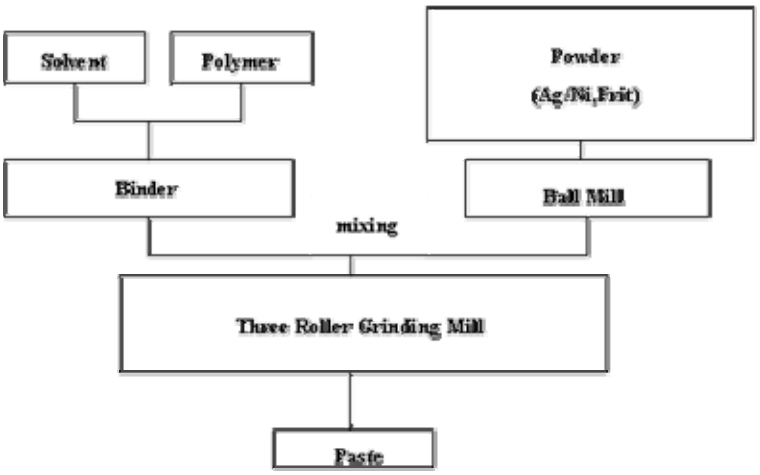


Fig. 4.2. The Procedure of Paste fabricating.

#### 4.1.2.3 Carbon nanotubes grow by MPCVD

The sample was placed in a MPCVD (model IMG 2502-S, IDX Tokyo, Japan) chamber and evacuated at $10^{-2}$ Torr with a mechanical pump. The Ag/Ni film was pretreated by hydrogen ($H_2$) plasma for 5 min at microwave power 150W to prepare Ni nanoparticles. The flow rate and the total pressure for the pretreatment were 200 sccm and 6 Torr, respectively. And then the CNTs were grown using gas mixtures of methane ($CH_4$) and $H_2$ under the total pressure of 6 Torr. In order to verify the samples, several parameters were used, including methane concentration, growth time, flow rate of reactive gas and the power of MPCVD.

### 4.1.3 Results and discussion

#### 4.1.3.1 Effect of MPCVD power

The MPCVD power were raised from 150 W to 200 W for growing excellent quality of carbon nanotubes. Undoubtedly, the plasma temperature also increased from about 530 ℃ to about 625 ℃ measured by IR thermocouple. However, the sample was damaged and bent by heat at about 625 ℃ for 30 min when the MPCVD power over 200 W. In order to suit for

FED applications, the growth temperature has a limit below 550℃ to avoid glass substrate deformation. Therefore, in this work we controlled the MPCVD powder at 150W.

#### 4.1.3.2 Effect of hydrogen plasma pretreatment

The thickness of Ni/Ag electrode film on glass substrate is about 20 $\mu$m, as shown in Fig. 4.3. The film was coated by screen printing technology and commonly used for practical FEDs and PDPs applications. The surface morphology of catalyst-Ni on Ag film before and after hydrogen plasma activating treatment is shown in Fig. 4.4a and 4.4b, respectively. $H_2$ flow rate was 200 sccm, microwave power was 150 W, and treatment time was 5 min. It was found that Ni nanoparticles were not formed before hydrogen treating. It is well known that such a smooth surface without catalytic seed nanoparticles is not suitable for CNTs growing (Fig. 4.4a). After being treated for 5 min with hydrogen plasma, the Ni nanoparticles of 30-60 nm were formed (Fig. 4.4b). The Ni nanoparticles were not so uniform because the nanoparticles were not formed simultaneously and particles formed earlier were etched away by the hydrogen plasma activating.

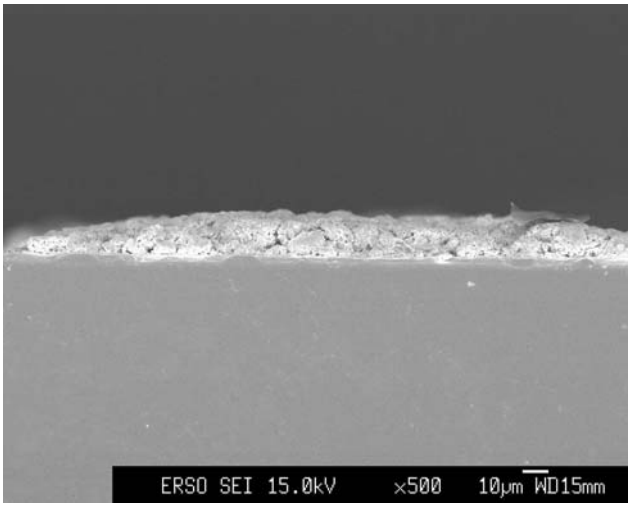


Fig. 4.3. SEM cross-section image of the Ag electrode film on glass substrate.

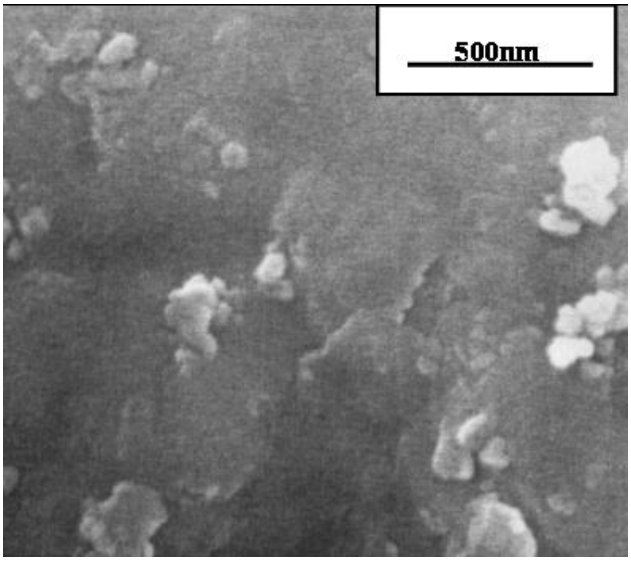


(a)

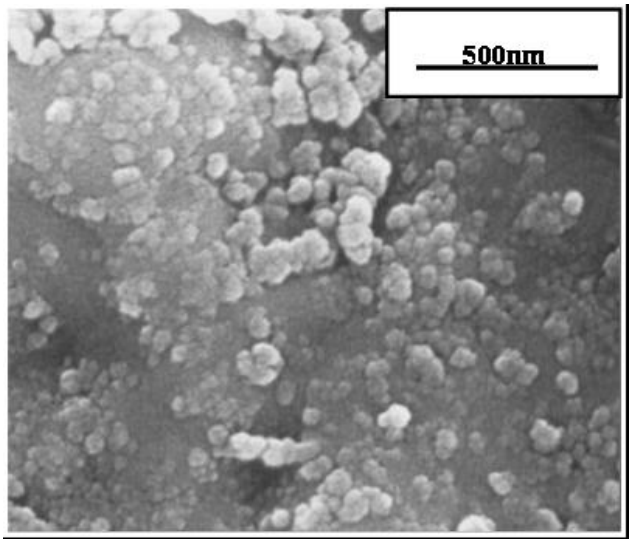


(b)

Fig. 4.4. SEM images of surface morphologies of catalyst-Ni on Ag film, (a) before, and (b) after hydrogen plasma activating treatment.

#### 4.1.3.3 Effect of methane concentration

Fig. 4.5a, 4.5b and 4.5c show the SEM images of CNTs grown at total pressure 6 Torr with a $CH_4$ flow rate of 10 sccm, and $H_2$ flow rate of 40, 20,10 sccm. The growth time was kept constant at 30 min. The microwave power was 150 W and the temperature was below 550℃. The temperature depends on the soda-lime glass substrates without bending. CNTs were grown uniformly on the substrates. However, lengths of CNTs increased with a decreasing $H_2$

flow rate due to the decrease of the etch rate of CNTs by hydrogen plasma with a decreasing $H_2$ flow rate. In these images, the $H_2$ flow rate of 10 sccm grown CNTs shows clean and longer tubes, as shows in Fig. 4.5c and 4.5d. The CNTs synthesized in this study seemed to be curly and suggested CNTs to be highly defective. This is expected that the growth temperature is below 550℃, which is relatively lower than in other researches using such as arc discharge or CVD methods. At low temperature, carbon atoms synthesized at the edge of the tubes do not have enough driving force and time to diffuse, and thus formed defective edges with pentagons and heptagons which would eventually induce the curvature of nanotubes. Many researchers reported that the lower growth temperature is, the more curved CNTs are [31,117].

The diameters of CNTs were ranged from 30 to 50 nm. As shown in Fig. 4.5d, Ni catalytic nanoparticles were observed at the ends of the tubes, which were reported in other studies [108,117]. We suppose that it is a tip growth mechanism. In this growth mechanism, Ni catalytic metals play an important role for the nanotube growth. Carbon-containing gas was decomposed into carbon atoms under plasma pyrolysis process and reacted with Ni catalytic metals. The carbon atoms diffused around the metal particles, and precipitated at the side of particles. As the process proceeded, the CNTs were formed and lifted up the metal from the substrate. It has been proposed that the surface melting point of nanoparticles can be as low as 40% of the bulk melting point by the surface curvature effect [163,164]. In addition, Ni nanoparticle could form a eutectic mixture with carbon and/or hydrogen, which can also reduce the melting point. According to both mechanisms described above, the melting point of Ni can be effectively reduced from 1450℃ and CNT synthesis temperature is as low as 550℃ in our system. It promoted the growth of the CNTs at low temperature. Carbon atoms were nucleated on the metal particles, and carbon-metal eutectic alloys were immediately formed. Then carbon atoms diffused in the metal particles, aggregated and formed CNTs. As the process proceeded, the metal was given rise to tip of the tube.

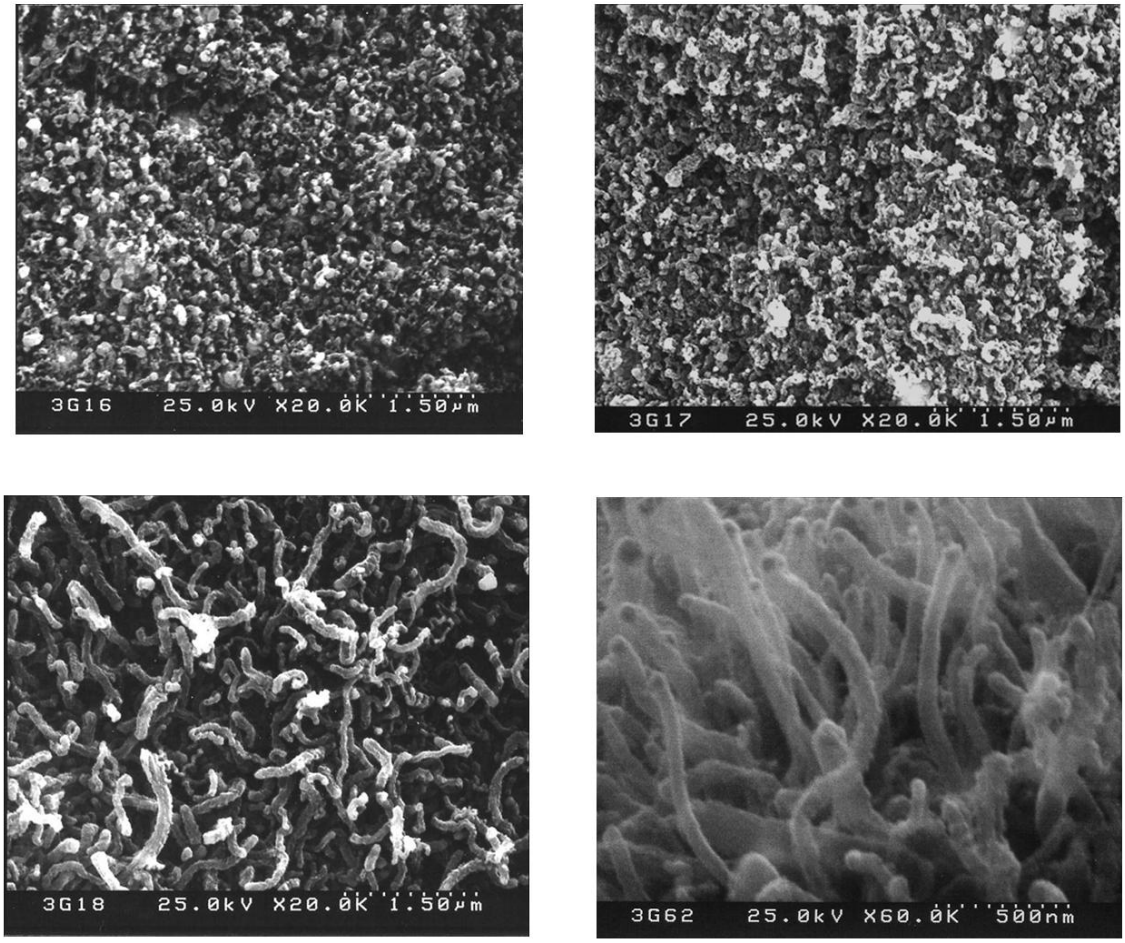


Fig. 4.5. SEM images of surface morphologies of CNTs grown at total pressure 6 Torr with a $CH_4$ flow rate of 10 sccm and $H_2$ flow rate of (a) 40 sccm, (b) 20 sccm, and (c) 10 sccm. (d) shows the higher-magnification image of Fig. 4c.

#### 4.1.3.4 TEM and Reman analysis

A TEM image of the CNTs produced from the sample, as shown in Fig. 4.6a. The multiwall carbon nanotubes (MWNT) of herringbone-like type structure were observed. The diameter of MWNTs was in range of 40-50 nm. The tip of CNTs were closed and encapsulated with catalytic nanoparticles. From the EDX analysis of TEM, the catalytic nanoparticle at the tip of the CNT was Ni indeed, indicating that Ni was suitable as a catalytic metal for CNTs growth at low temperature not Ag. It was also observed that the CNTs were not straight and the crystalline graphite layers were not as good as those of grown at high temperature [165]. The

defective graphitic sheets were resulted from the low growth temperature. Besides CNTs, a few of carbon nanofibers were also produced, as shown in Fig. 4.6b. It was observed the formation of amorphous carbons obviously. The diameter of nanofibers was about 60-70 nm. In previous studies, many researchers reported that the synthesis of carbon nanotubes accompanied production of carbon nanofibers at low temperature [30,166].

Carbon nanotubes were also characterized by Reman spectroscopy [167]. Only two peaks were observed in Reman spectrum of CNTs growth with a $CH_4$ flow rate of 10 sccm and $H_2$ flow rate of 10 sccm for 30 min, as shown in Fig. 4.7. The spectrum shows two strong peaks clearly at points: 1360 and 1590 $cm^{-1}$, respectively. Peak at 1360$cm^{-1}$ is related to disorder of graphite structure. This spectrum peak indicates that amorphous carbons exist at the wall of CNTs. The other spectrum peak at 1590 $cm^{-1}$ corresponding to the high frequency $E_{2g}$ first-order mode of graphite structure [168] indicated the formation of graphitized carbon nanotubes. The CNTs with higher disordered graphite structure was detected by a peak at 1360 $cm^{-1}$ with respect to that at 1590 $cm^{-1}$. This means that amorphous carbons adhered at CNT walls, a small amount of carbon nanofibers produced, and defective pentagon and heptagon structure in the graphitized walls exist due to low growth temperature [167,169].

Fig. 4.8 shows the Raman data of the multiwall carbon nanotubes were grown using gas mixtures of methane ($CH_4$) and $H_2$ by MPCVD. The $I_D/I_G$ ratio decreased with increasing methan concentration. The results implied the amounts of amorphous carbonaceous by product adhered to wall and defective structure in multiwall layer decreased.

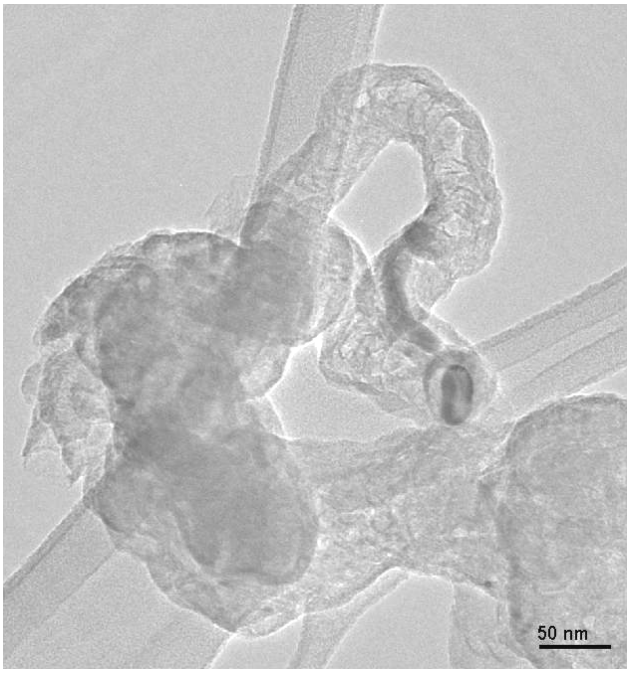


(a)

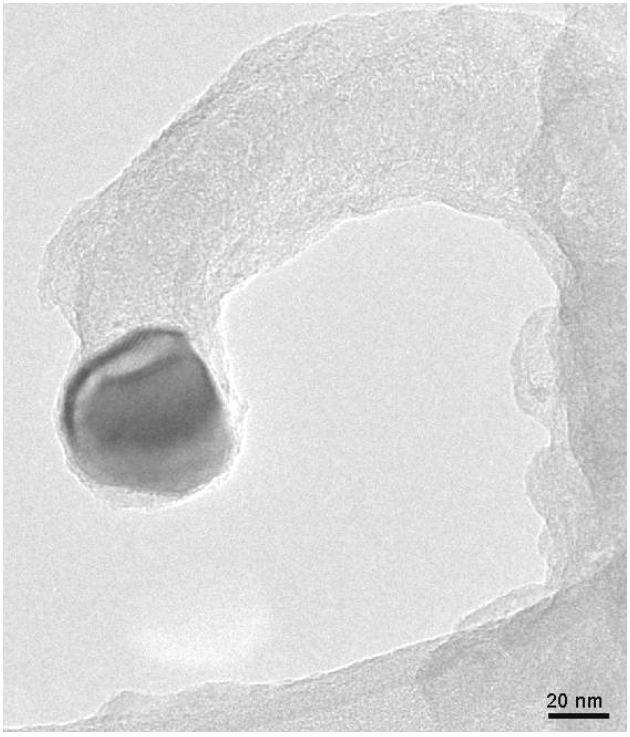


(b)

Fig. 4.6. TEM image of the sample: (a) herringbone-like carbon nanotube (b) carbon nanofiber. The samples were grown at total pressure 6 Torr with a $CH_4$ flow rate of 10 sccm and $H_2$ flow rate of 10 sccm for 30 min.

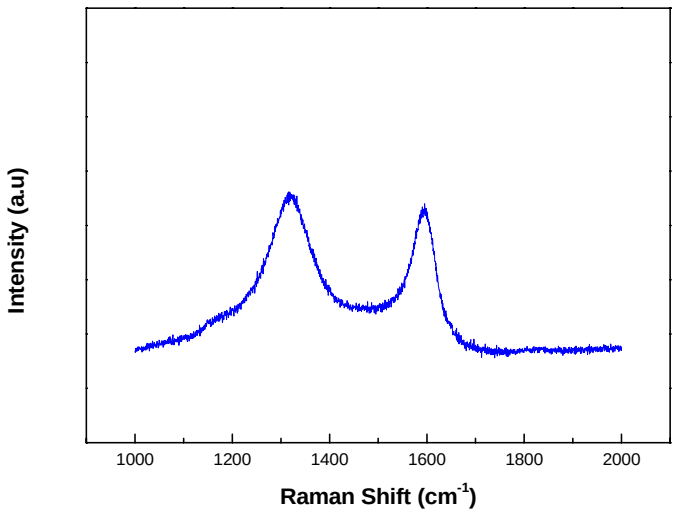


Fig. 4.7. Raman spectrum at the surface of the as-grown sample.

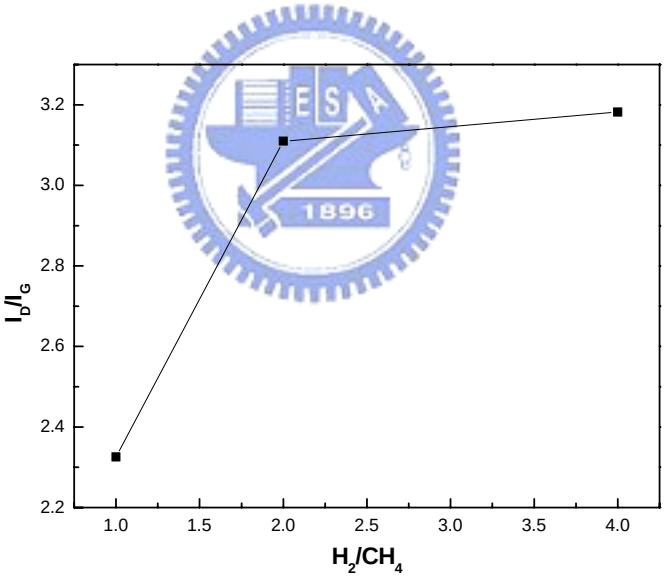


Fig. 4.8. $I_D/I_G$ ratio varied with $H_2/CH_4$ ration at the power of 150 W and the pressure of 6 Torr for 30 min.

### 4.1.3.5 Field emission properties

Fig. 4.9 shows the emission current density vs. electric field curve and the corresponding F-N plots. The CNTs were grown at total pressure 6 Torr with a $CH_4$ flow rate of 10 sccm and $H_2$ flow rate of 10 sccm for 30 min. A turn on field was defined as the field to give an

emission current density of 10 $\mu$A/cm$^2$. The turn on field value at this case was 3.2 V/$\mu$m. The turn on field value of growth non-aligned MWNTs is well agreed by earlier reports [2,167]. An inserted diagram shows the Fowler-Nordheim plot. If ln (I/E$^2$) vs.1/E in the F-N plot were a straight line, this indicated that field electron emission was intrinsically driven by electric field. However, the ln (I/E$^2$) vs.1/E which is exhibits a line in the intermediate range but shows saturation at higher fields in agreement with many other works [119,170]. Actually, the current density of 0.1mA/cm$^2$ is known to be sufficient for practical displays operating. A parallel-plate configuration is shown in Fig. 3.3. The anode is a glass substrate with an indium-tin-oxide film (ITO) and green phosphor film. The thickness of spacers is 100 $\mu$m. The diode structure field emission at applied field 10 V/$\mu$m produced sufficient brightness, as shows in Fig. 4.10. The bright square area is 0.25 cm$^2$.

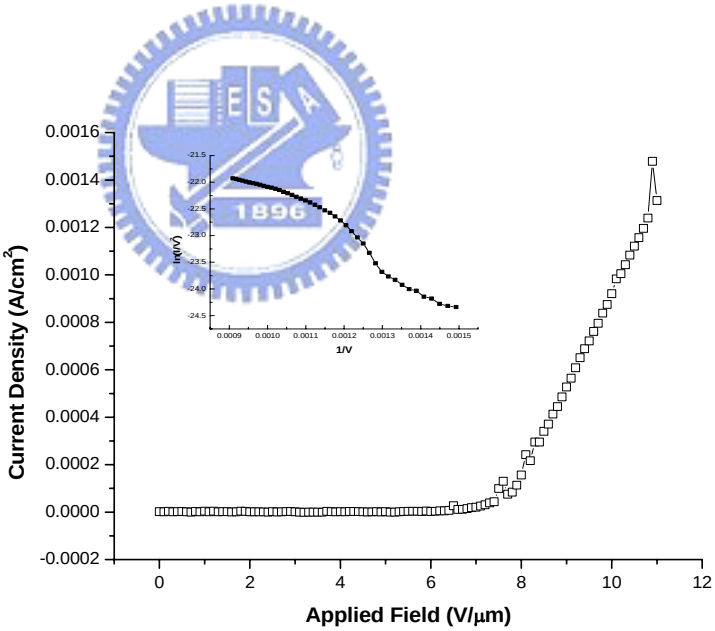


Fig. 4.9. Emission current density vs. electric field curve. Insert is Fowler-Nordheim plot.

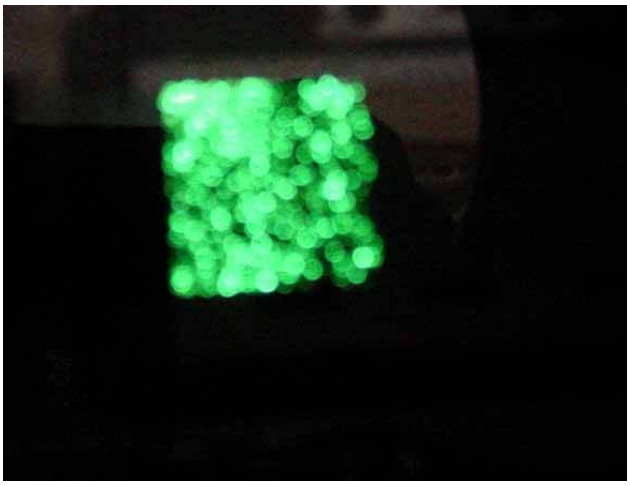

Fig. 4.10. Emission image at applied field 10 V/μm

#### 4.1.3.6 Summary

We successfully combined the advantages of screen printing process and MPCVD process to pattern catalyst/Ag cathode by screen printing technology and grow CNTs on patterned Ni-catalyst of cathode electrode on glass substrates below 550℃. A novel way can be applied to coat catalyst-Ni with Ag powders in solution phase by solution deposition method. Carbon nanotubes can be grown at total pressure 6 Torr with a $CH_4$ flow rate of 10 sccm and $H_2$ flow rate of 10 sccm for 30 min. Both herringbone-like type structure multiwall carbon nanotubes (MWNT) and nanofibers were observed. The tip of CNTs were closed and encapsulated with Ni catalytic nanoparticles. The turn on field value at this case was 3.2 V/$\mu$m. Uniform electron emission was also observed on the electrode with good emission current and brightness.

### 4.2 The growth of carbon nanotubes on patterned catalyst-Ni of cathode by MPCVD: catalyst preparation by sol-gel method

#### 4.2.1 Introduction

Carbon nanotubes (CNTs) were first discovered by Iijima in 1991 under observation of

transmission electron microscopy (TEM) [1]. Owing to the unique aspect ratios, CNTs exhibit excellent field emission characteristics. High mechanical strength and high chemical stability are also the advantages of CNTs for field emitters [18-21]. Numerous methods to grow CNTs have been developed, including arc-discharge, chemical vapor deposition and pulsed laser ablation [22-24]. Among various methods, both arc-discharge [25] and CVD [26] were usually reported to be used for field emission display. A low cost process combining arc-discharge produced CNTs and screen-printing technologies was developed to prepare field emitters on glass substrate [27]. Unfortunately, using CNTs paste by screen-printing technology has a relatively low resolution and needs a surface rubbing technology or other activated steps to enhance field emission characteristics [27].

For CVD process, it can directly grow on the predefined catalyst layer and has high yield and uniformity. Many researchers have succeeded in synthesizing CNTs on Si substrate at a relatively high temperature by various CVD methods [28]. In order to suit for FED applications, the growth temperature has a limit below 550℃ to avoid glass substrate deformation. Recently, the study of direct growth CNTs at low temperature on glass substrates by CVD method has been reported [29-31]. However, in previous works, it is required to deposit patterned catalyst metal on cathode electrode on glass substrate by semiconductor processes, such as sputtering or thermal evaporating etc. As we know, the cost increase of the semiconductor processes is many times larger than screen-printing processes. Therefore, development of the direct growth CNTs on glass substrates at low temperature by a low cost technology will play an important role in practical FED applications.

In this work, we combined the advantages of screen printing process and MPCVD process to pattern catalyst/Ag cathode by screen printing technology and grew CNTs on patterned Ni-catalyst of cathode electrode on glass substrate at low temperature. A novel way can be applied to coat catalyst-Ni with Ag powders in solution phase by sol-gel method.

### 4.2.2 Experimental procedures

#### 4.2.2.1 Catalyst preparation by sol-gel Method

For preparing the catalysts, two solutions were prepared individually and then well-mixed. The first solution was 100 ml anhydrous alcohol (Ethyl alcohol) with 29g $Ni(NO_3)_2 \cdot 6H_2O$, while the second solution was made by mixing 50 ml TEOS and 50 ml anhydrous alcohol. Next, the above two solutions were mixed to be Ni/TEOS alcohol solution under stirring for 24 hr. The Ni/TEOS alcohol solution was then well-mixed with conductive Ag powders, frit ,and organic vehicles by using ball mill and three-roller mill to make a printable paste. Then the Ag paste was printed on the soda-lime glass substrate as a cathode. After printing the Ag electrode, we removed organic solvents at 400℃ for 2 hr and sintered frit at 560℃ for 15 min. The catalyst and sample fabrication process is illustrated in Fig. 4.11.

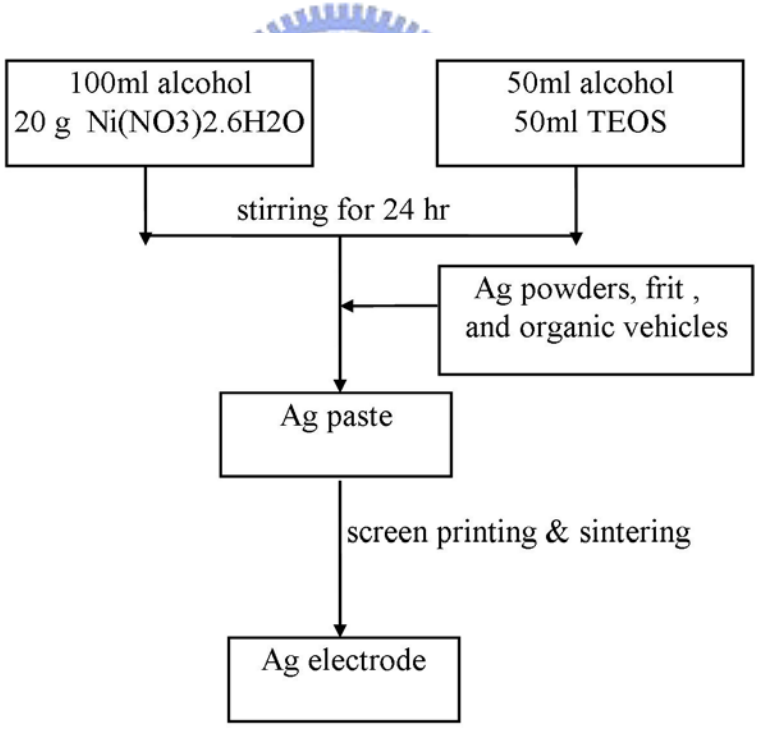


Fig. 4.11. A schematic illustration of the catalyst and sample fabrication processes.

#### 4.2.2.3 Carbon nanotubes grow by MPCVD

The sample was placed in a MPCVD (model IMG 2502-S, IDX Tokyo, Japan) chamber and

evacuated at $10^{-2}$ Torr with a mechanical pump. The Ag/Ni film was pretreated by hydrogen ($H_2$) plasma for 5 min at microwave power 150W to prepare Ni nanoparticles. The flow rate and the total pressure for the pretreatment were 200 sccm and 6 Torr, respectively. And then the CNTs were grown using gas mixtures of methane ($CH_4$) and $H_2$ under the total pressure of 6 Torr. In order to verify the samples, several parameters were used, including methane concentration, growth time, flow rate of reactive gas and the power of MPCVD.

### 4.2.3 Results and discussion

#### 4.2.3.1 Effect of hydrogen plasma pretreatment

The thickness of Ni/Ag electrode film on glass substrate is about 10 $\mu$m, as shown in Fig. 4.12. The film was coated by screen printing technology and commonly used for practical FEDs and PDPs applications. The surface morphology of catalyst-Ni on Ag film before and after hydrogen plasma activating treatment is shown in Fig. 4.13a and 4.13b, respectively. $H_2$ flow rate was 200 sccm, microwave power was 150 W, and treatment time was 5 min. It was found that Ni nanoparticles were not formed before hydrogen treating. It is well known that such a smooth surface without catalytic seed nanoparticles is not suitable for CNTs growing (Fig. 4.13a). After being treated for 5 min with hydrogen plasma, the Ni nanoparticles of ~40 nm were formed (Fig. 4.13b). The Ni nanoparticles were uniform to suit for CNTs growing.

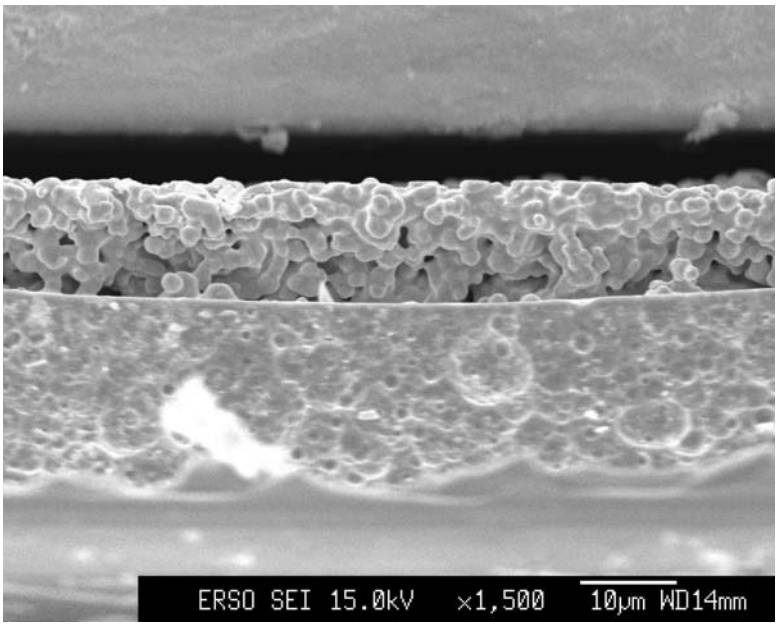


Fig. 4.12. SEM cross-section image of the Ag electrode film on glass substrate.

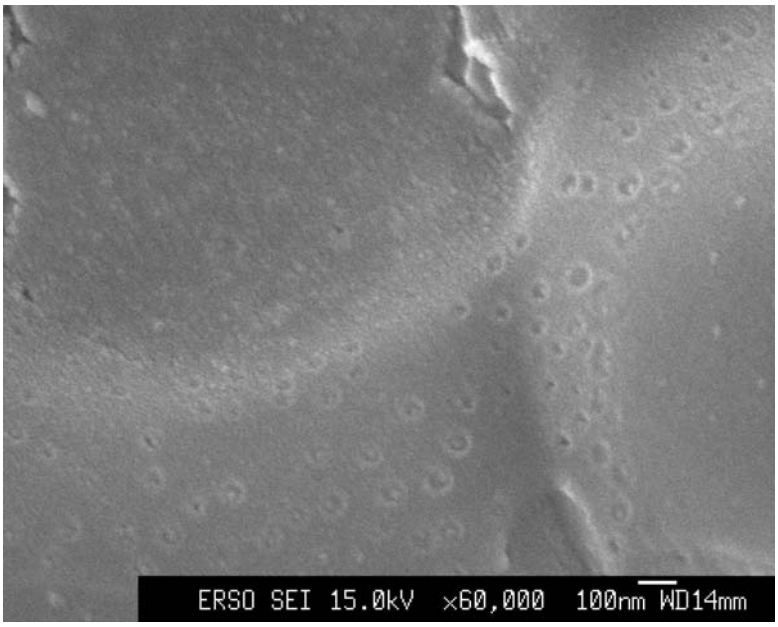


(a)

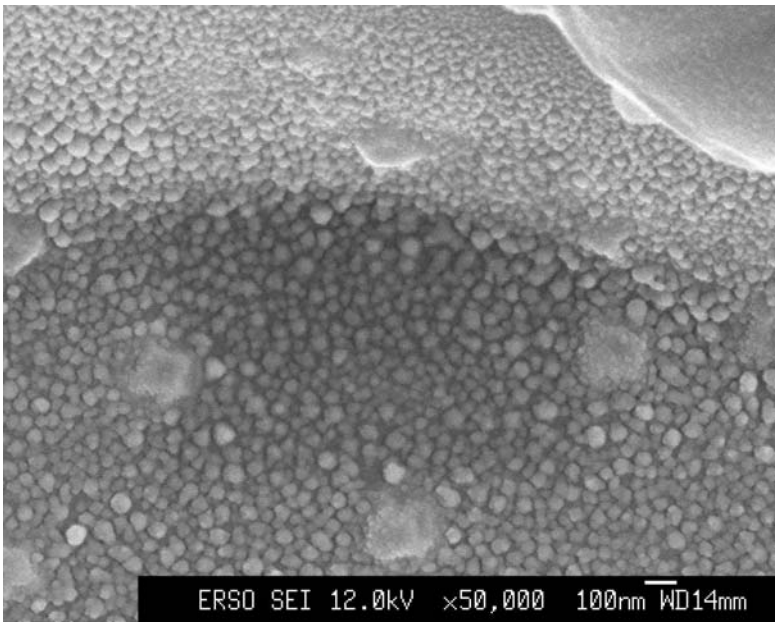


(b)

Fig. 4.13. SEM images of surface morphologies of catalyst-Ni on Ag film, (a) before, and (b) after hydrogen plasma activating treatment.

#### 4.2.3.2 Effect of methane concentration

Fig. 4.14 shows t the SEM images of CNTs grown at total pressure 6 Torr with a $CH_4$ flow rate of 10 sccm, and $H_2$ flow rate of 40, 20,10 sccm. The growth time was kept constant at 30 min. The microwave power was 200 W. The power depends on the soda-lime glass substrates without bending. As the concentration of carbon source increase, the diameter and the length also increases in our experiments. Carbon nanotubes were uniformly grown on a large area with high density.

In Fig. 4.15, it showed the Raman data. The $I_D/I_G$ ratio decreased with increasing methan concentration. It implied the amorphous carbonaceous adhered to the wall and defective structure in multiwall layer decreased.

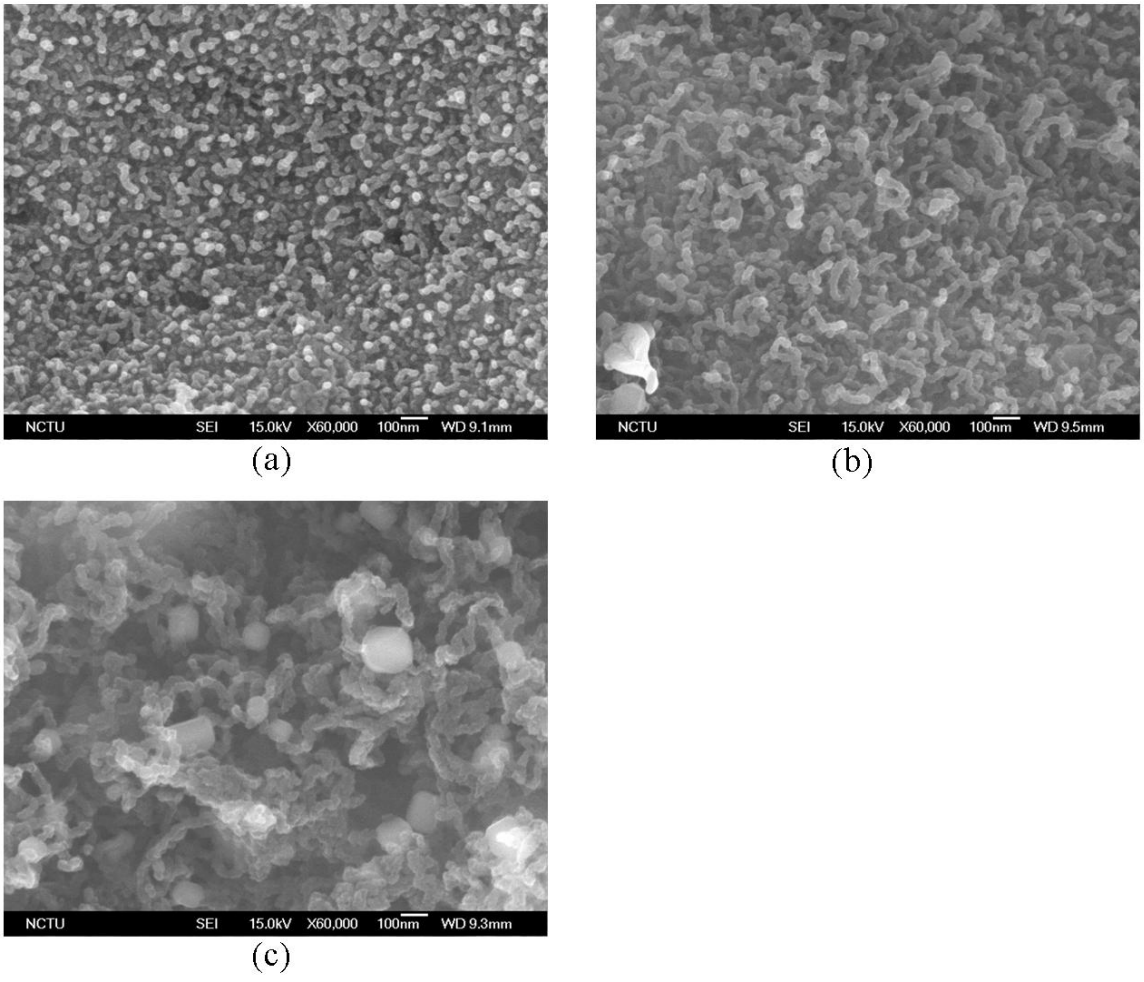


Fig. 4.14. SEM images of surface morphologies of CNTs grown at total pressure 6 Torr with a $CH_4$ flow rate of 10 sccm and $H_2$ flow rate of (a) 40 sccm, (b) 20 sccm, and (c) 10 sccm at 200 W for 30 min.

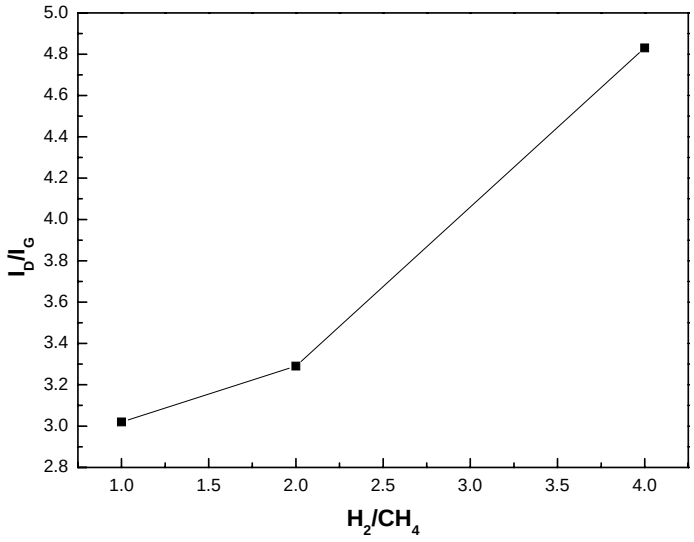


Fig. 4.15. $I_D/I_G$ ratio varies with $H_2/CH_4$ ration at the power of 200 W and the pressure of 6 Torr for 30 min.

#### 4.2.3.3 Effect of growth time of carbon nanotubes

Fig. 4.16 shows the SEM image of surface morphologies of the CNTs grown at the power of 150 W (555 ℃) for different growth time with $H_2$-$CH_4$ gases. The growth time were 15 min, 30 min, 45 min, and 60 min, respectively. Randomly oriented CNTs have grown on cathode at any growth time. The diameter and length of CNTs increased with increasing the growth time. The diameter of CNTs was from the rage of about 20 nm for 15 min to about 70 nm for 60 min. The tubes showed curved structures. Most of the tubes had a bright dot at the tip, indicating electron reflection from metal particles. Two growth modes, tip growth and base growth, have been identified for the catalytic growth mechanism of carbon filaments. In this work, the growth of CNTs was found to be the tip growth type.

In Fig. 4.17, it shows the SEM images of different growth time of the CNTs at the power of 200 W and the pressure of 6 Torr. Unlike the samples fabrication by solution deposition method, the samples were not bendind or damaging under the power of 200 W (about 620 ℃). The reason was catalyst metal particles prepared by sol-gel method, which were covered with

surfactant, might be more stable at higher temperature, allowing high temperature MWNT growth [171]. As the growth time increased, the CNT became larger from the range of about 20 nm for 15 min to about 80 nm for 60 min.

Fig. 4.18 showes the $I_D/I_G$ ratio of Raman spectrum under the power of 150 W and 200 W, respectively. The $I_D/I_G$ ratio decrease as increasing the growth time at 150 W. The same result also shows at 200 W. The $I_D/I_G$ ratio curve slants toward down, indicating a better graphitization as growth increasing.

Compared Fig. 4.16 and Fig. 4.17, as MPCVD power increasing, the diameter and length of CNTs obviously increase from the SEM observation. In Fig. 4.18, the $I_D/I_G$ ratio decreased as power increased from 150 W to 200 W under the same growth time. It implied that the defective structure containing amorphous carbonaceous particles were effectively removed by plasma during growth at higher temperature.

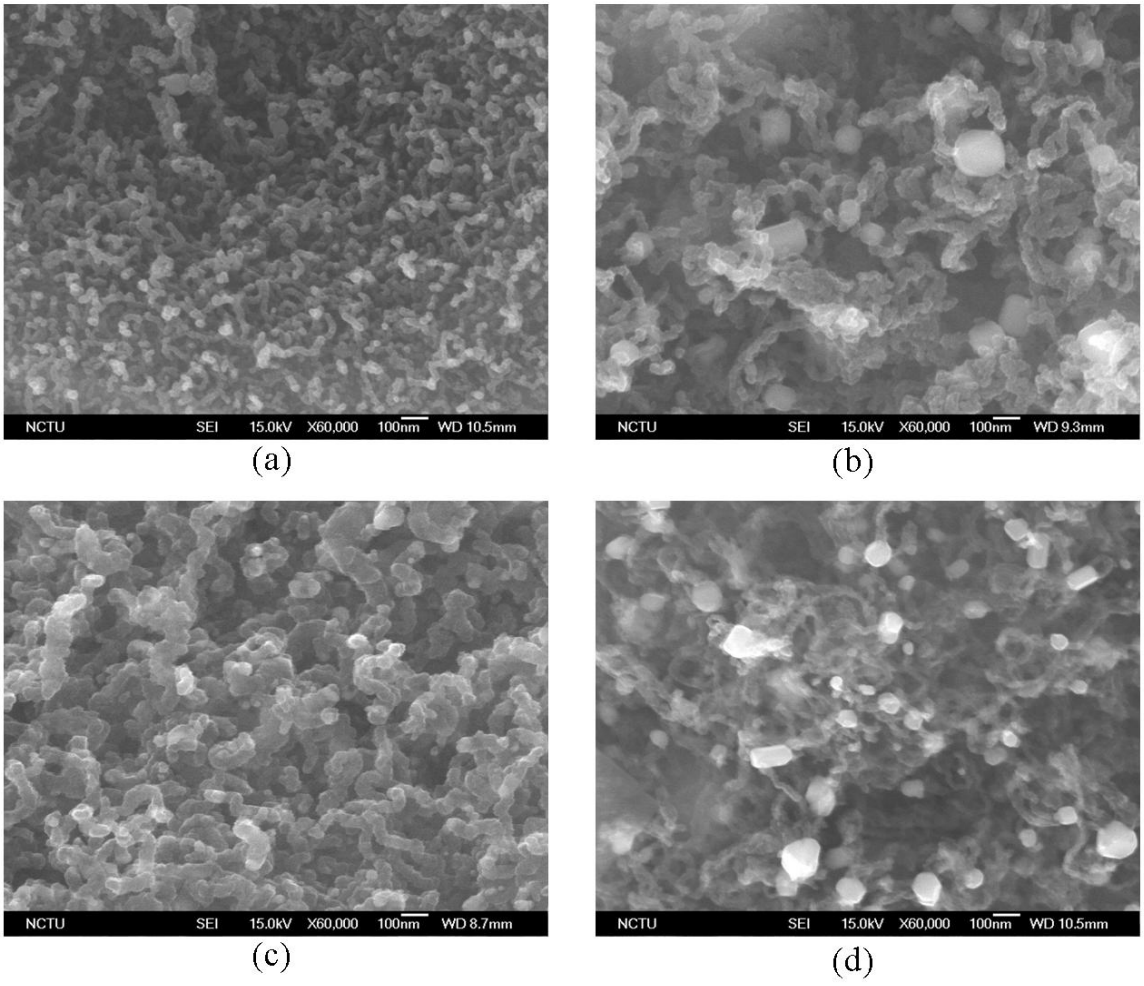


Fig. 4.16. SEM images of surface morphologies of the CNTs grown under the condition of $H_2/CH_4$=10/10 at the power of 150 W and the pressure of 6 Torr: (a) for 15 min, (b) 30 min, (c) 45 min, and (d) 60 min.

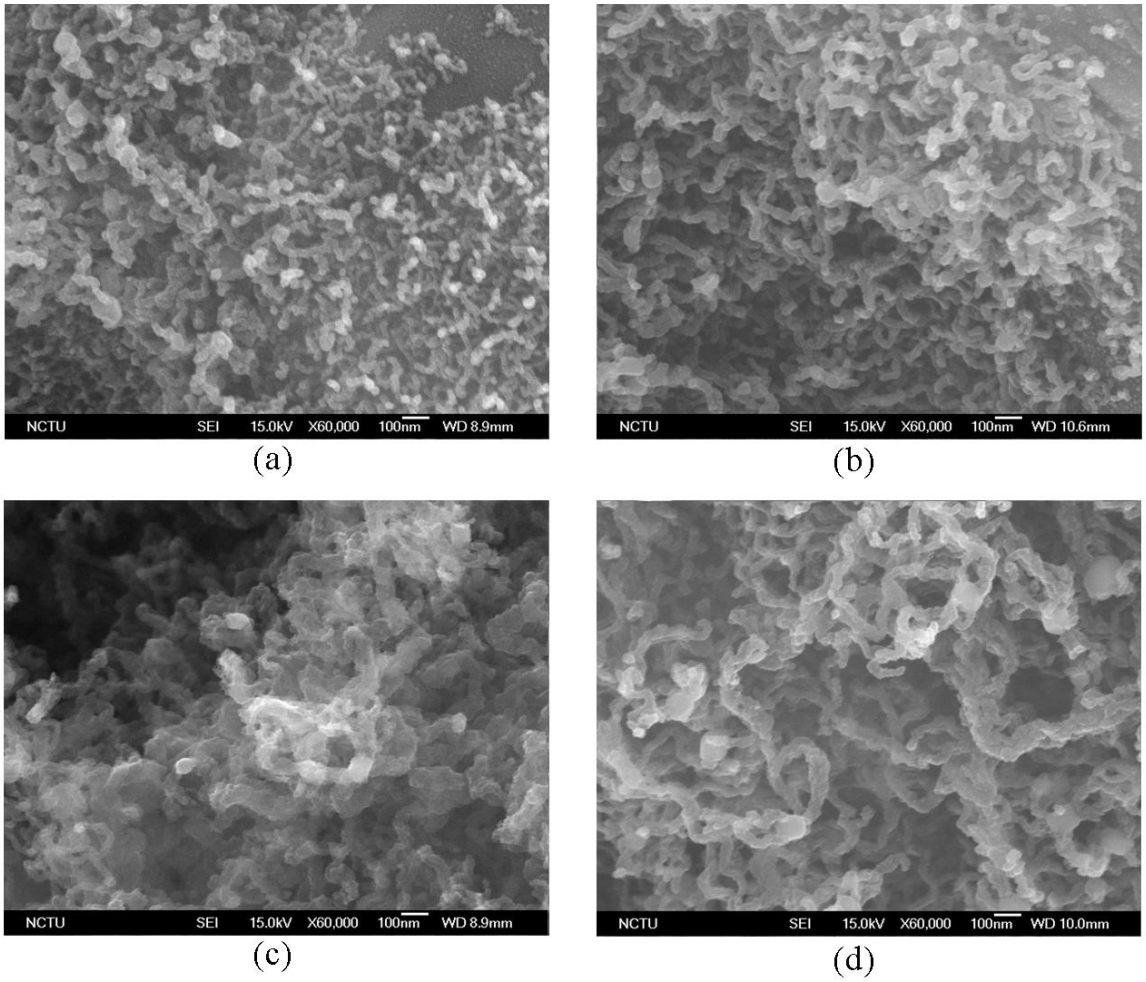


Fig 4.17. SEM images of surface under the growth condition of $H_2/CH_4$=10/10 at the power of 200 W and the pressure of 6 Torr: (a) for 15 min, (b) for 30 min, (c) for 45 min, and (d) for 60 min.

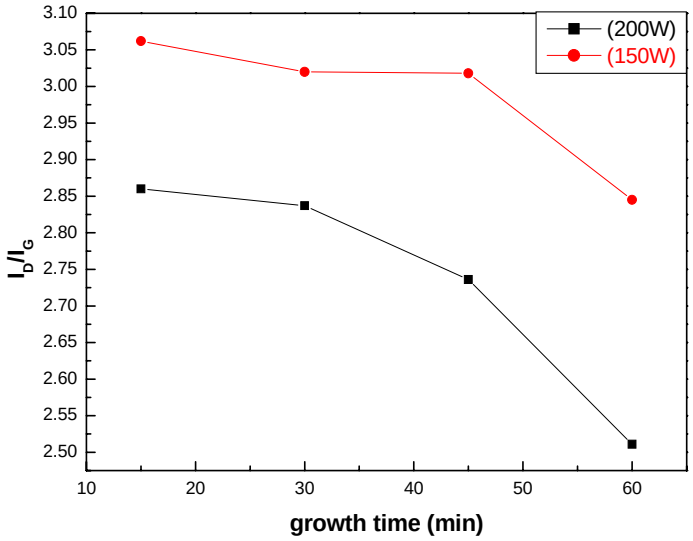


Fig. 4.18. $I_D/I_G$ ratio varied with different growth time of $H_2/CH_4$=10/10 at the power of 150W and 200 W.

### 4.2.4 TEM analysis of carbon nanotubes

Fig. 4.19 showed the TEM image of CNTs grown on the cathode prepared by sol-gel method under the power of 200 W for 60 min. The herringbone-like strucrure MWNTs were observed. The diameter of MWNTs was in the range of 50-100 nm. The tip of CNTs were closed and encapsulated with catalytic nanoparticles. From the EDX analysis of TEM, the catalytic nanoparticle at the tip of the CNT was Ni indeed, indicating that Ni was suitable as a catalytic metal for CNTs growth at low temperature not Ag. It was also observed that the CNTs were not straight and the crystalline graphite layers were not as good as those of grown at high temperature [165]. The defective graphitic sheets were resulted from the low growth temperature. It seems that the defective pentagons and heptagons induce the curvature of nanotubes.

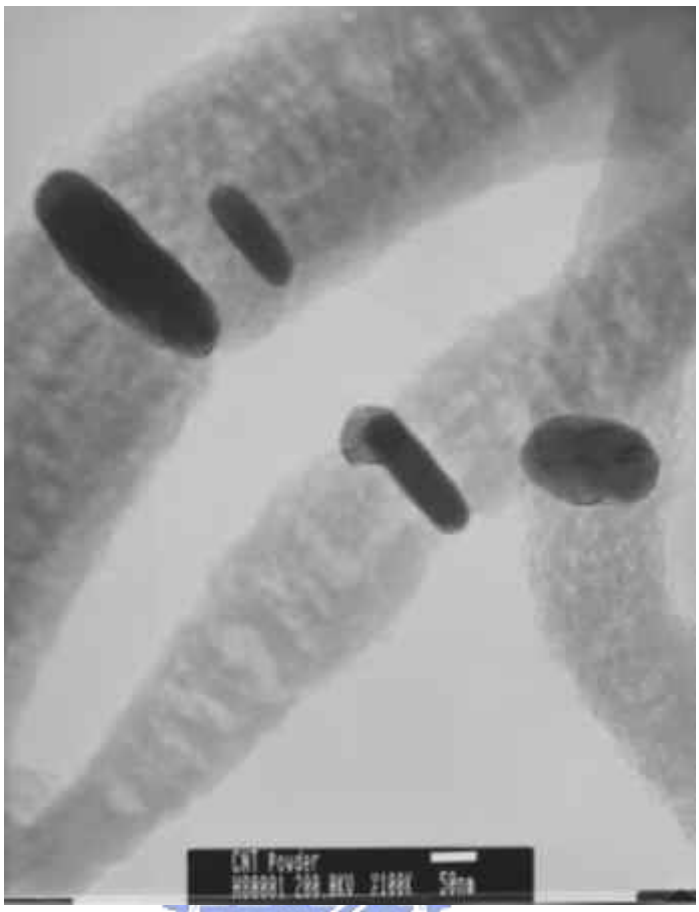


Fig. 4.19. TEM images of carbon nanotubes: herringbone-like structure.

### 4.2.5 Field emissiom properties

Fig.4.20 shows the I-V characteristics. The samples was grown at 150W for 30 min and 200W for 60 min, respectively. A turn on field was defined as the field to give an emission current density of 10 $\mu$A/cm$^2$. The turn-on fields were 5.4 V/$\mu$m for 200 W sample and 6.4 V/$\mu$m for 150 W sample. It shows that under higher power the longer length of CNTs could be obtained, and the current density becomes smaller leading to better field emission properties. However the turn-on field value is larger than the solution deposition method (3.2 V/$\mu$m). The reason is that the length of CNTs grown on the cathode prepared by solution deposition method is longer than sol-gel method. And the surface roughness of thick films prepared by solution deposition method is also larger. These properties contribute to the better field emission stability of the sample prepared by solution deposition method.

Actually, the current density of 0.1mA/cm$^2$ is known to be sufficient for practical displays operating. A parallel-plate configuration is shown in Fig. 3.3. The anode is a glass substrate with an indium-tin-oxide film (ITO) and green phosphor film. The thickness of spacers is 100 $\mu$m. The diode structure field emission at applied field 10 V/$\mu$m produced sufficient brightness, as shows in Fig. 4.21. The bright square area is 0.25 cm$^2$.

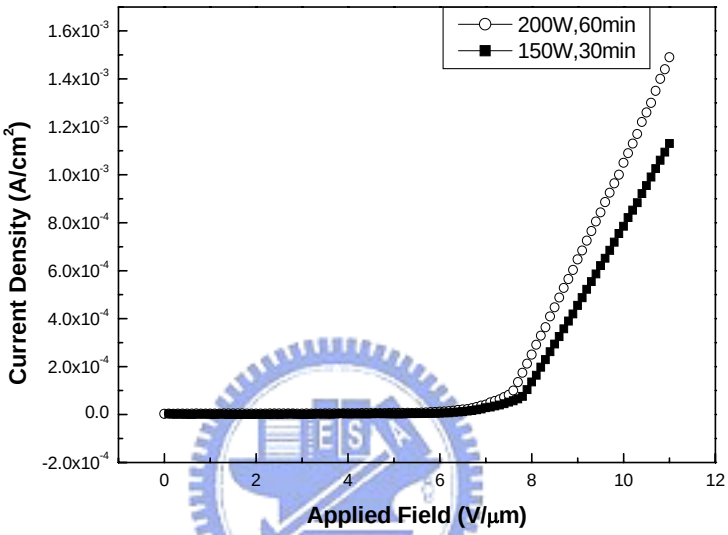


Fig. 4.20. Field emission curves for CNTs growing at 150W for 30 min and 200W for 60 min.

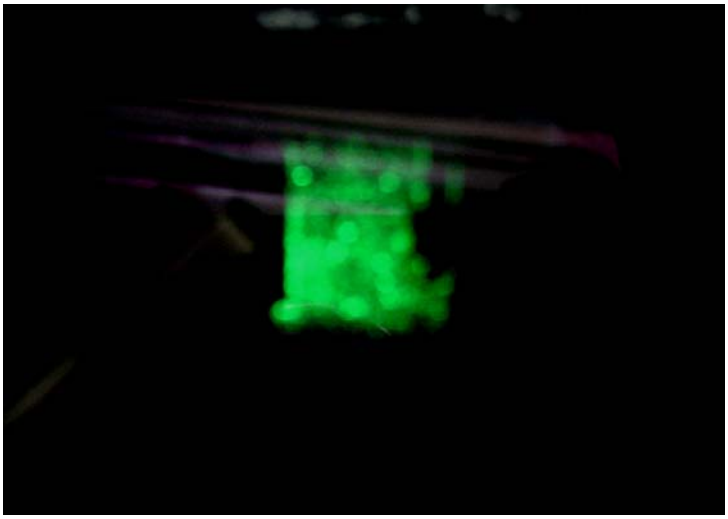

Fig. 4.21. Emission image at applied field 10 V/μm. The samples were grown at total pressure 6 Torr with a $CH_4$ flow rate of 10 sccm and $H_2$ flow rate of 10 sccm for 60 min under 200 W.

### 4.2.6 Summary

We successfully combined the advantages of screen printing process and MPCVD process to pattern catalyst/Ag cathode by screen printing technology and grow CNTs on patterned Ni-catalyst of cathode electrode on glass substrates below 550℃. A novel way can be applied to coat catalyst-Ni with Ag powders in solution phase by sol-gel method. Carbon nanotubes can be grown at total pressure 6 Torr with a $CH_4$ flow rate of 10 sccm and $H_2$ flow rate of 10 sccm for 60 min under 200W. Both multiwall carbon nanotubes (MWNT) and herringbone-like type structure multiwall carbon nanotubes were observed. The tip of CNTs were closed and encapsulated with Ni catalytic nanoparticles. The turn on field value at this case was 5.4 V/$\mu$m. Uniform electron emission was also observed on the electrode with good emission current and brightness.

## 4.3 The growth of carbon nanotubes on patterned catalyst-Ni of cathode by thermal CVD: catalyst preparation by sol-gel method

### 4.3.1 Introduction

Carbon nanotubes (CNTs) were discovered by Iijima in 1991 [1], which were predicted to be the next generation of field electron emitters due to its unique properties such as high aspect ratios, mechanical strength, metallic conductivity, and chemical stability [3,15,20,78]. Numerous methods to grow CNTs have been developed, including arc-discharge, chemical vapor deposition, pulsed laser ablation and so on [22,23,43]. For field emission display, fabrication methods can be roughly classified into two ways. One is coating of as-grown CNTs incorporated into paste by low cost screen-printing process [9], and the other is direct growth of CNTs on the cathode lines by CVD method [29-31].

At present, using CNTs paste by screen-printing technology has a relatively low resolution and needs a surface rubbing technology or other activated steps to enhance field emission properties [9]. For CVD method, it can directly grow CNTs on the predefined catalyst layer

without the following activated steps and has high yield and uniformity. However, the CNTs growth temperature is limited below 550℃ to avoid glass substrate deformation. In the previous works [29-31], semiconductor processes, such as sputtering or thermal evaporating are commonly used to pattern catalyst metals on cathode electrodes. It is well-known that the cost of the semiconductor processes is much higher than screen-printing processes. Therefore, development of the direct CNTs growth on glass substrates at low temperature by a low cost technology will play an important role in practical FED applications. In order to combine advantages of screen printing processes and CVD processes, both catalyst and electrodes were screen printed; while CNTs emitters were uniformly grown on electrodes below 500℃ by CVD. A novel way can be applied to coat catalyst-Ni with Ag powders in solution phase by sol-gel method.

### 4.3.2 Experimental procedures

#### 4.3.2.1 Catalyst preparation by sol-gel Method

For preparing the catalysts, two solutions were prepared individually and then well-mixed. The first solution was 100 ml anhydrous alcohol (Ethyl alcohol) with 29g $Ni(NO_3)_2 \cdot 6H_2O$, while the second solution was made by mixing 50 ml TEOS and 50 ml anhydrous alcohol. Next, the above two solutions were mixed to be Ni/TEOS alcohol solution under stirring for 24 hr. The Ni/TEOS alcohol solution was then well-mixed with conductive Ag powders, frit ,and organic vehicles by using ball mill and three-roller mill to make a printable paste. The catalyst fabrication process is illustrated in Fig. 4.11.

#### 4.3.2.2 Samples preparation by screen printing

The planar triode structure fabrication process is illustrated in Fig. 4.22. The above catalyst/Ag paste was printed on the soda-lime glass substrate as a cathode (Step 1). Another commercial Ag paste was printed next to the cathode line as a gate (Step 2). After printing the

Ag electrode, we removed organic solvents at 400℃ for 2 hr and sintered frit at 560℃ for 15 min (Step 3). The geometric sizes of cathode and gate lines were ~130 μm width with ~5 μm thickness, and the space between the cathode and gate line was ~90 μm.

After sintering, the sample was etched by 0.7 wt% $HNO_3$ for 20 min to clean the surface impurities and glass/oxide covered on Ni (Step 4). After sintering, the sample was etched by 0.7 wt% $HNO_3$ for 20 min to clean the surface impurities and glass/oxide covered on Ni (Step 4).

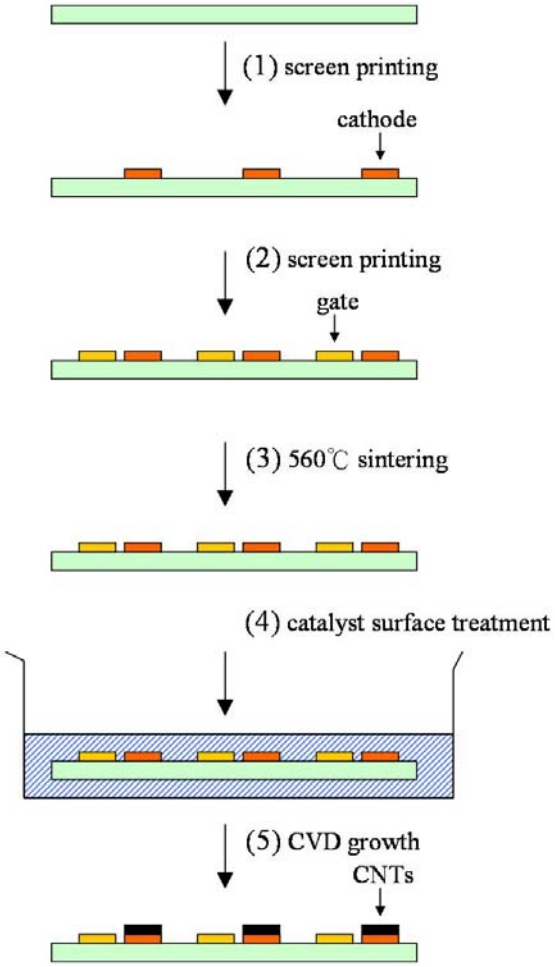


Fig. 4.22. A schematic illustration of the planar triode structure fabrication processes

### 4.3.2.3 Carbon nanotubes fabricating by thermal CVD

Then the sample was loaded into a thermal CVD quartz chamber and heated to a synthesis

temperature in the range of 420-480℃. The reduction step proceeded under $H_2$ and Ar atmospheres for 20 min, followed by the CNTs growth step under $H_2$ (100 sccm), Ar (500 sccm), and acetylene ($C_2H_2$) (25 sccm) atmospheres for 10 min (Step 5).

The morphologies and structures of CNTs were observed by scanning electron microscope (SEM, Hitachi S-4000) and optical microscope (OM). The field emission behavior of CNTs was characterized in the diode and triode method, with a phosphor-coated ITO glass as anode. The spacer thickness is 100 $\mu$m for diode measurement and 4.8 mm for triode measurement, respectively. The current-voltage characteristics were measured using Keithley 237 under $10^{-6}$ Torr.

### 4.3.3 Results and discussion

The surface morphologies of catalyst-Ni after hydrogen reducing treatment were illustrated in Fig. 4.23, showing that Ni nanoparticles were formed after 20 min treatment. It is well known that $H_2$ provides a reducing and activating environment for the catalytic nanoparticles and such catalytic seeds are suitable for CNTs growing at low temperature [163,173]. Figs. 4.24 show the SEM images of CNTs grown at four different temperatures (420, 440, 460, 480℃). It can be seen that the lengths of CNTs increased with the increasing of the growth temperature. Compared to the 440℃ grown CNTs, the 420℃ grown CNTs appear shorter and thinner, and there are also carbonaceous particles on the Ag surface. The CNTs do not form in our system when the growth temperature is lower than 420℃. This is attributed to insufficient growth kinetic energy at the lower growth temperature [174]. The CNTs grown over 440℃ appear longer and denser relatively and the average lengths are over 3μm, as shown in Fig. 4.24b to 4.24d. The CNTs synthesized in this study seemed to be curly and highly defective [30,117,175]. This is suggested that the growth temperature is below 500℃, which is relatively lower than other researches such as arc discharge or CVD methods [1, 28].

A TEM image of the CNTs produced from the sample is shown in Fig. 4.25a. The closed capped multi-walled carbon nanotubes (MWNTs) were observed. The diameter of MWNTs was in range of 30-50 nm. From the EDX analysis of TEM, the catalytic nanoparticle at the tip of the CNT was Ni indeed, indicating that Ni was suitable as a catalytic metal for CNTs growth at low temperature. It was also observed that the CNTs were not straight and the crystalline graphite layers were not as good as those grown at high temperature [28,176]. The defective graphitic sheets were resulted from the low growth temperature. Besides CNTs, a few of carbon nanofibers were also produced, as shown in Fig. 4.25b. It was observed the formation of amorphous carbon obviously. In previous studies, many researchers reported that the synthesis of carbon nanotubes accompanied production of carbon nanofibers at low temperature [131,163].

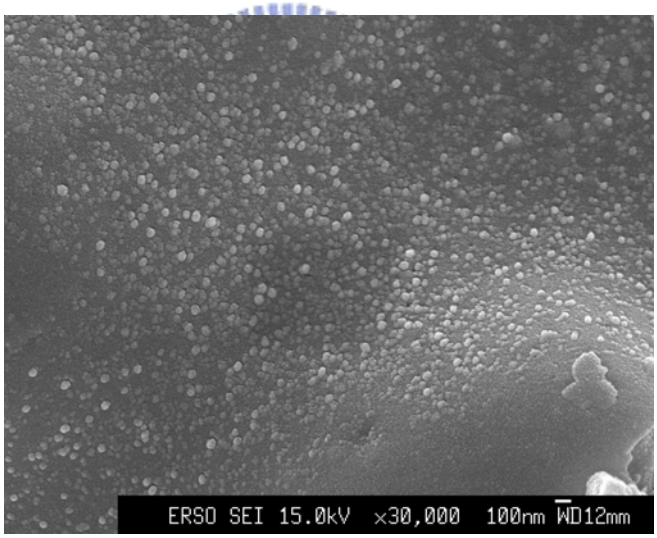


Fig. 4.23. Surface morphologies of catalyst-Ni after hydrogen reducing treatment

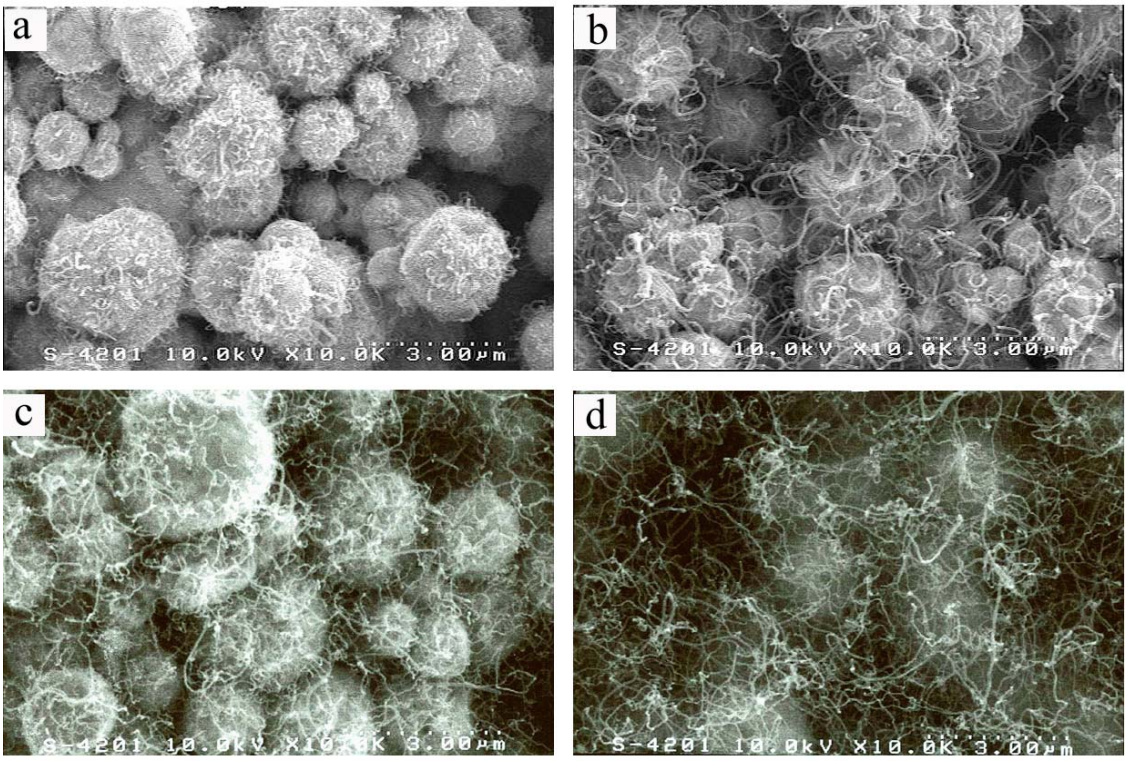


Fig. 4.24. Surface morphologies of CNTs grown at (a) 420, (b) 440, (c) 460, and (d) 480℃ for 10min with a $C_2H_2$ flow rate at 25 sccm, $H_2$ flow rate at 100 sccm, and Ar flow rate at 500 sccm.

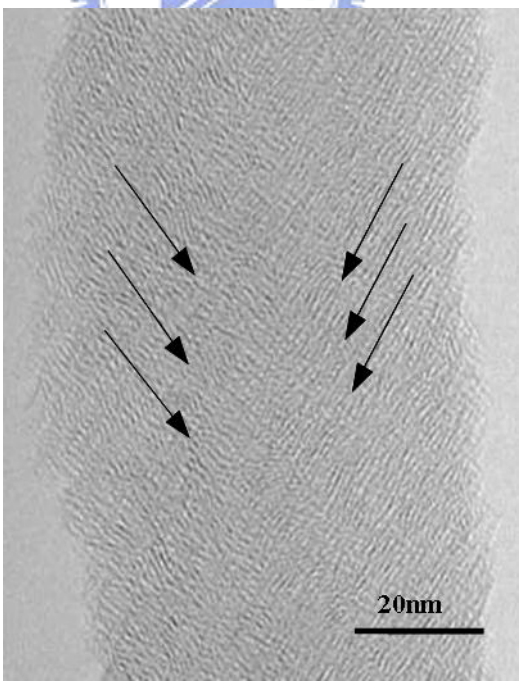


(a)

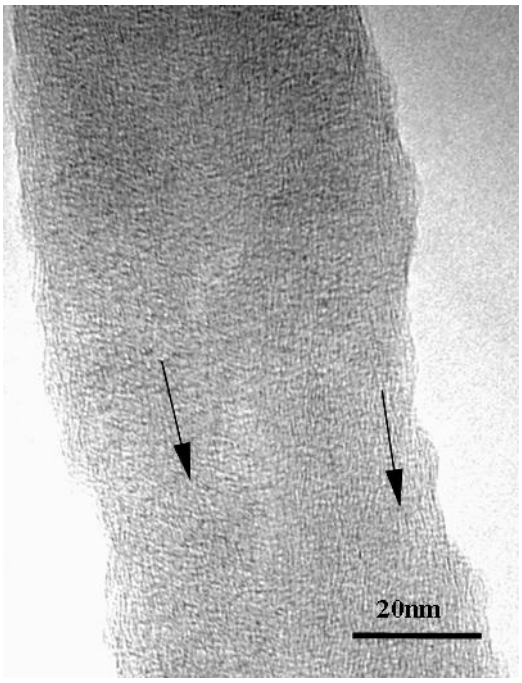


(b)

Fig. 4.25. TEM image of the sample: (a) closed capped multi-walled carbon nanotube (b) carbon nanofiber. The samples were grown at 480℃ for 10min with a $C_2H_2$ flow rate at 25 sccm, $H_2$ flow rate at 100 sccm, and Ar flow rate at 500 sccm.

The emission current was measured in the vacuum chamber under $10^{-6}$ Torr. Fig. 4.26 shows the emission curves for CNTs growing at (a) 420℃, (b) 440℃, (c) 460℃, and (d) 480℃. A turn-on field is defined as the applied electric field to drive an emission current density of 10 $\mu$A/cm$^2$. The field values for these four samples were (a) 9.86, (b) 5.71, (c) 4.70, and (d) 3.85 V/$\mu$m. It can be seen that the turn-on field value decreased with the increasing of the growth temperature. The CNTs grown at 480℃ begin to emit electrons at a lower electric field than other CNTs grown at lower growth temperature, indicating that the emission properties of CNTs depends on the growth temperature. At higher temperature, carbon atoms have enough driving force to diffuse, and thus formed more perfect structure and longer tube, which would eventually affect the emission properties of nanotube. It can be also observed that the CNTs grown at 480℃ show longer and "clean" surfaces relatively, as shown in Fig. 4.24d. Compared to the emission current density of 440℃ grown CNTs, the 420℃ grown CNTs was detected a little emission current at the same electric field which was

due to a small amount and higher defective nanotubes, relatively, as shown in Fig. 4.26 [176]. The inset in Fig. 4.26 shows Fowler-Nordheim (F-N) plot of the CNTs grown at 480℃ which indicates that field electron emission was intrinsically driven by electric field [131]. The extremely uniform and bright diode emitting image (over 500 nits) of the anode (coated by the green phosphor) for the CNTs grown at 480℃ at the electric field of 5.5 V/$\mu$m was shown in Fig. 4.27.

Fig. 4.28 shows the obtained current-gate voltage characteristics of the planar triode device [177] (the CNTs grown at 480℃) under a constant anode voltage of 1100 V. The cathode and gate lines were ~130 μm width, and the space between the cathode and gate line was ~90 μm, as shown in Fig. 4.29. Most of electric current was introduced toward the anode at gate voltage over 300 V. The ratio of anode and gate current was much lower than that expected at the gate voltage 400 V. It is resulted from non-uniform emission behaviors of the CNTs on cathode. The CNTs at the edge of the cathode get stronger electric field (originating from the cathode geometric effect) than those on the top of cathode. High electric field introduces the leakage current from cathode to gate for this planar triode structure. Even though the leakage current was occurred, the planar triode emission image of the anode (coated by the white phosphor) for the CNTs grown at 480℃ was observed with uniform electron emission current and high brightness (no less than 500 nits), as shown in Fig. 4.30.

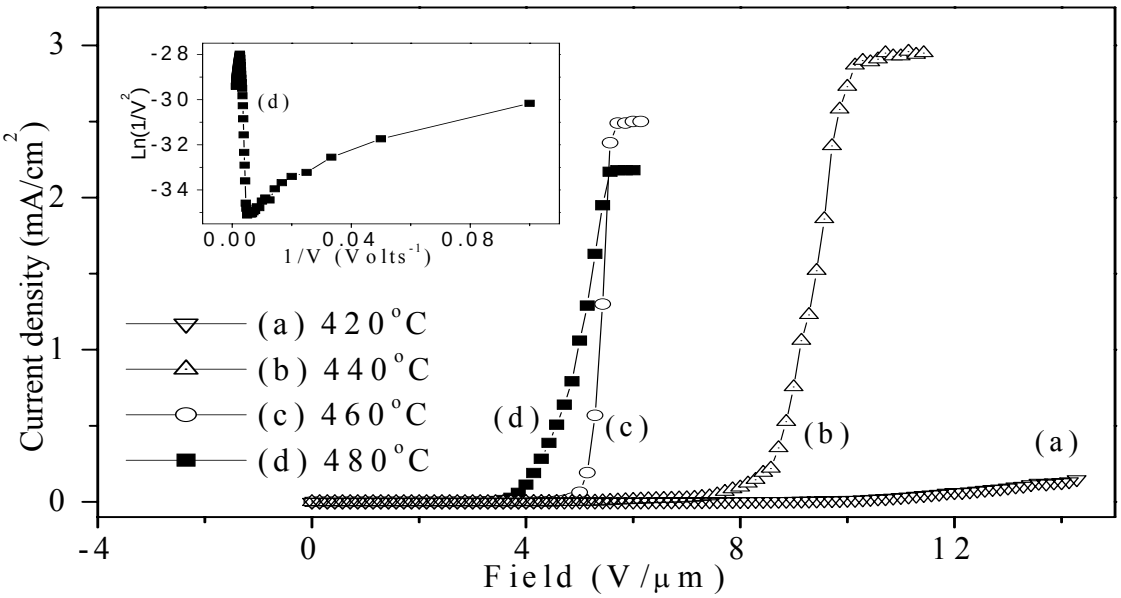


Fig. 4.26. Field emission curves for CNTs growing at different temperatures (The insert is the Fowler-Nordheim plot at 480℃ growth temperature)

Fig. 4.27. Emission image at applied field 5.5 V/ $\mu$m for diode testing

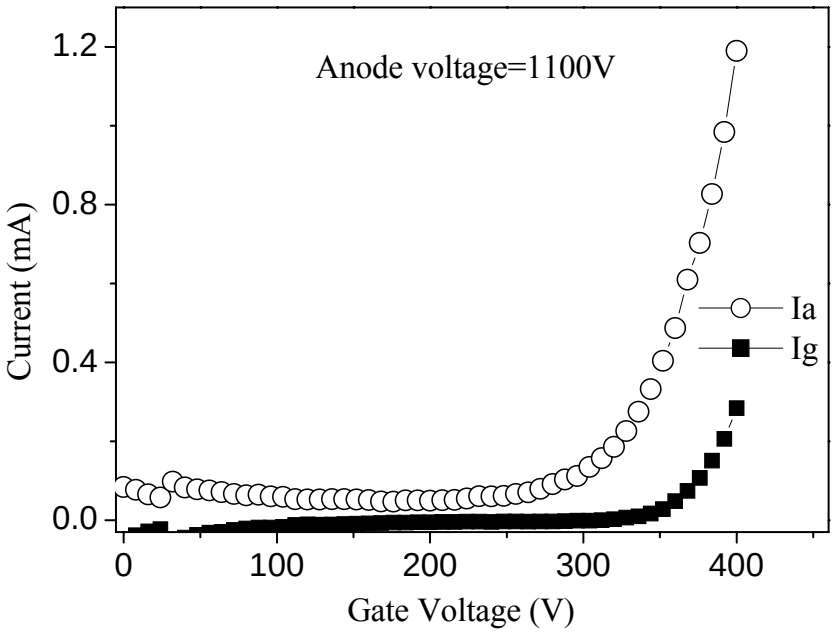


Fig. 4.28. Current-gate voltage characteristics of the planar triode device under a constant anode voltage of 1100 V

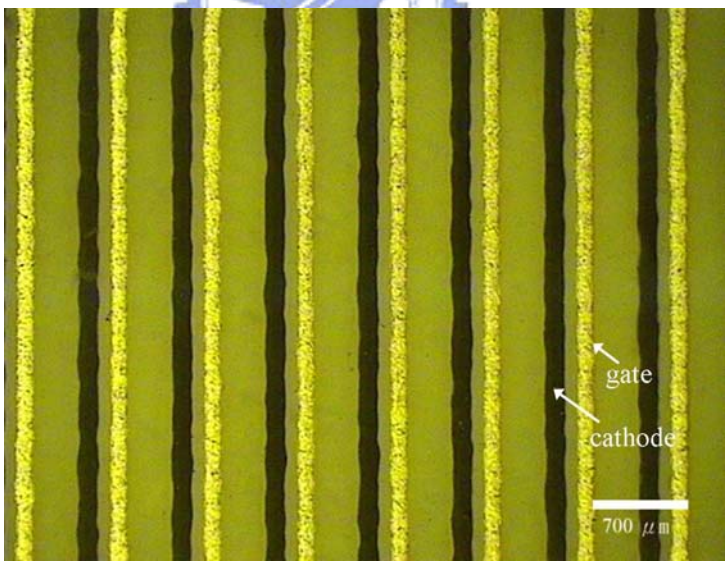


Fig. 4.29. OM image of cathode electrodes with growing CNTs and gate electrodes

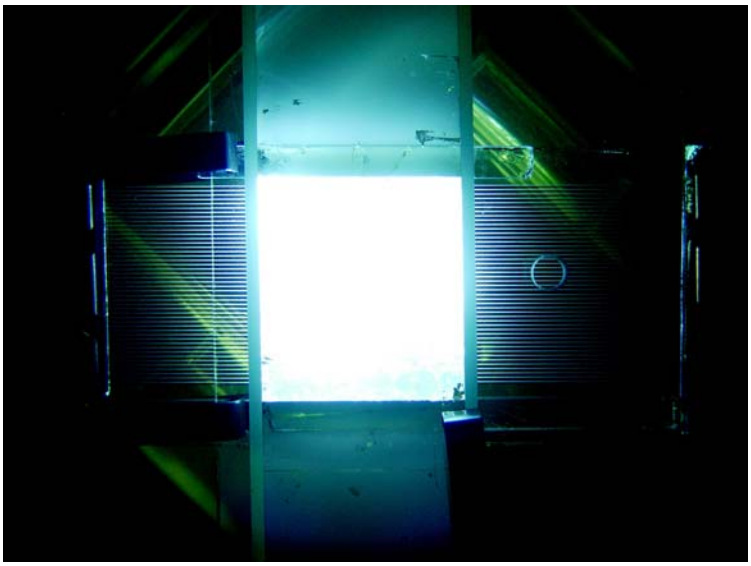

Fig. 4.30. Emission image at anode voltage of 1100 V and gate voltage of 400 V for triodetesting

### 4.3.4 Summary

In conclusion, CNTs with superior field emission properties (uniform emission and high brightness) are synthesized under 500℃ by CVD growth on the thick-film constructed cathode structures. Although gate current leakage phenomenon can not be avoided in this work, the field emission results of diode and triode measurements demonstrate the successful application of CNTs emitters incorporated into thick-film cathode structure. It is suggested that preventing of gate current leakage by cathode structure design can reinforce the field emission performance future more.

## 4.4 Thick-film structure geometry effect on carbon nanotubes synthesized by chemical vapor deposition method

### 4.4.1 Introduction

The discovery of carbon nanotubes (CNTs) by Iijima in 1991 has promised a new scientific research in both academic and industrial field [1]. CNTs have aroused great attention due to their unique properties, such as high mechanical strength, high chemical stability, and high aspect ratio for field emission application [15,18-20,178]. Recently, chemical vapor deposited

CNTs, arc-discharge, and pulsed laser ablation produced CNTs were reported to exhibit excellent field emission characteristics such as low turn-on voltage and high current density [22-24]. Among above methods, both arc-discharge and CVD were usually reported to be used for field emission display [25,26]. A low cost process combining arc-discharge produced CNTs and screen-printing technologies was developed to prepare field emitters on glass substrates [27,179]. Unfortunately, using CNTs paste by screen-printing technology has a relatively low resolution and needs a surface rubbing technology or other activated steps to enhance field emission characteristics [27]. Oppositely, using CVD methods can directly grow CNTs on the predefined catalyst layer and has high yield and uniformity without activated methods [176].

Many researchers have succeeded in synthesizing CNTs on Si substrate at a relatively high temperature by various CVD methods [28,180]. In order to suit for field emission display (FED) applications, the growth temperature has a limit below 550℃ to avoid glass substrate deformation. Consequently, the study of direct growth CNTs at low temperature on glass substrates by CVD methods has been reported [29-31]. However, in previous works, it is required to construct the triode structure on glass substrates by semiconductor processes, such as sputtering, thermal evaporating, or CVD methods, etc. It is well-known that the cost of the semiconductor processes is much higher than screen-printing processes. Therefore, development of the direct growth CNTs in the triode structure at low temperature by a low cost technology will play an important role in practical FED applications. In order to achieve these requirements, our work was combining the thick-film screen printing and photolithography technology to construct the triode electronic structure, in which CNTs were then synthesized in the selected-area by CVD method. Under controlling the pumping system and precursor concentration during the CVD process, cathode for field emission devices was properly produced.

### 4.4.2 Experimental procedures

(a) Structure construction

In order to investigate structure geometric effects on CVD CNT process, we constructed three different types of structures with different morphologies. The conductive electrodes in three structures were all screen printed with silver paste and patterned by photolithography methods. The organic solvents were removed by the following 400℃ firing process, and then glass frits were sintered at 550℃ for 15 minutes.

The first type (type Ⅰ) structure was the planar electrode structure, as seen in Fig. 4.31a. The width and thickness of the cathode electrode were ~300 μm and ~10 μm, respectively. Catalyst were selectively deposited on these patterned electrodes by assistance of photo-resist. In type Ⅱ (Fig. 4.31b), we printed and patterned trench-morphology dielectric layer on conductive electrode. The depth of the trench was ~15 μm, while the open width was ~180 μm. Catalyst was coated on the both dielectric layer and conductive electrode in order to trace the difference in these two positions (on the top area and at the bottom of the trench structure).

Type Ⅲ was a conventional normal triode structure (Fig. 4.31c). The pixel size was ~350 μm × ~110 μm, with the depth of ~15 μm. The structure in type Ⅲ appeared a smaller open-size and deeper hole morphology, compared to type Ⅰ and type Ⅱ. Catalyst was selective deposited on the cathode electrode at the bottom of the dielectric hole. Type Ⅰ, type Ⅱ, and type Ⅲ were observed by scanning electron microscopy (SEM), and shown in Figs. 4.32a, 4.32b, and 4.32c, respectively.

A schematic flow diagram of fabrication for the normal-gate triode structure(Type Ⅲ) on glass substrate was illustrated in Fig. 4.31c. The photosensitive Ag paste was first screen-printed over the whole area on the soda-lime glass substrate. The patterned cathode electrodes were formed by photolithography process with 150 mJ/cm$^2$ UV light source (Step 1). After developing the cathode electrodes with a water solution containing 0.5% $Na_2CO_3$,

organic solvents were removed at 400℃ firing for 2 hr, and then glass frits were sintered at 560℃ for 15 min (Step 2). The geometric sizes of cathode lines were 90 μm width with ~5 μm thickness, and the interspace between the cathode lines was 110 μm. Then, the insulator paste was screen-printed on the cathode lines (Step 3), followed by firing at 400℃ for 2 hr and then sintering at 550℃ for 15 min (Step 4).

Another photosensitive Ag paste (serving as gate electrodes) was screen-printed over a whole area on the insulator. After drying at 90℃, the gate holes and gate lines were exposed to a UV light through the photo-mask with the energy density of 120 mJ/cm$^2$ (Step 5). After developing the gate electrodes, they were heated at 400℃ for 2 hr to remove the organic solvents and sintered at 500℃ for 15 min (Step 6).

Photo-resist with a thickness of 20 μm was patterned to protect the gate holes and gate lines from insulator etching as well as to define the regions where Ni would be deposited (Step 7 and 8). Ni catalyst was deposited by sputtering through photo-resist the patterned areas. After the photo-resist stripping, the normal-gate triode structure with Ni on cathode was produced (Step 9).

(b) CVD process

The samples were loaded into a thermal CVD chamber and heated to a synthesis temperature of 500℃. The reduction step was proceeded under 600 sccm $H_2$ atmospheres for 10 min, followed by the CNTs growth step under 300 sccm $H_2$ and 300 sccm acetylene ($C_2H_2$) atmospheres for 15 min. The structures and morphologies of CNTs were observed by scanning electron microscope (SEM, Hitachi S-4000) and optical microscope (OM).

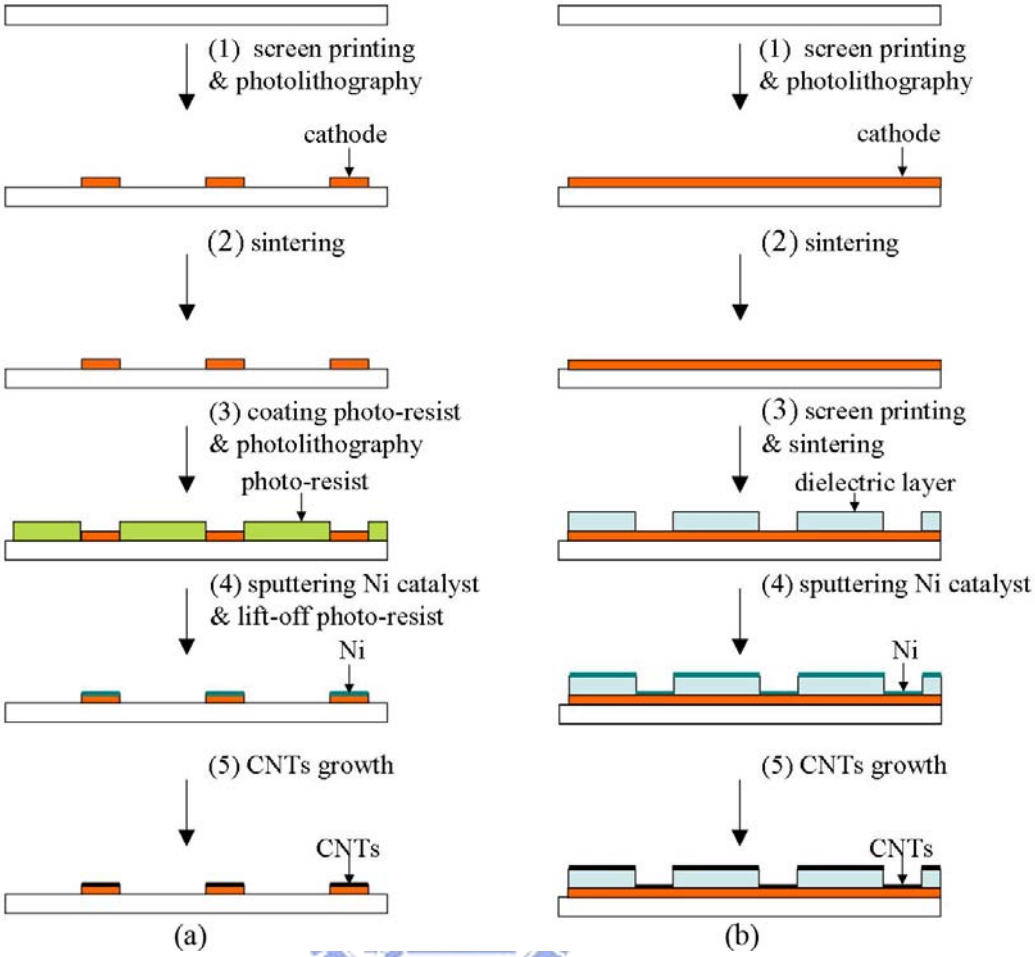
(1) screen printing
& photolithography
cathode
(2) sintering
(3) coating photo-resist
& photolithography
photo-resist
(4) sputtering Ni catalyst
& lift-off photo-resist
Ni
(5) CNTs growth
CNTs
(a)
(1) screen printing
& photolithography
cathode
(2) sintering
(3) screen printing
& sintering
dielectric layer
(4) sputtering Ni catalyst
Ni
(5) CNTs growth
CNTs
(b)

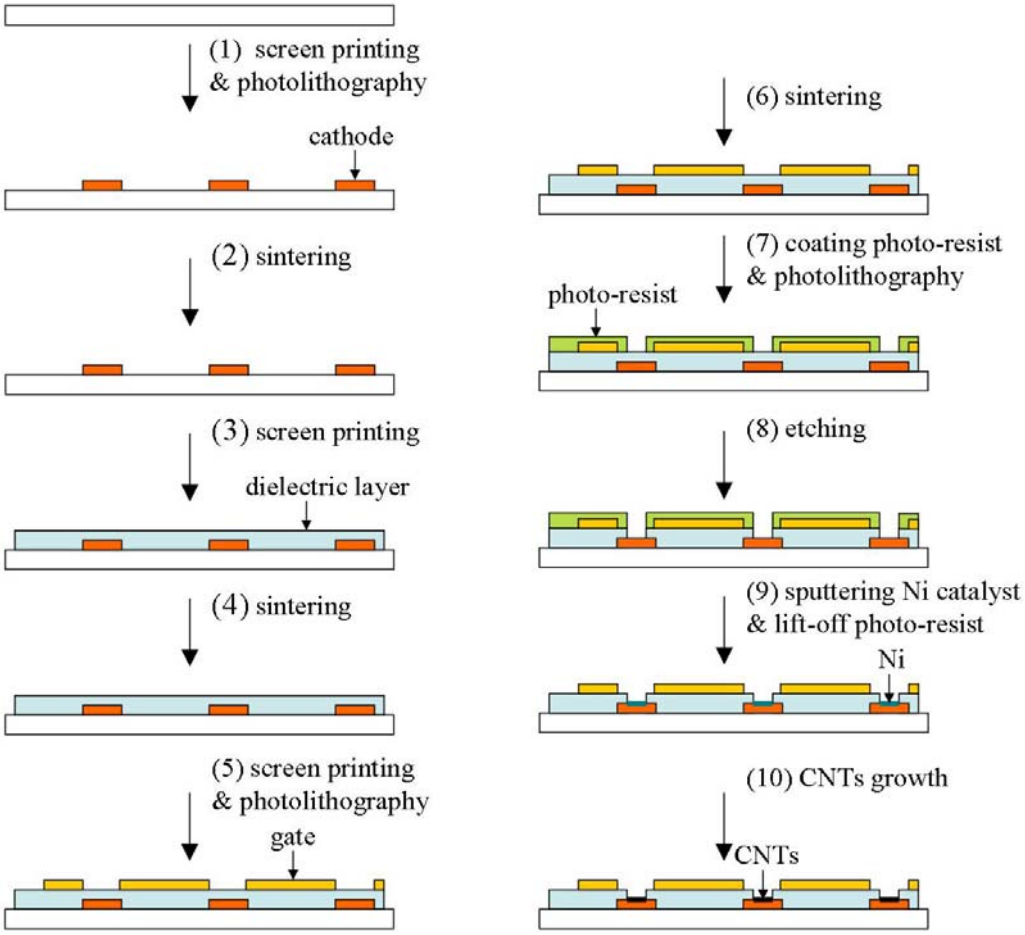


Fig. 4.31. Schematic illustrations of the (a) type Ⅰ, (b) type Ⅱ, and (c) type Ⅲ structure fabrication processes.

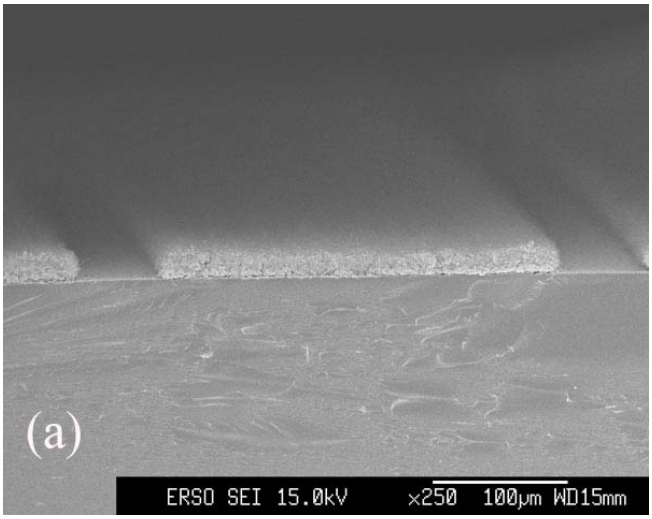

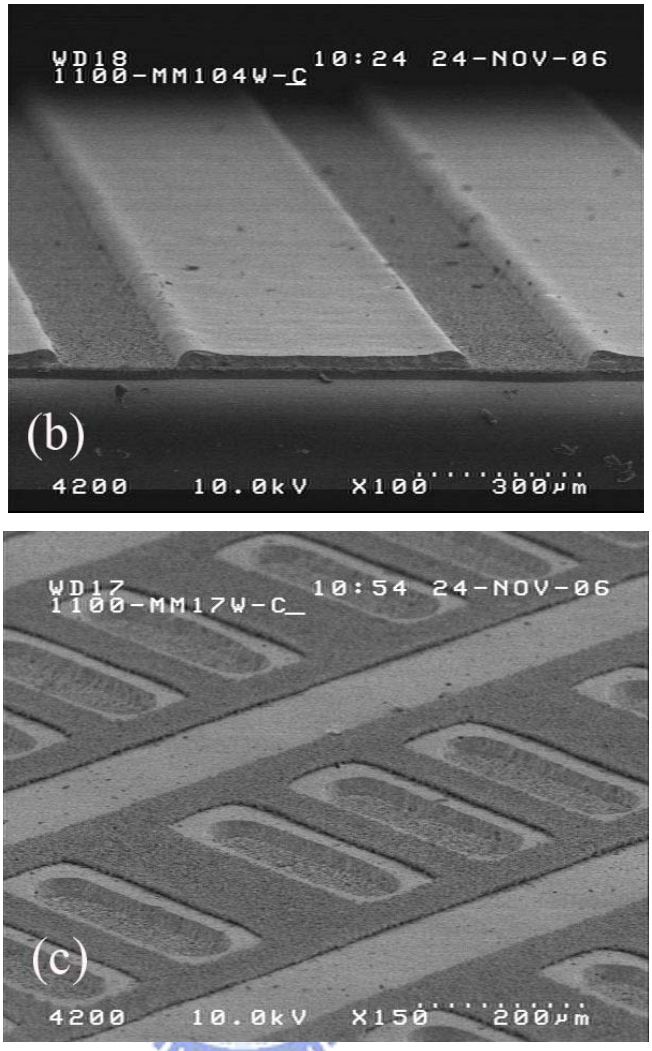


Fig. 4.32. SEM images of cross-section view of (a) type Ⅰ,(b) type Ⅱ, and (c) type Ⅲ structure.

### 4.4.3 Result and discussions

In type Ⅰ, precursor gases loaded into chamber are able to react with catalyst coated on conductive electrode without any difficulty. Carbon atoms can transport from gas phase to catalyst metal, supersaturate in catalyst and then precipitate to form CNTs (as shown in Fig. 4.33). There is no obstacle which can restrict or influence gas flowing behavior.

Then, we build the environment of "side-walls" surrounding the conductive electrode electrodes, as shown in type Ⅱ. The goal is to investigate whether such trench morphology can play an important role on influencing gas flowing. Results show that CNTs can be synthesized both "on the top of the trench structure" and "at the bottom of the trench

structure", shown in Fig. 4.34a and 4.34b, respectively. The morphologies of CNTs at these two different positions are similar without any obvious difference. It was implied that the depth of trench structure and the aspect ratio of trench can not make effects on CNTs growth. The gas flowing and transport path is still unobstructed inside the trench.

In practical FED devices, matrix of pixels is fabricated in the cathode plate. The CNTs emitters located at the bottom of the dielectric holes, while the gate electrodes over CNTs emitters serve as driving electrodes. For high-resolution display application, the pixel size is reduced to a much smaller scale. Thus, dielectric holes become much more narrow and deeper. In the type Ⅲ structure, such holes perform a morphology in which gas flowing and transport is not smooth any more. Fig. 4.35a shows that only amorphous carbon particles are synthesized at the bottom of dielectric holes under the same growth recipes as those in type Ⅰ and type Ⅱ structures. Although different ratios of precursor gases are tested, we still get the same results. It implies that the problem originating from hole geometry morphology can not be solved merely by turning precursor ratios. If the original atmosphere existing inside dielectric holes can not exchange with active precursor gases, the decomposed carbon atoms can move toward catalyst only by concentration gradient driving. The precursor gases might from the steady flowing state just over the dielectric holes (but not flow into the holes and then out of the holes). Amount of carbon atoms just by concentration gradient driving are not enough to proceed supersaturation and precipitation reaction. Thus, only carbon particles are coated at the bottom of dielectric holes.

This phenomenon can not appear in the normal triode structure fabricated by completely thin-film processes [31]. The depth of dielectric holes in the thin-film processes is commonly no more than 1 μm. The effect resulting from depth of such dielectric holes is not obvious for precursor gases flowing behavior. But in the thick-film processes, it does play an important role on synthesizing CNTs.

In order to solve this problem, we adopt the pumping procedure before hydrogen

reduction step and before CNTs growth step. The background pressure is pumped to 460 Torr, and then hydrogen gas is feeding into the chamber to activate catalyst under 600 Torr background pressure. After activating step, another pumping proceeds to maintain background pressure at 460 Torr again. At the following step, mixture of hydrogen and acetylene is loaded to grow CNTs. Pumping assistance can help to drive the original existing gas out of dielectric holes and force precursor gas to flow into the holes. Fig. 4.36a shows the cathode plate after growth under optical microscopy observation, while Fig. 4.36b shows CNTs growth results at the bottom of the dielectric hole under SEM observation. The density of CNTs is about $10^6$ CNTs/$cm^2$, still lower than those in Fig. 4.34a and 4.34b.

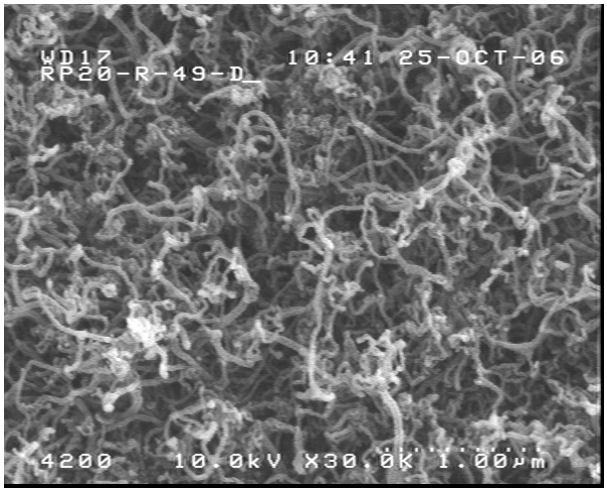


Fig. 4.33. SEM image of surface morphology of CNTs grown at 500℃ for 15min with 300 sccm $C_2H_2$ and 300 sccm $H_2$.

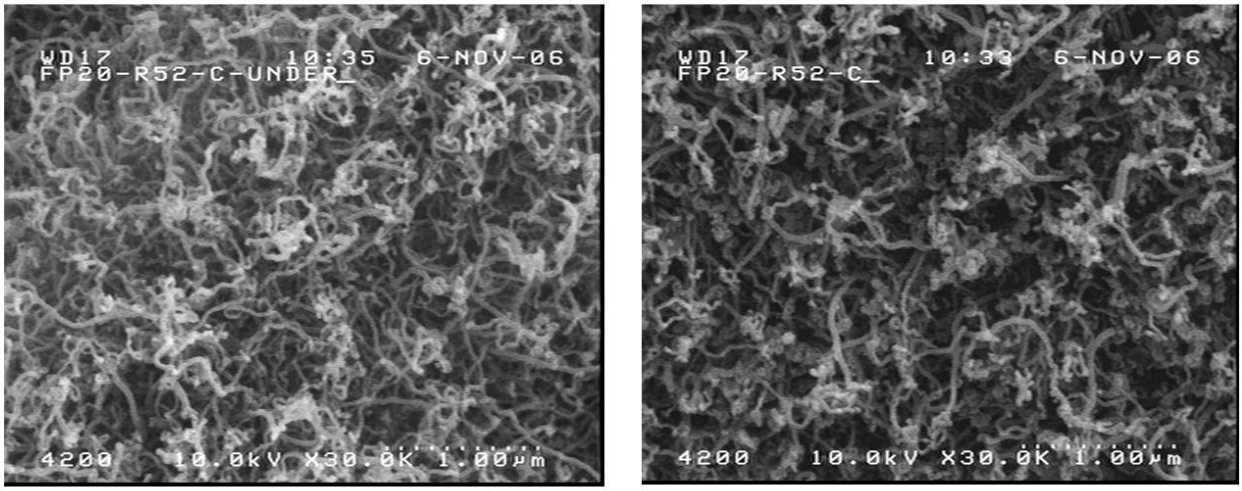


(a) (b)

Fig. 4.34. SEM images of surface morphology of CNTs grown (a) at the bottom and (b) on the top area of the trench structure at 500℃ for 15min with 300 sccm $C_2H_2$ and 300 sccm $H_2$.

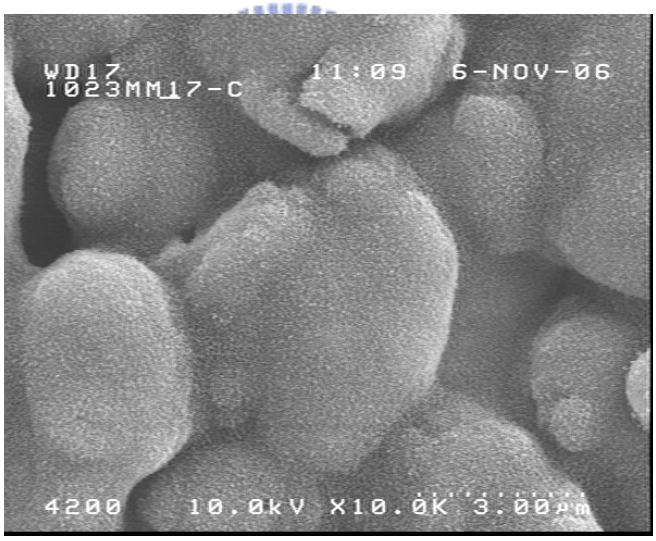


Fig. 4.35. SEM image of surface morphology of CNTs grown at the bottom of the dielectric hole at 500℃ for 15min with 300 sccm $C_2H_2$ and 300 sccm $H_2$ without pumping assistance.

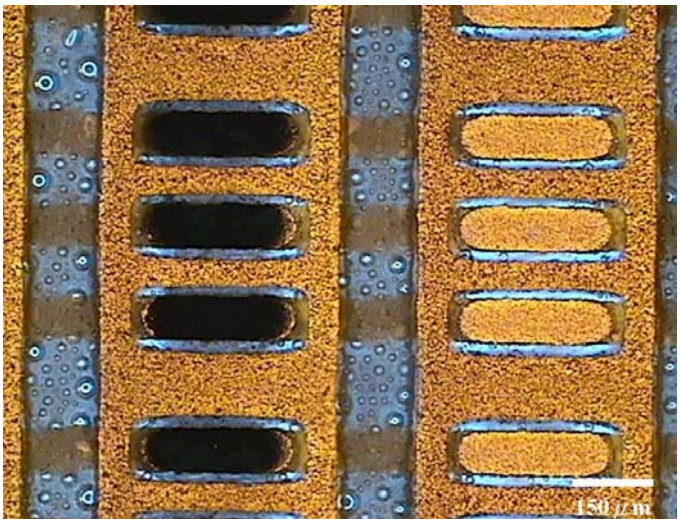


(a)


(b)

Fig. 4.36. (a) OM image and (b) SEM image of CNTs grown at the bottom of the dielectric hole at 500℃ for 15min with 300 sccm $C_2H_2$ and 300 sccm $H_2$ at 600 Torr. with pumping assistance. (In the left-hand of Fig. 4.36a shows the CNTs selective growth on the cathode electrode with catalyst deposited, but in the right-hand of Fig. 4.36a shows clear cathode electrode without catalyst deposited.)

### 4.4.4 Summary

In this work, we have demonstrated that precursor gas flowing and transport is unobstructed in both planar electrode and trench morphology structures. As to the thick-film normal triode structure, additional pumping assistance is required in order to solve the gas transport problem in such narrow and deep dielectric holes.

## 4.5 Selected-area deposition of CNTs in triode structure for field emission device

### 4.5.1 Introduction

CNTs were first discovered by Iijima in 1991 under observation of transmission electron microscopy (TEM) [1]. Owing to the unique aspect ratio, CNTs exhibit excellent field emission characteristics such as lower turn-on voltage and larger emitting current than any other field emission devices [15,18,20,22,178]. In the related research [181-185], it remains a challenge to deposit CNTs into the selected-area of the triode structure by electrophoretic deposition (EPD) method. The typical solution is to apply a sacrificial layer covering the unwanted-depositing site and then to remove this sacrificial layer after EPD treatment, which are inconvenient processes. Thus, it is worth developing selected-area deposition technology during EPD. Furthermore, low-cost, low-temperature, large-scaled area and homogeneous deposition are main issues on the subjects of manufacture for the CNTs field emission display (CNT-FED) [172,186]. In order to achieve these requirements, our work was combining the thick-film screen printing and photolithography technology to construct the triode electronic structure, in which CNTs were then deposited in the selected-area by EPD method. Under controlling the solution content and voltage supplies during the EPD process, cathode for field emission devices was properly produced.

### 4.5.2 Experimental procedures

(a) Structure construction

A schematic flow diagram of fabrication for the normal-gate triode structure on glass substrate was illustrated in Fig. 4.37c. The pixel size of panel was 500 micron × 500 micron, the gate hole size was about 80 μm, and the dielectric thickness was about 25 μm. The photosensitive Ag paste was first screen-printed over the whole area on the soda-lime glass substrate. The patterned cathode electrodes were formed by photolithography process with 150 mJ/cm$^2$ UV light source (Step 1). After developing the cathode electrodes with a water

solution containing 0.5% $Na_2CO_3$, organic solvents were removed at 400℃ firing for 2 hr, and then glass frits were sintered at 560℃ for 15 min (Step 2). The geometric sizes of cathode lines were 90 μm width with ~5 μm thickness, and the interspace between the cathode lines was 110 μm. Then, the insulator paste was screen-printed on the cathode lines (Step 3), followed by firing at 400℃ for 2 hr and then sintering at 550℃ for 15 min (Step 4).

Another photosensitive Ag paste (serving as gate electrodes) was screen-printed over a whole area on the insulator. After drying at 90℃, the gate holes and gate lines were exposed to a UV light through the photo-mask with the energy density of 120 $mJ/cm^2$ (Step 5). After developing the gate electrodes, they were heated at 400℃ for 2 hr to remove the organic solvents and sintered at 500℃ for 15 min (Step 6).

Photo-resist with a thickness of 20 μm was patterned to protect the gate holes and gate lines from insulator etching as well as to define the regions where Ni would be deposited (Step 7 and 8). Ni catalyst was deposited by sputtering through photo-resist the patterned areas. After the photo-resist stripping, the normal-gate triode structure with Ni on cathode was produced (Step 9).

(b) EPD process

Before proceeding the EPD process, the cathode was immersed in the Tritron solution for 10 minutes in order to enhance the adhesion behavior for CNTs. In order to control CNTs depositing behavior efficiently, 1 ppm $Na_2CO_3$ was chosen as the charging additive to the solution with DI water of 50 ppm CNTs, and solution conductivity increased from 0.444 ms/m to 0.702 ms/m.

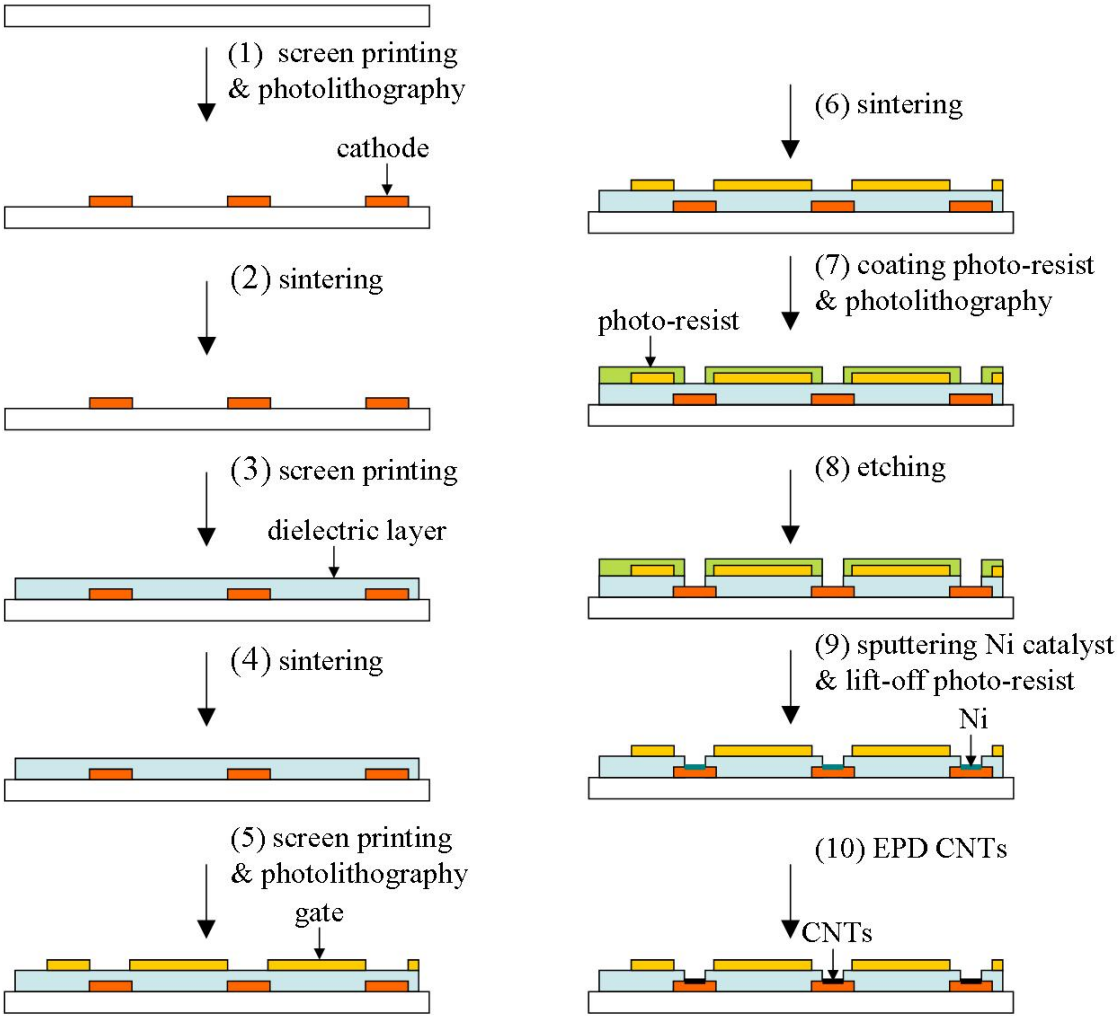


Fig. 4.37. Schematic illustrations of the normal-gate triode structure fabrication processes.

### 4.5.3 Result and discussions

The EPD equipment is illustrated in Fig. 4.38. The anode was made of the mesh structure, instead of plane sheet, in order to homogenize the electric field distribution. During selected-area electrophoretic deposition, positive 100 V was applied to the gates while negative 30V was applied to the cathodes with respect to the ground voltage at the anode plate. Depositing substance in EPD process can mainly be driven by three factors: diffusion, convection and drifting. Because CNTs powders were well-mixed in the solution and no stirring was proceeding during EPD, diffusion and convection effects were much less

significant. Under applied electric field in the solution, one dimensional nano-materials (such as linear polymer, nano-rod and CNTs) are easily polarized along the longitude axis, and these polarized dipoles can drift by the effect of dielectrophorectic force. In our work, $Na_2CO_3$ additive assists CNTs to be charged on their surface. Thus, drifting behaviors of CNTs substance is sensitive to the applied electric field. By suitable designing electric field supply environment, CNTs drifting is able to be well-controlled. According to our voltage controlling situation, the electric field distribution is illustrated in Fig. 4.39. The positive gate voltage repels the CNTs and prevents them from depositing in the neighborhood of the gate. Thus, CNTs are pulled through the gate hole by electrical force from the negative cathode voltage, and then deposit onto the surface of the cathode.

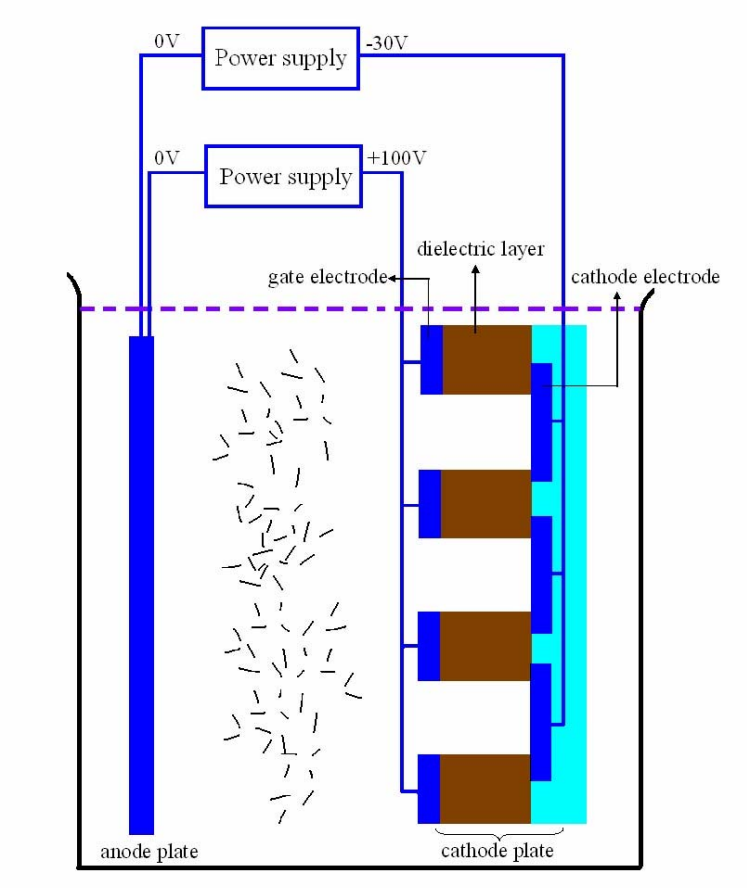


Fig. 4.38. Illustration of EPD equipment.

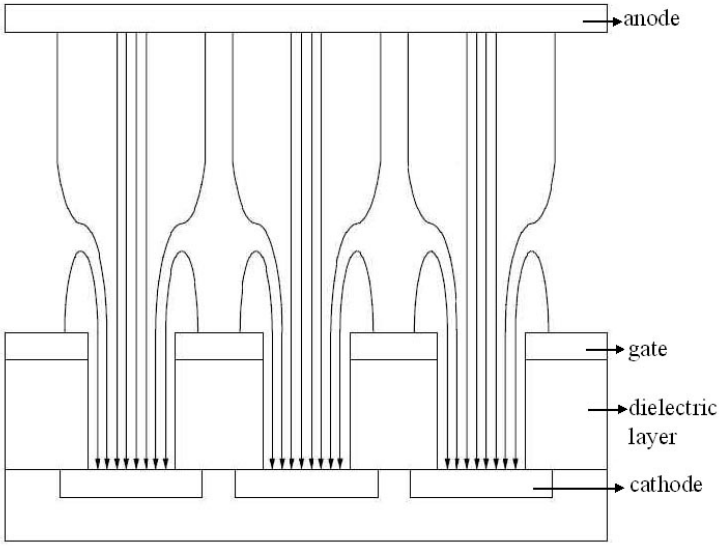


Fig. 4.39. Electric field distribution of EPD experiment.

Cathode plates before and after EPD process were shown in Figs. 4.40(a) and (b), respectively. Vertical electrode lines are cathode lines, while horizontal electrode lines are gate lines. The substance between gate lines and cathode lines is dielectric layer. The pixel size of panel was 500 micron × 500 micron, the gate hole size was about 80 μm, and the dielectric thickness was about 25 μm. All cathode lines appeared black color in Fig. 4.40(b), implying that CNTs were selectively deposited on cathode lines. In Fig. 4.40(c), the morphology of the CNTs-coated cathode is shown by SEM observation. A great amount of CNTs were coated on the cathode line. Because CNT powders were not purified in the pre-treatment, there still existed some carbon particles coated on the cathode line. It is suggested that removal of these particles can both enhance the field emission properties and improve the vacuum situation during the panel package process.

The filed emission properties of CNTs in EPD method were shown in Fig. 4.41. The turn-on electric field intensity was as low as 4.5 volt/μm, while current density reached 3.5 mA/cm$^2$ at 9.5 volt/μm. The anode coated by P22 green phosphor was bombarded by the accelerated electron emitting from cathode and showed the 4-inch light image in the inserted figure of Fig.

4.41. It is found that the homogeneous emitting behavior for CNTs is still needed to be improved in the future application for panel display industry.

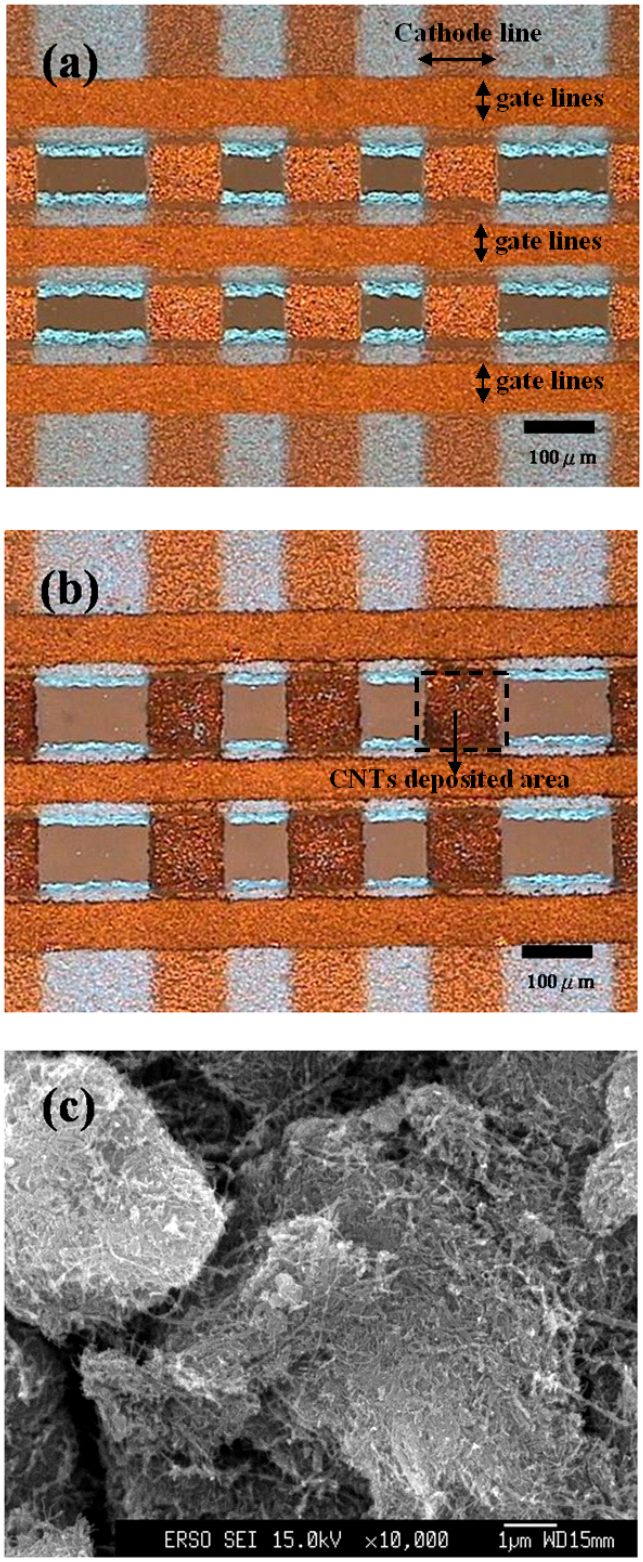


Fig. 4.40. OM images of cathode (a) before coating, (b) after coating, and (c) SEM image of CNT-coated cathode line.

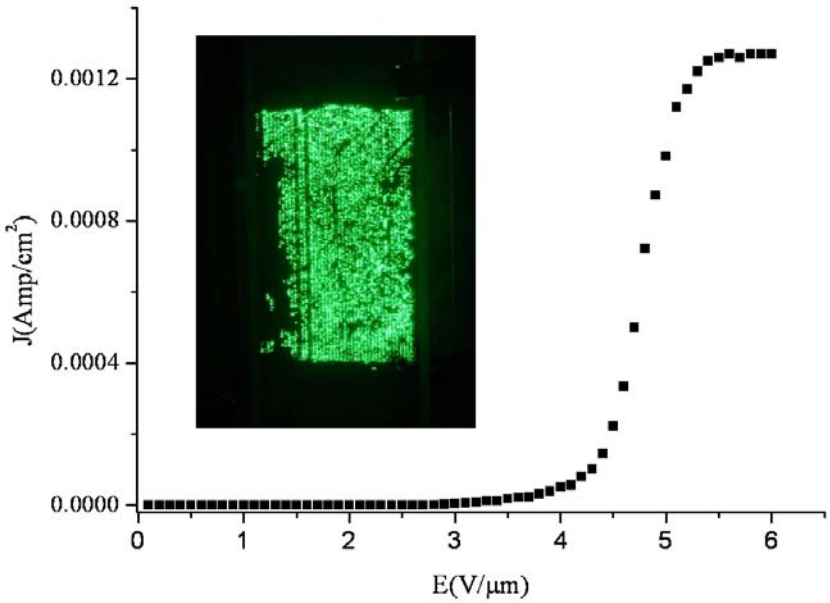


Fig. 4.41. Field emission results for EPD sample. The inset shows the field emission image of the phosphor-coated anode.

### 4.5.4 Summary

In conclusion, we have successfully demonstrated that the EPD method can be applied to deposit CNTs into the selected-area of the triode structures for FED devices. By suitable solution content and voltage controlling situation, photo-resist or sacrificial layer can be omitted. Comparing with other processes, this work was combining the advantages of thick-film technology and EPD method which can scale up to large size panel with low-cost and operate at low-temperature environment.

# Chapter 5 Conclusions

In this thesis, the CNTs were synthesized successfully by using MPCVD and thermal CVD at low temperature. The CNTs were also synthesized on the cathode with high aspect ratio dielectric holes by controlling the pumping system and precursor concentration during the thermal CVD process. We also have successfully demonstrated that the EPD method can be applied to deposit CNTs into the selected-area of the triode structures for FED devices.

**Concluding Remarks**

1. We successfully combined the advantages of screen printing process, MPCVD and thermal CVD process to pattern catalyst/Ag cathode by screen printing technology and grew CNTs on patterned Ni-catalyst of cathode electrode on glass substrates at low temperature. These processes are simple, low-cost and easy to scale up for large sized panels.
2. Two novel ways can be applied to coat catalyst-Ni with Ag powders in solution phase by solution deposition method and sol-gel method. These methods can be integrated with thick-film process by screen printing technology.
3. Carbon nanotubes can be grown at total pressure 6 Torr with a $CH_4$ flow rate of 10 sccm and $H_2$ flow rate of 10 sccm for 30 min below 550°C under the power of 150W(catalyst preparation by solution deposition method). The tip of CNTs were closed and encapsulated with Ni catalytic nanoparticles. The turn on field value at this case was 3.2 V/μm. Uniform electron emission was also observed on the electrode with good emission current and brightness.
4. Carbon nanotubes can be grown at total pressure 6 Torr with a $CH_4$ flow rate of 10 sccm and $H_2$ flow rate of 10 sccm for 60 min under the power of 200W(catalyst preparation by sol-gel method). The tips of CNTs were closed and encapsulated with Ni catalytic

nanoparticles. The turn on field value at this case was 5.4 V/μm. Uniform electron emission was also observed on the electrode with good emission current and brightness.

5. Carbon nanotube emitters were synthesized on the catalyst-mixed thick-film constructed cathode structures at 480℃ by thermal chemical vapor deposition (CVD) method. The field emission properties performed uniform emission image and high brightness (no less than 500 nits). The turn-on electric field was about 3.85 V/μm with an emission current destiny of 10 μA/cm$^2$, and the achieved current density was 1 mA/cm$^2$ driven by 5 V/μm.
6. Under controlling the pumping system and precursor concentration during the CVD process, cathode with high aspect ratio dielectric holes for field emission devices was properly produced.
7. We have successfully demonstrated that the EPD method can be applied to deposit CNTs into the selected-area of the triode structures for FED devices. By suitable solution content and voltage controlling situation, photo-resist or sacrificial layer can be omitted.
8. Comparing with other processes, this work was combined the advantages of thick-film technology and EPD method which can scale up to large size panel with low-cost and operate at low-temperature environment.

## References


[1] S. Iijima, Nature 354 (1991) 56.

[2] J.-M. Bonard, H. Kind, T. Stöckli, L.O. Nilsson, Solid State Electronics 45 (2001) 893.

[3] N. Hamada, S.-I. Sawada, A. Oshiyama, Phys. Rev. Lett. 68 (1992) 1579.

[4] R. Saito, M. Fujita, G. Dresselhaus, M.S. Dresselhaus, Appl. Phys. Lett. 60 (1992) 2204.

[5] J.W.G. Wildöer, L.C. Venema, A.G. Rinzler, R.E. Smalley, C. Dekker, Nature 391 (1998) 59.

[6] T.W. Odom, J.L. Huang, P. Kim, C.M. Lieber, Nature 391 (1998) 62.

[7] S. Xie, W. Li, Z. Pan, B. Chang, L. Sun, J. Phys. Chem. Solids 61 (2000) 1153

[8] M.R. Falvo, G.J. Clary, R.M. Taylor II, V. Chi, F.P. Brooks Jr, S. Washburn, R. Superfine, Nature 389 (1997) 582.

[9] E.W. Wong, P.E. Sheehan, C.M. Lieber, Science 277 (1997) 1971.

[10] J.-P. Salvetat, A.J. Kulik, J.-M. Bonard, G.A.D. Briggs, T. Stöckli, K. Méténier, S. Bonnamy, F. Béguin, N.A. Burnham, L. Forró, Adv. Mater. 11 (1999) 161.

[11] J.-P. Salvetat, G.A.D. Briggs, J.-M. Bonard, R.R. Bacsa, A.J. Kulik, T. Stöckli, N.A. Burnham, L. Forró, J. Phys. Rev. Lett. 82 (1999) 944.

[12] M.-F. Yu, O. Lourie, M.J. Dyer, K. Moloni, T.F. Kelly, R.S. Ruoff, Science 287 (2000) 637.

[13] L.A. Chernozatonskii, Yu.V. Gulyaev, Z.Ja. Kosakovskaja, N.I. Sinitsyn, G.V. Torgashov, Yu.F. Zakharchenko, E.A. Fedorov, V.P. Val'chuk, Chem. Phys. Lett. 233 (1995) 63.

[14] A.G. Rinzler, J.H. Hafner, P. Nikolaev, L. Lou, S.G. Kim, D. Tománek, P. Nordlander, D.T. Colbert, R.E. Smalley, Science 269 (1995) 1550.

[15] W.A. de Heer, A. Châtelain, D. Ugarte, Science 270 (1995) 1179.

[16] W. Zhu, C. Bower, O. Zhou, G. Kochanski, S. Jin, Appl. Phys. Lett. 75 (1999) 873.

[17] Z. Yao, C.L. Kane, C. Dekker, Phys. Rev. Lett. 84 (2000) 2941.

[18] P. G. Collins and A. Zettl, Appl. Phys. Lett. 69 (1996) 1969.

[19] S. Fan, M. G. Chapline, N. F. Franklin, T. W. Tombler, A.M. Cassel, H. Dai, Science 283 (1999) 512.

[20] Q. H. Wang, A. A. Setlur, J. M. Lauerhass, J. Y. Dai, E. W. Seeling, and R. P. H. Chang, Appl. Phys. Lett. 72 (1998) 2912.

[21] W. A. de Heer, A. Chatelain, and D. Ugarte, Science 270 (1995) 1179.

[22] P. M. Ajayan, S. Iijima, Nature 361 (1993) 333.

[23] Z. W. Pan, S. S. Xie, B. H. Chang, L. F. Sun, W. Y. Zhou, G. Wang, Chem. Phys. Lett. 299 (1999) 97.

[24] S. Bandow, A. M. Rao, K. A. Willianms, A. Thess, R. E. Smalley, P. C. Ejlund, J. Phys. Chem. B 101 (1997) 8839.

[25] P. G. Collins and A. Zettl, Phys. Rev. B 55 (1997) 9391.

[26] Y. Chen, D. T. Shaw, and L. Guo, Appl. Phys. Lett. 76 (2000) 2469.

[27] W.B. Choi, D.S. Chung, J.H. Kang, H.Y. Kim, Y.W. Jin, I.T. Han, Y.H. Lee, J.E. Jung, N.S. Lee, G.S. Park, and J.M. Kim, Appl. Phys. Lett. 75 (1999) 3129.

[28] G. S.Choi, Y. S. Cho, S. Y. Hong, J. B. Park, K. H. Son, and D. J. Kim, J. Appl. Phys. 91 (2002) 3847.

[29] H. S. Kang, H. J. Yoon, C. O. Kim, J. P. Hong, I. T. Han, S. N. Cha, B. K. Song, J. E. Jung, N. S. Lee, and J. M. Kim, Chem. Phys. Lett. 349 (2001) 196.

[30] C. J. Lee, J. Park, S. Han, and J. Ihm, Chem. Phys. Lett. 337 (2001) 398.

[31] J.-H. Han, S. H. Choi, T. Y. Lee, J.-B. Yoo, C.-Y. Park, H. J. Kim, I.-T. Han, S. Yu, W. Yi, G. S. Park, M. Yang, N. S. Lee, and J. M. Kim, Thin Solid Films 409 (2002) 126.

[32] M.S. Dresselhaus, G. Dresselhaus, P.C. Eklund, Academic Press, Boston (1996).

[33] R. Saito, G. Dresselhaus, M.S. Dresselhaus, “Physical properties of carbon nanotubes” Imperial College Press, London (1998).

[34] http://smalley.rice.edu/images/allotropes.jpg

[35] H.W. Kroto, J.R. Heath, S.C. O’Brien, R.F. Curl, R.E. Smalley, Nature 318 (1985) 162.

[36] J. Baggot, “Perfect symmetry the accidental discovery of buckminsterfullerence”, Oxford University Press (1994).

[37] H.W. Kroto, Rev. Mod. Phys. 69 (1997) 703.

[38] R.E. Smalley, Rev. Mod. Phys. 69 (1997) 723.

[39] H. Aldersey-Williams, “The most beautiful molecule”, Aurum Press, London (1995).

[40] M.S. Dresselhaus, J. Steinbeck, “Liquid carbon”, Tanso 132 (1988) 44.

[41] T.W. Ebbesen, “Carbon nanotube”, Phys Today 49 (June 1996) 26.

[42] P.M. Ajayan, T.W. Ebbesen, Rep. Prog. Phys. 60 (1997) 1025.

[43] B.I. Yakobson, R.E. Smalley, Am Sci 85 (1997) 324.

[44] C. Dekker, Phys. Today 52 (May 1999) 22.

[45] T.W. Ebbesen, “Carbon nanotubes: preparation and properties”, CRC Press, Boca Raton, FL. (1997).

[46] K. Tanaka, T. Yamabe, K. Fukui, “The science and technology of carbon nanotubes”, Amsterdam, Elsevier (1999).

[47] E.T. Thostenson, Z. Ren, T.-W. Chou, Composites Science and Technology 61 (2001) 1899.

[48] K. Tanaka, K. Okahara, M. Okada, T. Yamab, Chem. Phys. Lett. 191 (1992) 469.

[49] D. Bernaerts, M. Op De Beeck, S. Amelinckx, J. Van Landuyt, G. Van Tendeloo, Philos. Mag. A 74 (1996) 723.

[50] X.F. Zhang, X.B. Zhang, G. Van Tendeloo, S. Amelinckx, M. Op de Beeck, J. Van Landuyt, J. Cryst. Growth 130 (1993) 3.

[51] S. Iijima, T. Ichihashi, Y. Ando, Nature 356 (1992) 776.

[52] L. Chico, V.H. Crespi, L.X. Benedict, S.G. Louie, M.L. Cohen, Phys Rev Lett 76 (1996) 971.

[53] X. Blase, L.X. Benedict, E.L. Shirley, S.G. Louie, Phys. Rev. Lett. 72 (1994) 1878.

[54] J.W. Mintmire, C.T. White, Carbon 33 (1995) 893.

[55] C.L. Kane, E.J. Mele, Phys. Rev. Lett. 78 (1997) 1932.

[56] P.R. Wallace, Phys. Rev. 71 (1947) 622.

[57] L.C. Venema, J.W.G. Wildöer, C. Dekker, A.G. Rinzler, R.E. Smalley, Appl. Phys. A 66 (1998) S153.

[58] T.W. Odom, J.L. Huang, P. Kim, C.M. Lieber, J. Phys. Chem. B 104 (2000) 2794.

[59] L.C. Venema, J.W.G. Wildöer, J.W. Janssen, S.J. Tans, H.L.J. Temminck Tuinstra, L.P. Kouwenhoven, C. Dekker, Science 283 (1999) 52.

[60] P. Kim, T.W. Odom, J.-L. Huang, C.M. Lieber, Phys. Rev. Lett. 82 (1999) 1225.

[61] S.J. Tans, A.R.M. Verschueren, C. Dekker, Nature 393 (1998) 49.

[62] R. Martel, T. Schmidt, H.R. Shea, T. Hertel, Ph. Avouris, Appl. Phys. Lett. 73 (1998) 2447.

[63] M. Bockrath, D.H. Cobden, P.L. McEuen, N.G. Chopra, A. Zettl, A. Thess, R.E. Smalley, Science 275 (1997) 1922.

[64] S.J. Tans, M.H. Devoret, H. Dai, A. Thess, R.E. Smalley, L.J. Geerligs, C. Dekker, Nature 386 (1997) 474.

[65] S.J. Tans, M.H. Devoret, R.J.A. Groeneveld, C. Dekker, Nature 394 (1998) 761.

[66] M. Bockrath, D.H. Cobden, J. Lu, A.G. Rinzler, R.E. Smalley, L. Balents, P.L. McEuen, Nature 397 (1999) 598.

[67] A. Bachtold, C. Strunk, J.-P. Salvetat, J.-M. Bonard, L. Forró, T. Nussbaumer, C. Schönenberger, Nature 397 (1999) 673.

[68] H.T. Soh, C.F. Quate, A.F. Morpurgo, C.M. Marcus, J. Kong, H. Dai, Appl. Phys. Lett. 75 (1999) 627.

[69] C. Schönenberger, A. Bachtold, C. Strunk, J.-P. Salvetat, L. Forró, Appl. Phys. A 69 (1999) 283.

[70] J. Kong, C. Zhou, A. Morpurgo, H.T. Soh, C.F. Quate, C. Marcus, H. Dai, Appl. Phys. A 69 (1999) 305.

[71] K. Liu, M. Burghard, S. Roth, P. Bernier, Appl. Phys. Lett. 75 (1999) 2494.

[72] P.L. McEuen, M. Bockrath, D.H. Cobden, Y.-G. Yoon, S.G. Louie, Phys. Rev. Lett. 83 (1999) 5098.

[73] H. Dai, E.W. Wong, C.M. Lieber, Science 272 (1996) 523.

[74] L. Langer, V. Bayot, E. Grivei, J.-P. Issi, J.P. Heremans, C.H. Olk, L. Stockman, C. Van Haesendonck, Y. Bruynseraede, Phys. Rev. Lett. 76 (1996) 479.

[75] T.W. Ebbesen, H.J. Lezec, H. Hiura, J.W. Bennett, H.F. Ghaemi, T. Thio, Nature 382 (1996) 54.

[76] B.I. Yakobson, C.J. Brabec, J. Bernholc, Phys. Rev. Lett. 76 (1996) 2511.

[77] B.I. Yakobson, G. Samsonidze, G.G. Samsonidze, Carbon 38 (2000) 1675.

[78] M.M.J. Treacy, T.W. Ebbesen, T. M. Gibson, Nature 381 (1996) 678.

[79] D.A. Walters, L.M. Ericson, M.J. Casavant, J. Liu, D.T. Colbert, K.A. Smith, R.E. Smalley, Appl. Phys. Lett. 74 (1999) 3803.

[80] M.-F. Yu, B.S. Files, S. Arepalli, R.S. Ruoff, Appl. Phys. Lett. 84 (2000) 5552.

[81] http:// 140.114.18.223/~hcshih/diamond/nanotube.html (2000).

[82] T.W. Ebbesen, P.M. Ajayan, Nature 358 (1992) 220.

[83] S. Iijima, T. Ichihashi, Nature 363 (1993) 603.

[84] D.S. Bethune, C.H. Klang, M.S. de Vries, G. Gorman, R. Savoy, J. Vazquez, R. Beyers, Nature 363 (1993) 605.

[85] J. Abrahamson, P.G. Wiles, B.L. Rhoades, Carbon 37 (1999) 1873.

[86] P.A. Thrower, Carbon 37 (1999) 1677.

[87] X.K. Wang, X.W. Lin, V.P. Dravid, J.B. Ketterson, R.P.H. Chang, Appl. Phys. Lett. 66 (1995) 2430.

[88] P.J.F. Harris, “Carbon nanotubes and related structure”, Cambridge university press (1999).

[89] T.W. Ebbesen, H. Hiura, J. Fujita, Y. Ochiai, S. Matsui, K. Tanigaki, Chem. Phys. Lett. 209 (1993) 83.

[90] G.H. Taylor, J.D. Fitz Gerald, L. Pang, M.A. Wilson, J. Cryst. Growth 135 (1994) 157.

[91] D.T. Colbert, J. Zhang, S.M. McClure, P. Nikolaev, Z. Chen, J.H. Hafner, D.W. Owens, P.G. Kotula, C.B. Cater, J.H. Weaver, A.G. Rinzler, R.E. Smalley, Science 266 (1994) 1218.

[92] W.K. Maser, J.M. Lambert, P.M. Ajayan, O. Stephan, P. Bernier, Synthetic Metals 77 (1996) 243.

[93] C. Journet, P. Bernier, Appl Phys A 67 (1998) 1.

[94] T. Guo, P. Nikolaev, A.G. Rinzler, D. Tománek, D.T. Colbert, R.E. Smalley, J. Phys. Chem. 99 (1995) 10694.

[95] A. Thess, R. Lee, P. Nikolaev, H. Dai, P. Petit, J. Robert, C. Xu, Y.H. Lee, S.G. Kim, A.G. Rinzler, D.T. Colbert, G.E. Scuseria, D. Tománek, J.E. Fischer, R.E. Smalley, Science 273 (1996) 483.

[96] A.G. Rinzler, J. Liu, H. Dai, P. Nikolaev, C.B. Huffman, F.J. Rodriguez-Macias, P.J. Boul, A.H. Lu, D. Heymann, D.T. Colbert, R.S. Lee, J.E. Fischer, A.M. Rao, P.C. Eklund, R.E. Smalley, Appl. Phys. A 67 (1998) 29.

[97] P.L. Walker Jr, J.F. Rakszawski, G.R. Imperial, J. Phys. Chem. 63 (1959) 133.

[98] M.S. Kim, N. M. Rodriguez, R.T.K. Baker, J. Catal. 131 (1991) 60.

[99] M. José-Yacamán, M. Miki-Yoshida, L. Rendón, J.G. Santiesteban, Appl. Phys. Lett. 62 (1993) 657.

[100] V. Ivanov, J.B. Nagy, P. Lambin, A. Lucas, X.B. Zhang, X.F. Zhang, D. Bernaerts, G. Van Tendeloo, S. Amelinckx, J. Van Landuyt, Chem. Phys. Lett. 223 (1994) 329.

[101] K. Hernadi, A. Fonseca, J.B. Nagy, D. Bernaerts, J. Riga, A. Lucas, Synthetic Metals 77 (1996) 31.

[102] A. Fonseca, K. Hernadi, P. Piedigrosso, J.-F. Colomer, K. Mukhopadhyay, R. Doome, S. Lazarescu, L.P. Biro, Ph. Lambin, P.A. Thiry, D. Bernaerts, J.B. Nagy, Appl. Phys. A 67 (1998) 11.

[103] P. Nikolaev, M.J. Bronikowski, R.K. Bradley, F. Rohmund, D.T. Colbert, K.A. Smith, R.E. Smalley, Chem. Phys. Lett. 313 (1999) 91.

[104] J. Kong, A.M. Cassell, H. Dai, Chem. Phys. Lett. 292 (1998) 567.

[105] M. Ge, K. Sattler, Appl. Phys. Lett. 64 (1994) 710.

[106] G. Che, B.B. Lakshmi, C.R. Martin, E.R. Fisher, R.S. Rouff, Chem. Mater. 10 (1998) 260.

[107] S. Seraphin, J. Electrochem. Soc. 142 (1995) 290.

[108] W.Z. Li, S.S. Xie, L.X. Qian, B.H. Chang, B.S. Zou, W.Y. Zhou, R.A. Zhao, G. Wang, Science 274 (1996) 1701.

[109] Z.W. Pan, S.S. Xie, B.H. Chang, C.Y. Wang, L. Lu, W. Liu, W.Y. Zhou, W.Z. Li, L.X. Qian, Nature 394 (1998) 631.

[110] M. Terrones, N. Grobert, J. Olivares, J.P. Zhang, H. Terrones, K. Kordatos, W.K. Hsu, J.P. Hare, P.D. Townsend, K. Prassides, A.K. Cheetham, H.W. Kroto, D.R.M. Walton, Nature 388 (1997) 52.

[111] O.M. Küttel, O. Groening, C. Emmenegger, L. Schlapbach, Appl. Phys. Lett. 73 (1998) 2113.

[112] Z.F. Ren, Z.P. Huang, J.W. Xu, J.H. Wang, P. Bush, M.P. Siegal, P.N. Provencio, Science 282 (1998) 1105.

[113] S. Fan, M.G. Chapline, N.R. Franklin, T.W. Tombler, A.M. Cassell, H. Dai, Science 283 (1999) 512.

[114] C.J. Lee, D.W. Kim, T.J. Lee, Y.C. Choi, Y.S. Park, Y.H. Lee, W.B. Choi, N.S. Lee, G.-S. Park, J.M. Kim, Chem. Phys. Lett. 312 (1999) 461.

[115] H. Araki, H. Kajii, K. Yoshino, Jpn. J. Appl. Phys. 38 (1999) L1351.

[116] H. Kind, J.-M. Bonard, C. Emmenegger, L.-O. Nilsson, K. Hernadi, E. Maillard-Schaller, L. Schlapbach, L. Forró , K. Kern, Adv. Mater. 11 (1999) 1285.

[117] Y.C. Choi, D.J. Bae, Y.H. Lee, B.S. Lee, I.T. Han, W.B. Choi, N.S. Lee, J.M. Kim, Synthetic Metals 108 (2000) 159.

[118] Y. Chen, D.T. Shaw, L. Guo, Appl. Phys. Lett. 76 (2000) 2469.

[119] H. Murakami, M. Hirakawa, C. Tanaka, H. Yamakawa, Appl. Phys. Lett. 76 (2000) 1776.

[120] Z. P. Huang, J. W. Xu, Z. F. Ren, J. H. Wang, M. P. Siegal, P. N. Provencio, Appl. Phys. Lett. 73 (1998) 3845.

[121] M. Okai, T. Muneyoshi, T. Yaguchi, S. Sasaki, Appl. Phys. Lett. 77 (2000) 3468.

[122] C. Bower, W. Zhu, S. Jin, O. Zhou, Appl. Phys. Lett. 77 (2000) 830.

[123] Y.C. Choi, Y.M. Shin, Y.H. Lee, B.S. Lee, G.S. Park, W.B. Choi, N.S. Lee, J.M. Kim, Appl. Phys. Lett. 76 (2000) 2367.

[124] A. Gorbunov, O. Jost, W. Pompe and A. Graff, Carbon, 40 (2002) 113.

[125] R. S. Wagner and W. C. Ellis, Appl. Phys. Lett., 4 (1964) 89.

[126] G. G. Tibbetts, J. Cryst. Growth, 66 (1984) 632.

[127] Y. Saito, T. Yoshikawa, M. Inagaki, M. Tomita and T. Hayashi, Chem. Phys. Lett., 204 (1993) 277.

[128] Y. Saito, Carbon, 33 (1995) 979.

[129] T. J. Trentler, K. M. Hickman, S. C. Goel, A. M. Viano, P. C.Gibbons and W. E. Buhro, Science, 270 (1995) 1791.

[130] T. J. Trentler, K. M. Hickman, S. C. Goel, A. M. Viano, P. C.Gibbons, W. E. Buhro, M. Y. Chiang and A. M. Beatty, J. Am. Chem. Soc. 119 (1997) 2172.

[131] R.H. Fowler and L. Nordheim, Roy. Soc. Proc. A, (1928) 173 .

[132] R. Gomer, “Field Emission and Field Ionization”, Harvard University Press, Cambridge, MA (1961)

[133] I. Brodie and P.R. Schwoebel, “Vacuum microelectronic devices”, Proceedings of the IEEE, 82 (1964) 1006.

[134] R. Gomer, “Field Emission and Field Ionization”, Harvard University Press, Cambridge, MA, 1961.

[135] R. Stratton, Proc. Phys. Soc. London B, 68 (1955) 746.

[136] N.A. Cade, R. Johnston, A. J. Miller, and C. Patel, J. Vac. Sci. Technol. B, 13 (1995) 549.

[137] R. Greene and H.F. Gray, “A simple theory of semiconductor field emission saturation,” Proc. 1st Int. Vacuum Microelectronics Conf., Williamsburg, VA (1988).

[138] L.M. Baskin, O.I. Lvov and G.N. Fursey, Phys. Stat. Sol., 47 (1971) 49.

[139] H.F. Gray, G.J. Campisi and R.F. Greene, Technical Digest of the IEDM, 86 (1986) 776.

[140] S. Kanemaru, T. Hirano, H. Tanoue, J. Itoh, J. Vac. Sci. Technol., B 14 (1996) 1885.

[141] K.L. Jensen and A.K. Ganguly, J. Vac. Sci. Technol. B 11 (1993) 371.

[142] K.L. Jensen and A.K. Ganguly, J. Vac. Sci. Technol. B 12 (1994) 770.

[143] K.L. Jensen, J. Vac. Sci. Technol. B 13 (1995) 516.

[144] L. Nilsson, O. Groening, C. Emmenegger, O. Kuettel, E. Schaller, L. Schlapbach, H. Kind, J. M. Bonard and K. Kern, Appl. Phys. Lett., 76 (2000) 2071.

[145] Y. Tu, Z. P. Huang, D. Z. Wang, J. G. Wen and Z. F. Ren, Appl. Phys. Lett., 80 (2002) 4018.

[146] A.A. Talin, K.A. Dean, J.E. Jaskie, Solid State Electronics 45 (2001) 963.

[147] Q.H. Wang, A.A. Setlur, J.M. Lauerhaas, J.Y. Dai, E.W. Seelig, R.P.H. Chang, Appl. Phys. Lett. 72 (1998) 2912.

[148] W.B. Choi, D.S. Chung, J.H. Kang, H.Y. Kim, Y.W. Jin, I.T. Han, Y.H. Lee, J.E. Jung, N.S. Lee, G.S. Park, J.M. Kim, Appl. Phys. Lett. 75 (1999) 3129.

[149] D.S. Chung, W.B. Choi, J.H. Kang, H.Y. Kim, I.T. Han, Y.S. Park, Y.H. Lee, N.S. Lee, J.E. Jung, J.M. Kim, J. Vac. Sci. Technol. B18 (2000) 1054.

[150] W.B. Choi, D.S. Chung, J.H. Kang, H.Y. Kim, Y.W. Jin, I.T. Han, Y.H. Lee, J.E. Jung, N.S. Lee, G.S. Park, J.M. Kim, EuroFE'99 meeting, Toledo, Spain, 15-19 November (1999).

[151] J.M. Kim, N.S. Lee, W.B. Choi, J.E. Jung, I.T. Han, D.S. Jung, S.H. Park, S.S. Hong, H.Y. Kim, 14th International Winterschool on Electronic Properties of Novel Mater. (IWEPNM2000), Kirchberg, Austria, 4-11 March (2000).

[152] Y. Saito, S. Uemura, K. Hamaguchi, Jpn. J. Appl. Phys. 37 (1998) L346.

[153] J.-M. Bonard, J.-P. Salvetat, T. Stöckli, L. Forró, A. Châtelain, Appl. Phys. A 69 (1999) 245.

[154] Y. Saito, S. Uemura, Carbon 38 (2000) 169.

[155] K.L. Jensen, Phys. Plasma 6 (1999) 2241.

[156] O. Zhou, 14th International Winterschool on Electronic Properties of Novel Mater. (IWEPNM2000), Kirchberg, Austria, 4-11 March, 2000.

[157] O. Zhou et al. (UNC Chapel Hill), W. Zhu (Lucent Technologies), pending US patents.

[158] R. Rosen, W. Simendinger, C. Debbault, H. Shimoda, L. Fleming, B. Stoner, O. Zhou, Appl. Phys. Lett. 76 (2000) 1668.

[159] R. Standler, “Protection of electronic circuits from over-voltages”, Wiley, New York (1989).

[160] W.D. Zhang, J.T.L. Thong, W.C. Tjiu, L.M. Gan, Diamond Relat. Mater. 11 (2002) 1638.

[161] B.R. Stoner, G.-H.M. Ma, S.D. Wolter, J.T. Glass, Phys. Rev. B 45 (1992) 11 067.

[162] Y. C. Choi, D. J. Bae, Y. H. Lee, B. S. Lee, I. T. Han, W. B. Choi, N. S. Lee, J. M. Kim, Synthetic Matals 108 (2000) 159.

[163] Z. L. Wang, J. M. Petroski, T. C. Green, M. A. El-Sayed, J. Phys. Chem. B 102 (1998) 6145.

[164] C. J. Lee, J. Park, S. Y. Kang, J. H. Lee, Chem. Phys. Lett. 323 (2000) 554.

[165] C. J. Lee, J. Park, S. Y. Kang, J. H. Lee, Chem. Phys. Lett. 326 (2000) 175.

[166] H. Neumayer, R. Haubner, Diamond and Related Materials 13 (2004) 1191.

[167] M. Sveningsson, R.-E. Morjan, O.A. Nerushev, Y. Sato, J. Bäckström, E.E.B. Campbell, F. Rohmund, Appl. Phys. A 73 (2001) 409.

[168] T. C. Chieu, M. S. Dresselhaus, M. Endo, Phys. Rev. B 26 (1982) 10530.

[169] P.C. Eklund, J.M. Holden, R.A. Jishi, Carbon 33 (1995) 959.

[170] X. Xu, G. R. Brandes, Appl. Phys. Lett. 74 (1999) 2549.

[171] Hiroki Ago, Jifa Qi, Kazuhito Tsukagoshi, Kazuhiro Murata, J. Electroanal. Chem. 559 (2002) 25.

[172] C. C. Lee, B. N. Lin, M. C. Hsiao, Y. Y. Chang, W. Y. Lin, L. Y. Jiang, SID Int. Symp. Dig. Tech. Pap. 36 (2005) 1716.

[173] M. H. Kuang, Z. L. Wang, X. D. Bai, J. D. Guo, E. G. Wang, Appl. Phys. Lett. 76 (2000) 1255.

[174] Y. M. Shyu, F. C. N. Hong, Materials Chemistry and Physics 72 (2001) 223.

[175] Y. S. Jung, D. Y. Jeon, Applied Surface Science 193 (2002) 129.

[176] K. C. Chen, C. F. Chen, J. S. Chiang, C. L. Hwang, Y. Y. Chang, C. C. Lee, Thin Solid films 498 (2006) 198.

[177] T.H. Tsou, M. H. Lin, B. N. Lin, W. Y. Lin, Y. C. Jiang, C. H. Fu, L. Y. Chiang, Y. Y. Chang, M. C. Hsiao, C. C. Lee, IDW/AD '05 (2005) 1695.

[178] K. A. Dean, B. R. Chalamala, Appl. Phys. Lett. 75 (1999) 3017.

[179] J. E. Jung, Y. W. Jin, J. H. Choi, Y. J. Park, T. Y. Ko, D. S. Chung, J. W. Kim, J. E. Jang, S. N. Cha, W. K. Yi, S. H. Cho, M. J. Toon, C. G. Lee, J. H. You, N. S. Lee, J. B. Yoo, J. M. Kim, Physica B 323 (2002) 71.

[180] V. K. Kayastha, Y. K. Yap, Z. Pan, I. N. Ivanov, A. A. Puretzky, D. B. Geohegan, Appl. Phys. Lett. 86 (2005) 253105.

[181] B. Gao, G. Z. Yue, Q. Qiu, Y. Cheng, H. Shimoda, L. Fleming, O. Zhou, Adv. Mater. 13 (2001) 1770.

[182] J. Tang, B. Gao, H. Geng, O.D. Velev, L.-C. Qin, O. Zhou, Adv. Mater. 15 (2003) 1352.

[183] K. Yamamoto, S. Akita, Y. Nakayama, J. Phys. D 31 (1998) L34.

[184] W. B. Choi, Y. W. Jin, H. Y. Kim, S. J. Lee, M. J. Yun, J. H. Kang, Y. S. Choi, N. S. Park, N. S. Lee, J. M. Kim, Appl. Phys. Lett. 78 (2001) 1547.

[185] S. J. Oh, J. Zhang, Y. Cheng, H. Shimoda, O. Zhou, Appl. Phys. Lett. 84 (2004) 3738.

[186] L. H. Chan, L. Y. Jiang, J. H. Liao, K. C. Chen, W. H. Wang, Y. Y. Chang, M. C. Hsiao, C. C. Lee, SID Int. Symp. Dig. Tech. Pap. 37 (2006) 641.

# List of Publications

## Journal Papers

1. **Low temperature growth of carbon nanotubes on printing electrodes by MPCVD**

Thin Solid films, 498 (2006) 198-201

**Kuang-Chung Chen**, Chia-Fu Chen, Jih-Shun Chiang, Chian-Liang Hwang, Yu-Yang Chang, and Cheng-Chung Lee

2. **Low-temperature CVD growth of carbon nanotube for Field Emission Application**

Diamond and Related Materials, 16 (2007) 566-569

**Kuang-Chung Chen,** Chia-Fu Chen, Jen-Hao Lee, Tai-Lin Wu, Chian-Liang Hwang, Nyan-Hwa Tai, and Ming-Chun Hsiao

3. **Selected Area Electrophoretic Deposition of Carbon Nanotubes in Triode Structure for Field Emission Device**

Japanese Journal of Applied Physics, 46 (2007) 4408-4409

**Kuang-Chung Chen,** Chia-Fu Chen, Wha-Tzong Whang, Kuo-Feng Chen, Jun-Dar Hwang, Kwan-Sin Ho, Yu-Yang Chang, and Lih-Hsiung Chan

4. **Thick-film structure geometry effect on carbon nanotubes synthesized by chemical vapor deposition method**

Japanese Journal of Applied Physics, 47 (2008) Articles in Press

**Kuang-Chung Chen,** Chia-Fu Chen, Wha-Tzong Whang, Shu-Hsing Lee, Kuo-Feng Chen, Chian-Liang Hwang, Nyan-Hwa Tai, Ming-Hung Lin, and Lih-Hsiung Chan

## Conference Papers and Presentations

1. Kuang-Chung Chen, Chia-Fu Chen, Jih-Shun Chiang, Chian-Liang Hwang, Yu-Yang Chang, and Cheng-Chung Lee, "Low temperature growth of carbon nanotubes on printing electrodes by MPCVD", The 3rd Asian Conference on Chemical Vapor Deposition, Taipei, Taiwan 2004.

2. Kuang-Chung Chen, Chia-Fu Chen, Jen-Hao Lee, Tai-Lin Wu, Chian-Liang Hwang, Nyan-Hwa Tai, and Ming-Chun Hsiao, "Low-temperature CVD growth of carbon nanotube for Field Emission Application", The International Conference on Metallurgical Coatings and Thin Films, San Diego, CA, USA. 2006.

3. Kuang-Chung Chen, Chia-Fu Chen, Wha-Tzong Whang, Shu-Hsing Lee, Kuo-Feng Chen, Chian-Liang Hwang, Nyan-Hwa Tai ,Ming-Hung Lin, and Lih-Hsiung Chan, "Thick-film structure geometry effect on carbon nanotubes synthesized by chemical vapor deposition method", The 3rd International Conference on Technological Advances of Thin Film & Surface Coatings, Singapore 2006

4. Lih-Hsiung Chan, Liang-Yua Jiang, Jane-Hway Liao, Kuang-Chung Chen, Wei-Hao Wang, Yu-Yang Chang, Ming-Chun Hsiao, and Cheng-Chung Lee, “A Highly Precise Processes for Cathode Structure of CNT-FEDs”, The Society for Information Display, International Symposium, Seminar, and Exhibition, San Francisco, CA, U.S.A. 2006

5. Tsung-Yen Tsai, Nyan-Hwa Tai, Lih-Hsiung Chan, Kuang-Chung Chen, Yu-Yang Chang “Low Temperature Growth of Carbon Nanotubes on Glass Substrate through the Thermal Chemical Vapor Deposition Method Using a Binary Catalyst System”, International Display Manufacturing Conference & FPD Expo, Taipei, Taiwan 2007

6. Kuang-Chung Chen, Liang-Yua Jiang, Jane-Hway Liao,Wei-Hao Wang, Yun-Jiau Shiau, Pao-Ming Tsai, Kuo-Feng Chen, Hsiao-Fen Wei, Shy-Wen Lai , Lih-Hsiung Chan, Ming-Hung Lin, Yu-Yang Chang, and Cheng-Chung Lee, “Triode Carbon Nanotubes Field Emission Display by highly precise thick film printing processes”, The 14th International Display Workshops, Sapporo, Japan 2007

7. Kuang-Chung Chen, Chia-Fu Chen, Wha-Tzong Whang, Shy-Wen Lai, Pao-Ming Tsai, Biing-Nan Lin, Yu-Yang Chang, Cheng-Chung Lee, and Lih-Hsiung Chan, “Floating Electrode Effects on Carbon Nanotubes Field Emission Display”, 台灣鍍膜科技研討會暨國科會計畫研究成果發表會 2007.

# 學經歷資料


- 姓名：陳光中
- 性別：男
- 生日：64 年 11 月 24 日，台北人
- 電子郵件信箱：northnose168@hotmail.com
- 聯絡電話：0910013990
- 通訊地址：新竹市 300 大學路 1001 號
  國立交通大學材料與工程研究所
  永久地址：台北縣新莊市化成路 32 號 7 樓


## 學歷

| | |
|---|---|
| 博士班：國立交通大學材料科學與工程學系暨研究所 | 2000. 9 ~ 2008. 6 |
| 研究所: 國立交通大學材料科學與工程學系暨研究所 | 1998. 9 ~ 1999. 6 |
| 大學：國立清華大學工程與系統科學系 | 1994. 9 ~ 1998. 6 |

## 專長

研究專長：

1. 奈米碳管合成與應用。
2. 厚膜製程與網印相關技術。
3. 顯示器技術。